# Embroidered textile connectors for wearable systems

Duarte Manuel de Sousa Fonseca

**Doctoral Thesis**

Submitted in partial fulfillment of the requirements
for the award of
Doctor of Philosophy of Loughborough University

Supervisors

Rob D. Seager, James A. Flint

Wolfson School of
Mechanical, Electrical and Manufacturing Engineering
Loughborough University

March 12, 2019

Loughborough University

Loughborough University

# Certificate of Originality
# Thesis Access Conditions and Deposit Agreement

Students should consult the guidance notes on the electronic thesis deposit and the access conditions in the University's Code of Practice on Research Degree Programmes

**Author D**uarte Manuel de Sousa Fonseca

**Title** Embroidered textile connectors for wearable systems

I Duarte Manuel de Sousa Fonseca, Agricolastrasse 8A, Munich, Germany, "the Depositor", would like to deposit Embroidered textile connectors for wearable systems, hereafter referred to as the "Work", once it has successfully been examined in Loughborough University Institutional Repository

**Status of access** OPEN / RESTRICTED / CONFIDENTIAL

**Moratorium Period**......................................years, ending............./...........20.............................

**Status of access approved by** (CAPITALS):.....R D SEAGER.............................................................

**Supervisor** (Signature)....... R D Seager ..................................................

**School of**...Mechanical, Electrical and Manufacturing Engineering.......................................

**Author's Declaration** *I confirm the following :*

CERTIFICATE OF ORIGINALITY
This is to certify that I am responsible for the work submitted in this thesis, that the original work is my own except as specified in acknowledgements or in footnotes, and that neither the thesis nor the original work therein has been submitted to this or any other institution for a degree

NON-EXCLUSIVE RIGHTS
The licence rights granted to Loughborough University Institutional Repository through this agreement are entirely non-exclusive and royalty free. I am free to publish the Work in its present version or future versions elsewhere. I agree that Loughborough University Institutional Repository administrators or any third party with whom Loughborough University Institutional Repository has an agreement to do so may, without changing content, convert the Work to any medium or format for the purpose of future preservation and accessibility.

DEPOSIT IN LOUGHBOROUGH UNIVERSITY INSTITUTIONAL REPOSITORY
I understand that open access work deposited in Loughborough University Institutional Repository will be accessible to a wide variety of people and institutions - including automated agents - via the World Wide Web. An electronic copy of my thesis may also be included in the British Library Electronic Theses On-line System (EThOS). I understand that once the Work is deposited, a citation to the Work will always remain visible. Removal of the Work can be made after discussion with Loughborough University Institutional Repository, who shall make best efforts to ensure removal of the Work from any third party with whom Loughborough University Institutional Repository has an agreement. Restricted or Confidential access material will not be available on the World Wide Web until the moratorium period has expired.

- That I am the author of the Work and have the authority to make this agreement and to hereby give Loughborough University Institutional Repository administrators the right to make available the Work in the way described above.

**Author's signature**......Duarte de Sousa Ferreira......Date...26/03/2018.........................................

| **user's declaration:** for signature during any Moratorium period (Not Open work): ***I undertake to uphold the above conditions:*** | | | |
|---|---|---|---|
| Date | Name (CAPITALS) | Signature | Address |
| | | | |
| | | | |
| | | | |
| | | | |

# Abstract

This thesis presents a novel textile microwave interconnect that can be easily attached and removed from textile devices. Interconnects perform a vital role in carrying RF signals between an amplifier and an antenna or other devices. Conventional interconnects used for interconnecting non-flexible circuits perform this function with very low losses, however the same is not true for transmission lines made on fabrics using conductive threads or inks. This scenario of using interconnects on fabric systems is challenging. Due to the necessity of washing fabrics, permanent attachments on the fabric have disadvantages. The connection presented in this thesis is done without any metal or rigid parts on the textile devices side. The connector is held in place by magnets which are shown to have no negative impact on the microwave connection. Two models are then explored, a microstrip connector and a grounded coplanar waveguide (CPW) connector. A detailed study of the models was done and it was found that both models have reasonable results up to 2GHz. The interconnects are fully characterized by de-embedding the connection part. This can be used to predict the effect the interconnect will have when used to connect a microwave equipment. The microstrip version of the interconnect is attached to an antenna and the results presented. The interconnect has no negative effect on the reflection coefficient measurement of the antenna. Repeatability tests were also performed with this model, with no visible change in the connection quality between measurements. Different embroidery patterns and stitching designs were also investigated. These are used to reduce the amount of conductive thread used up to 59% reduction in thread ammount. A wearable antenna was fully converted from rigid copper sheet to a full textile design.

# Acknowledgements

To begin with I would like to thank my supervisors Dr. Rob Seager and Dr. James Flint for the invaluable guidance and advice during my PhD. I would like to express my gratitude to Dr. William Whittow for finding me on LinkedIn and for the positive reinforcement during my PhD. The whole process was made much easier by being surrounded by great colleagues and friends. I would like to give a big thank you to my colleagues Anastasios, Shiyu, Yunfei, Isaac, Chuck, Abraham and Chinthana for the support and good times in Loughborough University. A big thank you for my housemate Jialin for being a good friend and for teaching me how to fry lettuce! I would like to thank my parents Maria Helena and Joaquim Francisco, without them none of this would have been possible. And lastly I would like to give big thanks to my girlfriend Anđela. For all the patience and support in times of need.

# List of publications

[1] A. Paraskevopoulos, D. d. S. Fonseca, R. D. Seager, W. G. Whittow, J. C. Vardaxoglou, and A. A. Alexandridis, "Higher-mode textile patch antenna with embroidered vias for on-body communication," IET Microwaves, Antennas Propagation **10,** 802–807 (2016).

[2] D. Fonseca, "Textile-to-rigid microstrip transition using permanent magnets," Electronics Letters **51,** 709–710(1) (2015).

[3] S. Zhang, D. Speight, A. Paraskevopoulos, D. Fonseca, C. Luxey, W. Whittow, and J. Pinto, "On-body measurements of embroidered spiral antenna," In *2015 Loughborough Antennas Propagation Conference (LAPC)*, pp. 1–5 (2015).

[4] D. S. Fonseca, R. D. Seager, and J. A. Flint, "Microwave interconnects between textile and rigid substrates using permanent magnets," In *2015 9th European Conference on Antennas and Propagation (EuCAP)*, pp. 1–2 (2015).

[5] T. R. Lovett, J. Flint, D. S. Fonseca, and I. H. Daniel, "Novel broadband antenna for wearables," In *2014 Loughborough Antennas and Propagation Conference (LAPC)*, pp. 178–181 (2014).

# Contents

# List of Figures

# List of Tables

# Chapter 1

# Introduction

The area of wearable technology is a growing phenomenon with constantly increasing choices of devices as well as use cases. At the consumer level these are mostly used as fitness monitors and contactless payment units. Fitness devices measure and monitor our physical activity in an attempt to quantitise and provide feedback data on our daily lives. Contactless payment units are also getting a lot of attention, these are usually a part of smartwatches and smartbands that use NFC to facilitate and quicken small payments. There is also interest in the more generic area of smart clothing which incorporates both conventional units and textiles. In an ever increasing search for ways to measure a users daily life, these smart clothes have the ability to provide a much greater amount of data while being completely hidden from plain sight. Smart clothing that can measure all kinds of user data, location, heart rate, pulmonary expansion, localized muscle use as well as body temperature can provide greater insights into a person's physical activity. These textile sensors are sewn directly in the clothes and have the advantage of not having the discomfort of wearing wires or bulky electronics under the clothes. With smart clothes it can be easier to keep track of the location of users with special needs that could get lost, this is done with circuitry directly embedded in the clothes without the need to carry other methods of location (smartphone, wristbands). In sports garments with heart rate, breathing sensors and muscle flexing sensors provide the athlete with the advantage of knowing if his training routine is exercising the specialized muscles he needs the most. For more hazardous lines of work, such as firefighters [1] or police officers, the garments can be equipped to track the vital signs of the user as well as location.

The materials used to create this textile electronic systems can range from conductive threads to conductive inks, with different techniques applied to them to create antennas or transmission lines on the fabric. When such systems are tested it is usual to connect them to traditional RF equipment, since the technology still doesn't allow the fabrication of textile transistors. This usually means that a rigid metal connector will have to be attached somehow to the conductive material on the textile, sometimes by direct soldering or by using a conductive epoxy glue. This has the drawbacks of having a permanent rigid connector attached to garments. These interconnects cannot be removed for washing and can get be uncomfortable.

## 1.1 Motivation

Wearable technology is just starting to make its appearance in the consumer market, especially within the area of smartbands and smartwatches. However the technology has a huge growing potential due to the number of industries that have begun using wearable technology [2]. Industry analysts are forecasting a huge growth in the wearable devices market reaching unit sales of around two and a half billion by 2019 globally as shown in Figure 1.1.

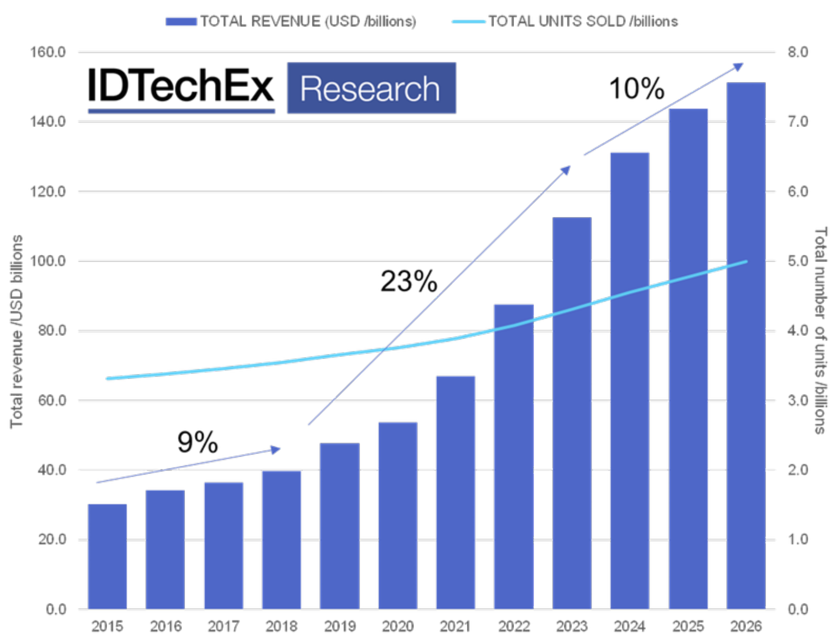


**Figure 1.1** Global wearable device unit shipments forecast as shown in [3]

Another technology that might give an increase to the wearable market is the Internet of Things or IoT, such as controlling the lights or heating in the home with your wearable mobile devices. The sport and fitness market has already begun the adoption of smart textiles with brands such as Ralph Lauren [4] suddenly introducing this technology in some of their merchandise.

The growing market of wearable electronics and the fact that it is a relatively new research area, makes this area a good topic of research both scientifically as well as economically. Another motivation for this research was lack of interconnects in the literature that could be easily removed. With this in mind, a novel approach in connecting textile electronics to traditional electronic equipment was developed. This interconnect should be fully removable while having no rigid parts on the textile side. The interconnect uses magnets in two ways. As a means of physically holding it in place and to apply contact force for a good electrical connection. This has the benefit of easy removal of external RF equipment.

Having a removable microwave interconnect for wearable applications has several advantages. It allows for easy removal when a device is not in use, leaving no permanent metal parts on the clothes which cause discomfort. It also allows for easy washing of the garments without worry for the removable interconnect. In a more commercial approach it can make a product more appealing by not having metallic or bulky electronics always on the garment.

## 1.2 Research novelty

The novel work done in this thesis in the area of textile electronics is summarized in following points:

- *A novel method of using magnets to create a high quality textile interconnect was studied.* By using magnets to secure the connection, after removing the interconnect RF equipment there are no permanent metallic parts on the textile system. This has several advantages when compared to other systems. If the textile garment has to be washed, there are no metallic connectors or cables that can be damaged by the water during washing. The magnets are also shown to be a critical part of the system, applying contact force between textile and copper connections and assuring a good electrical connection.

- *The interconnect was fully characterized and the effects of its use extracted.* By de-embedding the effect of the connection between textile and copper it is possible to observe the effect it has on a system. A reasonable connection was achieved up to 2 GHz.

- *Multiple measurements using a textile antenna were performed and it was found that the interconnect did not affect the results.* Some systems, such as push-buttons shown in the literature review, suffer negative effects after attaching and removing the connection multiple times. The interconnect presented here shows resilience to this negative effect when attaching or removing the connection multiple times.

There was a lack of good quality removable interconnects in the literature. The novel use of magnets as a means to secure the interconnect make it easy to attach and remove the device. When the interconnect is removed there are no permanent metallic parts on the textile system. A fully characterization of the interconnect was also performed. By de-embedding the attachment point of the interconnect it is possible to predict the effects it could have when attached to a RF device.

A short summary of the following chapters is now presented.

In Chapter 2 a review of the literature is presented with a short introduction to microwave transmission line theory. After this in Chapter 3, the textile microstrip model will be presented. In this chapter the simulations, measurements and later characterization of the textile microstrip are presented. In Chapter 4 a similar approach is taken but applied to the textile grounded coplanar waveguide. Finally in Chapter 5, different embroidery filling designs are used and compared to the regular embroidery filling.

## References

[1] C. Hertleer, L. Van Langenhove, H. Rogier, and L. Vallozzi, “A textile antenna for fire fighter garments,” In *AUTEX 2007 Conference (Association of Universities for Textiles): From Emerging Innovations to Global Business*, (2007).

[2] “Global wearable technology market forecast to experience strong growth in 2015,”, https://uk.finance.yahoo.com/news/global-wearable-technology-market-forecast-000000058.html, accessed: 20/02/2015.

[3] "Wearable Technology 2017-2027: Markets, Players, Forecasts Read more at: https://www.idtechex.com/research/reports/wearable-technology-2017-2027-markets-players-forecasts-000536.asp,", https://www.idtechex.com/research/reports/wearable-technology-2017-2027-markets-players-forecasts-000536.asp, accessed: 05/12/2017.

[4] "The polo tech shirt,", http://www.ralphlauren.com/shop/index.jsp?categoryId=46285296, accessed: 20/02/2015.

# Chapter 2

# Literature review and transmission line theory

## 2.1 Review of materials and techniques

There are a wide range of materials that can be used to manufacture textile antennas or transmission lines such as conductive paint, conductive thread, screen printing and many others [1, 2]. Insulated wire is a flexible silicone rubber insulated wire, conductive paint has a high content of silver that produces a low electrical resistance, conductive thread is usually coated with some sort of conductive material [3], screen printing has also been used [4] to create transmission lines.

In [1] the development and assessment of flexible, body wearable antennas is presented. Three antenna designs are considered, a spiral, a bowtie and a broadband wire dipole are considered from 100MHz to 1GHz. Various materials were tested such as conducting ribbon, insulated wire, conducting paint, conducting nylon, phosphor bronze mesh, conducting thread, screen print, liquid crystal polymer (LCP) and copper coated fabric. The phosphor bronze mesh, LCP and copper coated fabric have the advantage of being able to be soldered to. The nylon, painted and screen printed antennas were connected using conductive epoxy. Both nylon and painted antennas were able to hold the epoxy but on the screen print material the epoxy lost its bond. The authors were concerned that the conductive paint antenna might crack with repeated flexing of the fabric, while the nylon would not suffer from this problem. The conductive thread antenna shown in Figure 7.2 was flexible and has the advantage of being washable, however in terms of RF performance it performed worse than any other due to losses. This antenna was lossy possibly due to the way the conductive thread was embroidery. In Figure 7.2 the thread is embroidered perpendicularly to the spiral shape, if instead the thread were be embroidered in the direction of the spiral the resistance might be lower due to the threads being in the direction of the current flow.

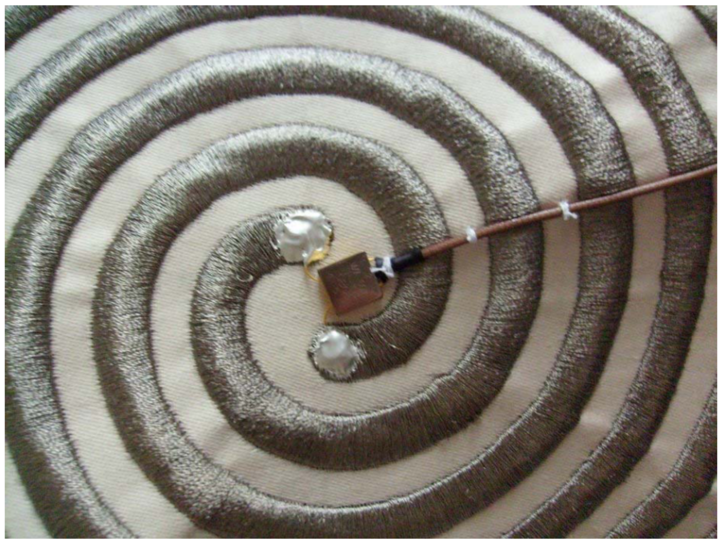

**Figure 2.1** Embroidered conductive thread spiral antenna after Matthews et al. [1]

The effects of environmental conditions on the electrical parameters of transmission lines is presented in [2]. The impact of moisture is assessed on this study, with characteristics of am EM wave passing along a dry and wet transmission line. It was found that with an increase in the humidity of the textile substrate, the attenuation of the signal transmitted also increases by several dB.

Weaving is also used to integrate electronics in textiles. In [5] the integration of e-stripes and conductive threads into woven textiles is studied, the process is compatible with commercial weaving processes. In this study the integration technology is based on weaving which involves two different sets of threads, the weft and warp. The principle of a weaving machine is shown in Figure 2.2, the warp threads are stored on the warp bean and threaded through the weaving machine. Shafts move the warp threads up and down to form a weaving pattern. The weft threads are then woven in the warp threads and are aligned against each other with a reed.

In this study the warp direction was used to integrate conductive threads into the textile, serving as bus lines. In Figure 2.3 along the weft direction the authors wove

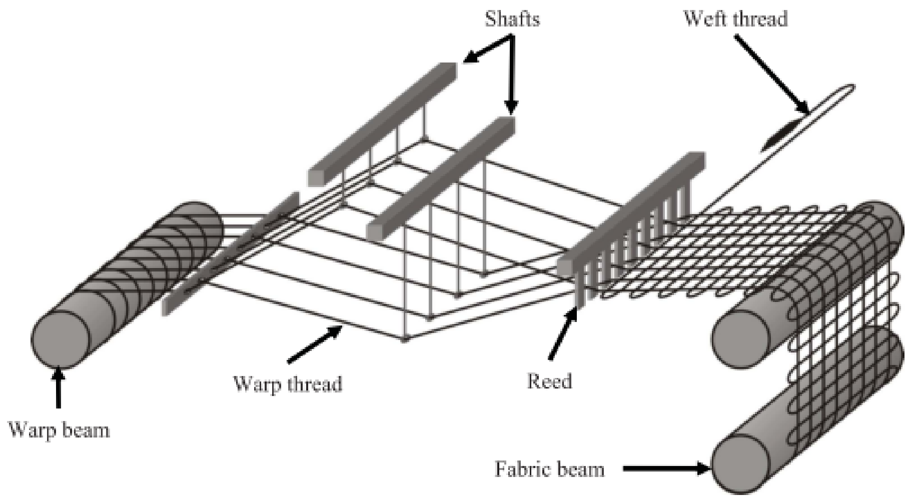


**Figure 2.2** Principle of a weaving machine after Zysset et al [5].

flexible plastic stripes which contain electronic devices (e-stripes) into the textile.

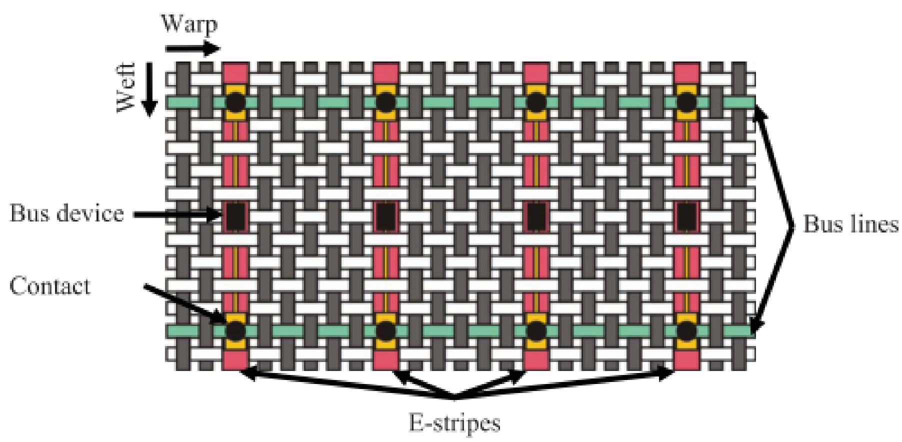


**Figure 2.3** Schematic of bus structure integrated into a woven textile after Zysset et al. [5].

In [6] flexible embroidered antennas made with computerized embroidery are investigated, the embroidery machine is shown in Figure 2.4. Different conductive threads were used and the findings indicate that hairy finer threads have to be embroidered at a slower speed to reduce thread breakage. Stiff threads and fine metal wires cannot go through the tension devices and cannot be wound into the looper wheel of the machine. Polymer based threads were found to be easier to process. Different conductive threads were tested and it was found that there was a great variation in the range of the resistance of the transmission lines created with different conductive threads.

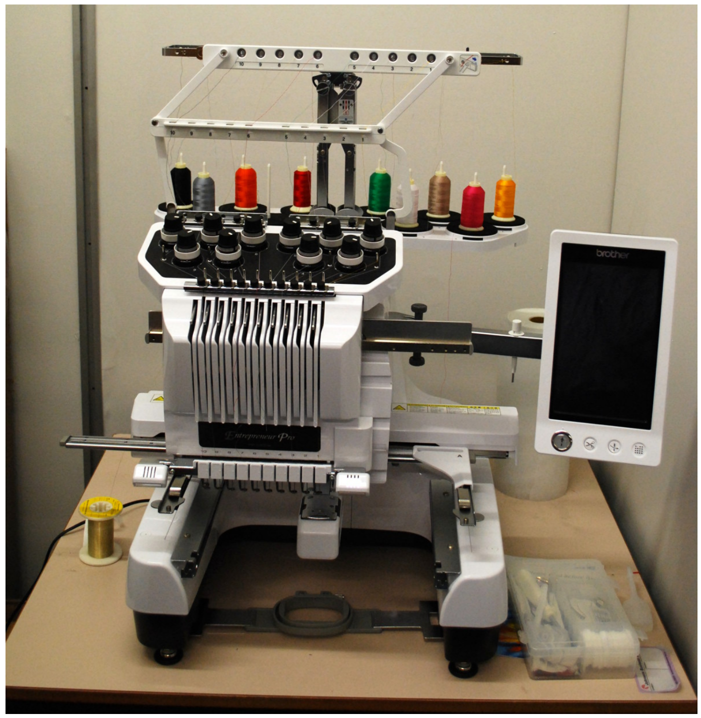

**Figure 2.4** Brother embroidery machine at Loughborough University

Different stitching properties were used in [6] when creating conductive thread embroidered patch antennas. In this work two fabric patch antennas were made and had their gain and efficiency compared with a copper patch reference antenna. The stitching direction was parallel to the longer side of the patch antennas and it was found that the antenna gain is affected by different spacing in between each stitch, the patch antenna and a close up of the 0.8mm stitching space is presented in Figure 2.5. The authors also found that the loss is introduced by the connection between stitches and when using closer stitching spacing, the electrical connection between neighbouring stitches improves and the antenna has better performance.

Another factor in the choice of the material was its availability. Research carried out at Loughborough University [7], [6] made use of the Brother Entrepreneur®PR1000 [8] embroidery machine and as this work was successful it was a natural choice for the work in the present thesis. The conductive thread available at the lab is Liberator™created by Syscom Advanced Materials [3] which has very good thermal and chemical properties, and was a good candidate for this research. The conductive

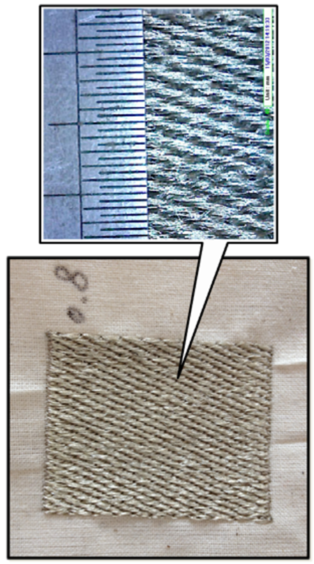

**Figure 2.5** 0.8mm stitch spacing and detail under microscope after Zhang et al. [7]

thread used is the Liberator Fiber-20 Ag which is made of 20 filaments composed of a lightweight, flexible and high strength fiber core with a conductive metal outer layer of copper and silver.

## 2.2 Transmission line review

Transmissions lines and waveguides are a medium used to transmit RF signals by the propagation of electromagnetic waves. They have very defined shapes in order to confine the electric and magnetic fields, if they are not well designed there could be losses in the transmission and some power is lost between the transmitter to the receiver. There are many types of transmission lines and waveguides as presented in [9] with planar transmission lines being widely used due to being compact, low cost and easily integrated with microwave circuits.

One type of transmission line suitable for this application is the Stripline, it consists of a conductive line covered by dielectric both on top and bottom and two parallel plates on either side acting as ground plane. In [10] a textile stripline is presented, it consists of a conductor strip sandwiched between two dielectric substrates acting as a spacer between two parallel conductive planes. It has a low reflection coefficient from dc to 8GHz and maintains a return loss of below 10 dB for a 180º bending condition.

Another type of transmission line which has been successfully implemented in textiles is coplanar waveguide. Cottet et al. in [11] have shown that this can be implemented using copper fibers in one or two directions with different yarn fineness. It was found that in this research the dielectric and ohmic losses do not determine the line insertions loss, but that the loss is mainly influenced by the nonuniform impedance profile along the transmission lines.

A screen printing technique has also been implemented [4] which presents the major advantage of having a very accurate design when comparing to other types of textile transmission lines. However the cured conductive silver paste suffers from brittleness when bending the fabric or creasing the fabric, the resistance goes up due to cracks in the silver paste.

## 2.3 Connector Review

After creating a wearable system it is usually measured and tested to evaluate its properties. This is normally done by connecting the textile antennas or transmission lines to Vector Network Analyzer (VNA) or other standard microwave measurement equipment. This measurements are usually done by connecting one end of a coaxial cable to the measurement equipment and the other end to the element selected for measurement. When using typical rigid antennas or transmission lines this connection is done by soldering a metal SMA connector to these devices.

In a textile system the rigid metal SMA connector is sometimes also used [12], however in a textile system where the elements need to be flexible and comfortable to wear, such rigid connectors get in the way of comfort as shown in Figure 2.6. Other techniques of ensuring a connection, include sewing the coaxial cable with conductive thread or by gluing it with conductive epoxy [13]. These techniques of attaching external equipment to the textile system often have the problem of being permanent. If one were to attach some kind of electronic equipment using this techniques, it would not be possible to remove it when the textile had to be washed.

Since most electronic systems cannot handle the washing procedure that textiles have to go through, there has to be a way to remove the electronic parts before washing the textile. This requires connections that allows electronics to be easily disconnected. Some work has been done on this by using a hook and loop connections as shown in [15] with insertion losses $< 1$ dB up to 2GHz when electroplating was used to increase hook and loop conductivity.

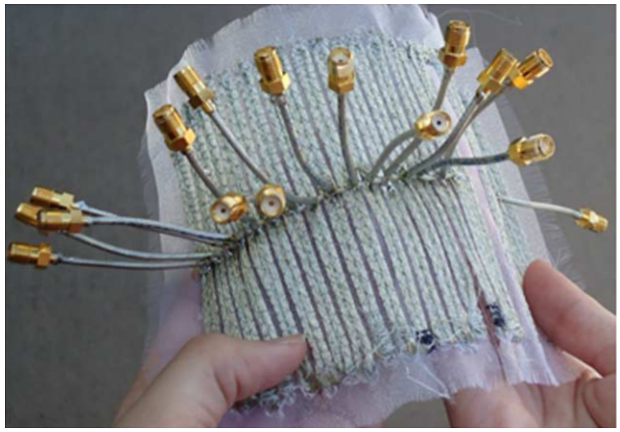

**Figure 2.6** Designed and fabricated textile lung sensor after Zhang L. et al. [14]

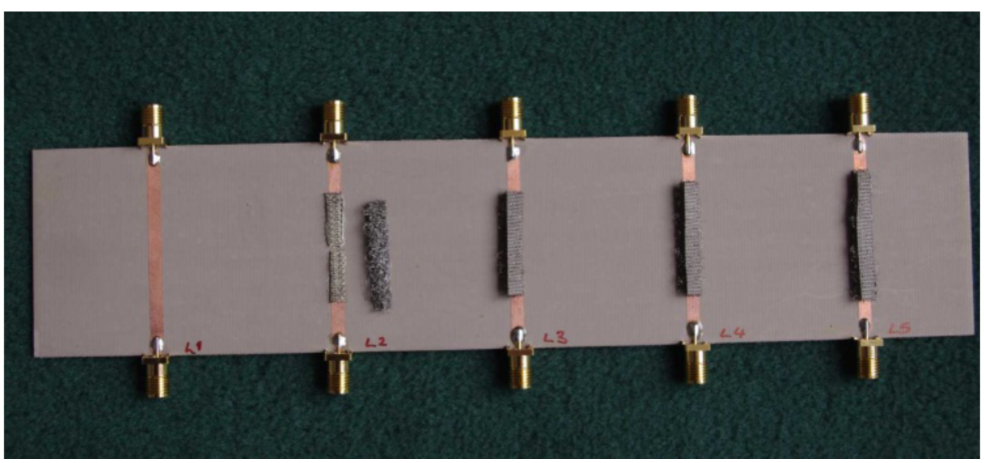

**Figure 2.7** Hook and loop test jig after Seager et al. [15]

Snap-on buttons have also been used in [16] and [17]. In [17] the study focuses the feeding system for disposable, single-use antennas. In this jig one button pair is used for the signal line and the other pair for the ground as shown in Figure 2.8.

**Figure 2.8** Snap-on button for coaxial-to-microstrip transition after Kellomäki et al. [17]

Here the buttons were punched through the microstrip line and ground plane. Using a time domain measurement the reflection coefficient of the buttons was found to be less than $-10$ dB within the frequency range up to 3GHz. The connection with the buttons was found to not be repeatable as with traditional RF connectors. The main reason was the bending of the coaxial inner conductor during the connection. It was noticed that bending the cables when in use, the torsion easily rips the copper foil tape off the substrate which dramatically changes the transition impedance.

In [16] the snap-on buttons are used as a detachable radio-frequency balanced connection between a garment-integrated textile dipole antenna and a passive sensor-enabled radio-frequency identification (RFID) tag. The flexible textile antenna that was developed has a reflection coefficient of $< -10$ dB ranging from 780MHz to 1030MHz. The snap-on buttons used are of sewn-on type as shown in Figure 2.9, the buttons were sown to the conductive textile using conductive thread.

Measurements on a 100mm length back-to-back balanced transmission line structure the buttons show an insertion loss from 0.29 dB to 0.76 dB up to 5GHz.

Another study on the subject of connectors was also developed in [18]. In this paper four connection strategies to connect an SMA connector to a textile transmission

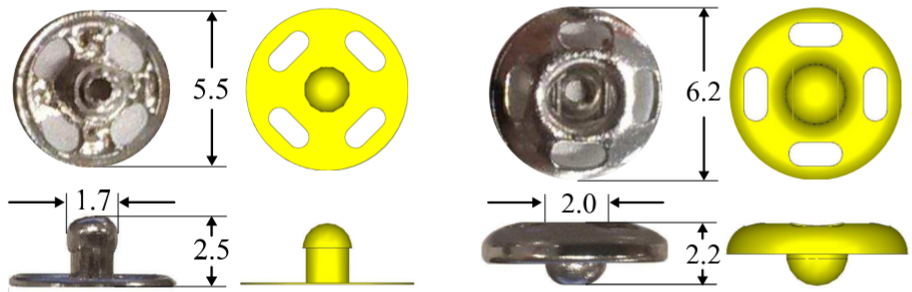


**Figure 2.9** Snap-on button and CST model dimensions [mm] after Chen et al. [17]

line are investigated. The connections are based on conductive epoxy, snap-on buttons, butterfly clasps and what the author calls wing solution. The snap-on connectors presented previously were attached to a textile antenna, while in this study they are attached to a textile microstrip line. However the authors noted a discrepancy when comparing the simulation results with the results measured with the snap-on buttons. The conclusion was that the snap-on buttons compress the dielectric too much, altering both physical and electrical properties.

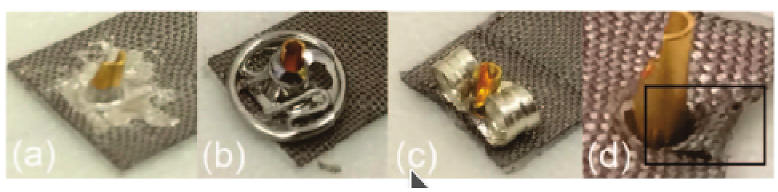


**Figure 2.10** Investigated connection strategies, from left to right, conductive epoxy, snap-on buttons, butterfly clasps and wing solution after Pinapati et al. [18]

The conductive epoxy has been mentioned before and the same conclusion applies here. It has excellent agreement between simulated and measured results but it is not suitable for practical applications, as bending the structure can crack the conductive epoxy.

Butterfly clasps are commonly used for earrings. In the authors solution the looped arms of the butterfly clasp, hold the central pin of the SMA connector. Although it is a feasible solution, the physical structure is non-planar. This can be uncomfortable to use on the body and the connection itself is easily disconnected. Movement will make the arms of the clasp move apart and not make the necessary pressure to have a good electrical connection to the SMA's inner conductor.

The last strategy is what the authors call 'wing' solution. They begin by first cutting a tail, or a thin strip of the conductive fabric where the connection will be. Then the inner pin of the SMA connector is removed and this thin strip of fabric is passed through the teflon part of the SMA. Finally, the SMA pin is put back in and the extra fabric removed. This connection has similar electrical to the conductive epoxy but is more resistant to bending and deforming.

Another type of connector that is used on textile electronics, due to its small size, is the Ultra Small Surface Mount Coaxial Connector (USSM). These connectors have a very small height of 1.9 or 2.4mm and a mounting area of 7.7mm$^2$. They are usually used in cellular phones, wireless communication devices, bluetooth and GPS among others due to their high frequency transmission of DC to 6GHz and their small size.

All this connectors can also be called microwave transitions, which are a mechanism by which electromagnetic waves on one type of transmission line couple to another type. As presented in [19] besides having a good impedance match between both transmission lines, it is also necessary to have a good field transition. A transition must provide an efficient field transition between two mediums by gradually changing physical boundary conditions. This field matching is a function of the change in the boundary conditions due to the transmission line shape changes. This is usually why step or tapper transitions are used to achieve a field and impedance match.

## 2.4 Transmission Line Design

In the early days of RF and microwave design, systems relied on two-wire lines, coaxial lines and waveguides for transmission. As everything in RF, these systems have their pros and cons. Two-wire lines are cheap to build but have no shielding and are subject to cross-talk interference. Coaxial lines on the other hand, are shielded but are difficult to implement in microwave components. Waveguides are low-loss and can handle high-power RF but can be heavy and bulky. The type of transmission line used in this work is the planar transmission line, these types of lines are compact, low-cost and are the easiest to integrate into microwave circuitry.

Transmission lines can be characterized by different aspects. Impedance, reflection coefficient, electrical length, voltage standing wave ratio or VSWR among others. These characteristics evaluate how well transmission lines behave.

### 2.4.1 Impedance and reflection coefficient

In its most basic form the characteristic line impedance $Z_0$ is the relation between the current and voltage on the transmission line. Shown in Equation 2.1 is the mathematical expression of the characteristic impedance. This impedance can approximately estimated using empirical formulas for specific transmission line types which will be demonstrated later.

$$\frac{V^+}{I^+} = Z_0 = -\frac{V^-}{I^-} \tag{2.1}$$

Impedance is useful to calculate how much power is transmitted across a transmission line and how much power is reflected back. This happens if there are impedance mismatches between a generator and a transmission line or a load. To calculate reflections the reflection coefficient $\Gamma$ is used. It is the ratio of reflected to incident voltage at a certain location.

In Fig 2.11 a schematic of a load impedance connected to a finite transmission line of length $l$ is presented. Here $\Gamma_0$ is the ratio of reflected to incident voltage wave at the load location z=0, shown in Equation 2.2.

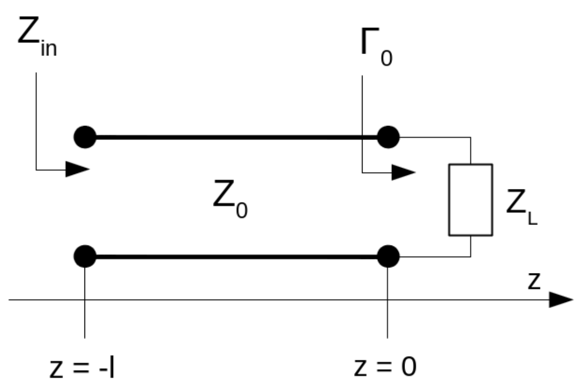


**Figure 2.11** Terminated transmission line at location z=0

$$\Gamma_0 = \frac{V^-}{V^+} \tag{2.2}$$

At location $z = -l$ the total input impedance $Z_{in}$ is calculated. At $z = 0$ the impedance is the load impedance where $Z_0$ is the characteristic impedance of the transmission line. From Equation 2.3 the reflection coefficient $\Gamma_0$ can be obtained as shown in Equation 2.4. As it can be seen, the reflection coefficient does not depend on the length of the line only on the impedance of the line and load. If the characteristic impedance of the line and the transmission line are equal, $\Gamma_0 = 0$ and there is no power reflected.

$$Z(0) = Z_L = Z_0 \frac{1+\Gamma_0}{1-\Gamma_0} \tag{2.3}$$

$$\Gamma_0 = \frac{Z_L - Z_0}{Z_L + Z_0} \tag{2.4}$$

### 2.4.2 Microstrip

Microstrip is one of the most used types of transmission lines, it is cheap to manufacture and easy to integrate in microwave circuitry. It can be considered to have evolved conceptually from a two-wire line. It is composed of a ground plane covered by a dielectric with thickness $d$ and a top conductor track of width $W$, the geometry can be seen in Fig. 2.12. The open top configuration of the microstrip line makes it very convenient for use with discrete lumped devices. However the open structure of the microstrip also has disadvantages. Due to the dielectric-air interface, the mode of propagation in a microstrip is a non-TEM hybrid mode. This happens due different phase velocities of the TEM fields on air and dielectric. Since the dielectric substrate is usually very thin $d \ll \lambda$, the fields are quasi-TEM [9]. Good approximations for the phase velocity, propagation constant and characteristic impedance can be obtained from static solutions. To obtain the approximate effective dielectric constant, equation 2.5 is used [9]. This equation treats the air and dielectric region as an homogeneous medium.

$$\epsilon_e = \frac{\epsilon_r + 1}{2} + \frac{\epsilon_r - 1}{2} \frac{1}{\sqrt{1 + \frac{12d}{W}}} \tag{2.5}$$

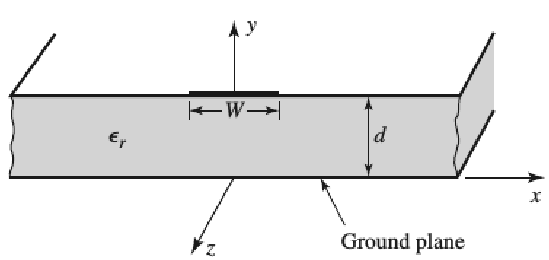


**Figure 2.12** Microstrip line geometry from Pozar et. al [9]

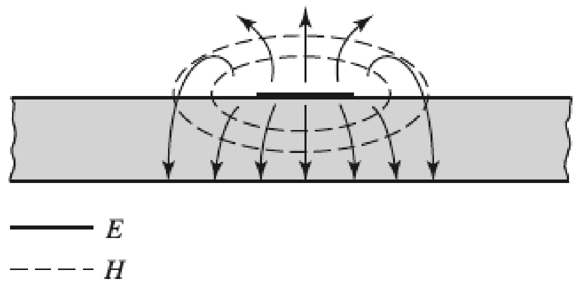


**Figure 2.13** Microstrip eletric and magnetic field lines from Pozar et. al [9]

As previously explained, an approximation of the characteristic impedance of a microstrip can be calculated using Equation 2.6 obtained from [9].

$$Z_0 = \left\{ \begin{array}{ll} \frac{60}{\sqrt{\epsilon_e}} \ln\left(\frac{8d}{W} + \frac{W}{4d}\right) & \text{for W/d} \leq 1 \\ \frac{120\pi}{\sqrt{\epsilon_e}\left[W/d + 1.393 + 0.667 ln\left(W/d + 1.444\right)\right]} & 2 \end{array} \right\} \tag{2.6}$$

In this work, microstrip was the first type of transmission line to be evaluated due to its widespread use. Patch antennas are widely used for on the body applications due to being low profile. And in many cases microstrip feed lines are the most common in these antennas. This and the fact that microstrip has a ground plane that reduces the effect of the body makes it a good candidate for this application.

### 2.4.3 Grounded co-planar waveguide

Coplanar waveguides are transmission lines that have all of the conductors in the same plane. While there are a few different models, the model that has been used in this work is the grounded coplanar waveguide or GCPW shown in Fig. 2.14. It has advantages when compared to microstrip when used with active circuitry due to the presence of the central conductor and the close ground planes on top. As this GCPW is to be worn close to the body, by including a conductor backing both the mechanical strength as well as resistance to the effects of the body are increased. However, conductor backed CPW lines support a parasitic microstrip mode as well as leaky modes which will be talked about later.

Shown in Fig. 2.15 is a traditional CPW, it consists of two slots of width $W$ and a central conductor $S$. The electric and magnetic fields are shown in Fig. 2.16. The fields of the CPW line are more sensitive to coupling above the line due to being less confined than in microstrips.

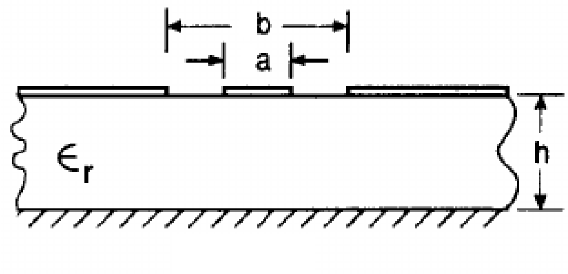


**Figure 2.14** Grounded CPW geometry from Gupta et. al [20]

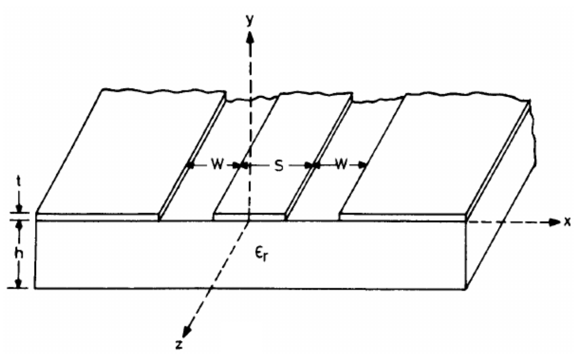


**Figure 2.15** CPW line geometry from Gupta et. al [20]

As with microstrip, it is possible to have an approximation of the characteristic impedance of the GCPW as shown in Equations 2.7 to 2.10. $Z_0$ is related to the width of the central conductor $S$ as well as the side gaps $W$. Also in order to avoid microstrip modes $h \gg b$.

$$\begin{aligned} a &= S \\ b &= S + 2W \end{aligned} \tag{2.7}$$

$$\begin{aligned} k &= a/b \\ k' &= \sqrt{1-k^2} \\ kl' &= \sqrt{1-kl^2} \\ kl &= \frac{tanh\left(\frac{\pi a}{4h}\right)}{tanh\left(\frac{\pi b}{4h}\right)} \end{aligned} \tag{2.8}$$

$$\epsilon_{eff} = \frac{1 + \epsilon_r \frac{K(k')}{K(k)} \frac{K(kl)}{K(kl')}}{1 + \frac{K(k')}{K(k)} \frac{K(kl)}{K(kl')}} \tag{2.9}$$

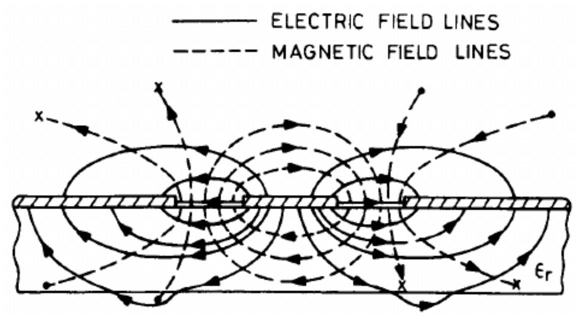


**Figure 2.16** CPW eletric and magnetic field lines from Gupta et. al [20]

$$Z_0 = \frac{60\pi}{\sqrt{\epsilon_{eff}}} \frac{1}{\frac{K(k)}{K(k')} + \frac{K(kl)}{K(kl')}} \tag{2.10}$$

Similar to microstrip, GCPW having a groundplane helps reduce the effect of the body in the transmission line. Although microstrip is more common, CPW is also present in many antennas and systems. The limitations of the textile CPW design are related to the small dimension of the gaps and difficulties with the embroidery as will be explained later.

## 2.5 Microwave Transition Design

As previously discussed, a microstrip transition was designed to connect textile RF equipment to traditional RF equipment. In transitions between different types of transmission lines reflections can occur due to different media, physical boundaries or impedance differences. According to [19], designing a transition must not only take into account impedance differences but also field transitions. Impedances should be matched in order to maximize coupling and minimizing reflections. As for field transitions, the change from one transmission line to the other should have a smooth and gradual transition in the boundary conditions. The gradual field match is related to the change in boundary conditions, as the transmission line changes shape the field geometry will also change.

## 2.6 Conclusion

As presented in this chapter several types of materials are used in textile wearable systems. For this study, conductive thread was chosen due to being more resilient to bending and washing. It was also found that there is a lack of high quality removable interconnects in the literature. Some work in the literature has been done with snap-on buttons and butterfly clasp but these have associated problems such as not being planar structures. For this work, small magnets were used to attach the interconnect to the system, which is a novel use for magnets in the area. The interconnect in study is also a planar structure which means that is conformable to the body. Work has been done as well on planar textile transmissions lines and shown to have good RF qualities. This is also why the interconnect was developed as a microstrip and coplanar design.

The transmission line theory presented in this chapter will be used in the design and analysis during the following chapters. An impedance of 50Ω at the required frequencies is desired, this will be obtained by designing a transmission line with the correct dielectric thickness and conductor width. A 50Ω will reduce the reflections due to impedance mismatch between the model and measurement cables. The focus of the next chapter is the design and full characterization of the textile microstrip model.

# References

[1] J. Matthews and G. Pettitt, "Development of flexible, wearable antennas," In *Antennas and Propagation, 2009. EuCAP 2009. 3rd European Conference on*, pp. 273–277 (2009).

[2] J. Leśnikowski, "Textile transmission lines in the modern textronic clothes," Fibres & Textiles in Eastern Europe **19,** 89 (2011).

[3] "Liberator™ conductive fiber,", http://www.metalcladfibers.com/liberator-fiber/, accessed: 21/11/2014.

[4] I. Locher and G. Troster, "Screen-printed Textile Transmission Lines," Textile Research Journal **77,** 837–842 (2007).

[5] C. Zysset, T. Kinkeldei, N. Munzenrieder, K. Cherenack, and G. Troster, "Integration Method for Electronics in Woven Textiles," Components, Packaging and Manufacturing Technology, IEEE Transactions on **2,** 1107–1117 (2012).

[6] T. Acti, S. Zhang, A. Chauraya, W. Whittow, R. Seager, T. Dias, and Y. Vardaxoglou, "High performance flexible fabric electronics for megahertz frequency communications," In *Antennas and Propagation Conference (LAPC), 2011 Loughborough*, pp. 1–4 (2011).

[7] S. Zhang, A. Chauraya, W. Whittow, R. Seager, T. Acti, T. Dias, and Y. Vardaxoglou, "Embroidered wearable antennas using conductive threads with different stitch spacings," In *Antennas and Propagation Conference (LAPC), 2012 Loughborough*, pp. 1–4 (2012).

[8] Brother, "Brother PE Design Next software,", 2017.

[9] D. M. Pozar, *Microwave Engineering, 4th Edition* (Wiley Global Education, 2011).

[10] Z. Xu, T. Kaufmann, and C. Fumeaux, "Wearable Textile Shielded Stripline for Broadband Operation," Microwave and Wireless Components Letters, IEEE **24,** 566–568 (2014).

[11] D. Cottet, J. Grzyb, T. Kirstein, and G. Troster, "Electrical characterization of textile transmission lines," Advanced Packaging, IEEE Transactions on **26,** 182–190 (2003).

[12] H. M. R. Nurul, F. Malek, P. J. Soh, G. A. E. Vandenbosch, V. Volski, S. L. Ooi, and I. Adam, "Evaluation of a wearable hybrid textile antenna," In *Antennas and Propagation Conference (LAPC), 2010 Loughborough*, pp. 337–340 (2010).

[13] K. Koski, L. Sydanheimo, Y. Rahmat-Samii, and L. Ukkonen, "Fundamental Characteristics of Electro-Textiles in Wearable UHF RFID Patch Antennas for Body-Centric Sensing Systems," Antennas and Propagation, IEEE Transactions on **62,** 6454–6462 (2014).

[14] L. Zhang, Z. Wang, and J. L. Volakis, "Textile Antennas and Sensors for Body-Worn Applications," Antennas and Wireless Propagation Letters, IEEE **11,** 1690–1693 (2012).

[15] R. D. Seager, A. Chauraya, S. Zhang, W. Whittow, and Y. Vardaxoglou, "Flexible radio frequency connectors for textile electronics," Electronics Letters **49,** 1371–1373 (2013).

[16] S. J. Chen, C. Fumeaux, D. C. Ranasinghe, and T. Kaufmann, "Paired Snap-On Buttons Connections for Balanced Antennas in Wearable Systems," Antennas and Wireless Propagation Letters, IEEE **PP,** 1–1 (2014).

[17] T. Kellomaki, "Snap-on buttons in a coaxial-to-microstrip transition," In *Antennas Propagation Conference, 2009. LAPC 2009. Loughborough,* pp. 437–440 (2009).

[18] S. P. Pinapati, T. Kaufmann, I. Linke, D. Ranasinghe, and C. Fumeaux, "Connection strategies for wearable microwave transmission lines and antennas," In *2015 International Symposium on Antennas and Propagation (ISAP),* pp. 1–4 (2015).

[19] J. Izadian, *Microwave transition design* (Artech House, Norwood, MA, 1988).

[20] K. Gupta, *Microstrip Lines and Slotlines*, *ARTECH HOUSE ANTENNAS AND PROPAGATION LIBRARY* (Artech House, 1996).

# Chapter 3

# Textile Microstrip Characterization

## 3.1 Introduction

This chapter will cover topics related to the study of a textile to FR-4 microstrip transition. The first section will present a proof of concept, to find whether holding the textile microstrip in place with magnets will negatively affect the connection. The following two sections 3.2 and 3.3, will present work done in trying to simulate this proof of concept model. A comparison between the results obtained from simulating the model using CST microwave studio software and the measurement of the built prototype are shown. On section 3.5 the the proof of concept is expanded by presenting a full textile microstrip prototype. This prototype is used to bridge a gap in a FR-4 microstrip and the results are shown. Afterwards in section 3.6, the full textile prototype is used to connect a textile antenna to a VNA and some repeatability measurements are also presented. Finally in the last section 3.7, the full jig of textile to FR-4 transition is characterized. Every part of the system is characterized and by de-embedding each individual part, the effect of the connection between textile and copper is presented.

## 3.2 Proof of Concept

The first step of the project was to envision what type of transition to build. Microstrip transmission lines are widely used to feed planar antennas and the fact the microstrip has a ground plane to reduce the negative effects of the proximity of the body makes it a good candidate. To have a removable connection it was thought to use small magnets to provide the mechanical strength. The magnets used are Neodymium Iron Boron (NdFeB) Nickel coated magnets and two sizes were tested. The smaller magnets are $3 \times 1$ mm cylindrical magnets and the larger ones are $10 \times 3 \times 2$ mm rectangular magnets [1]. However, to be sure about the effect that these magnets would have on a microstrip two test boards were created. One consisted of a 50Ω microstrip transmission line etched in FR-4 and the other was a similar prototype but with some of the top conducting layer etched out. These schematics are shown in Fig. 3.1 and pictures of the manufactured boards boards are shown in Fig. 3.2.

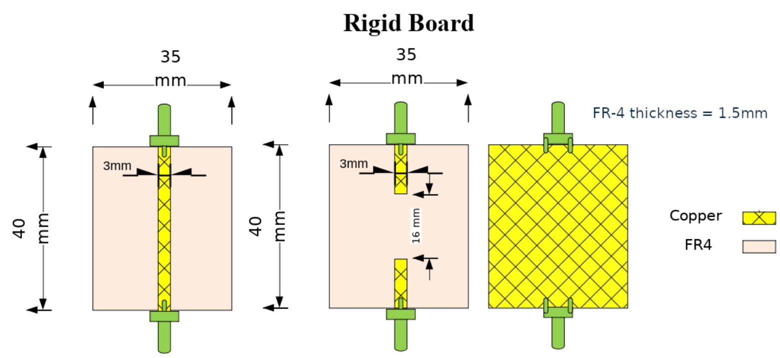


**Figure 3.1** Schematics of the boards used to test the effect of permanent magnets on the performance of a microstrip line

Also to test the effect of the magnets, a copper line was etched on a very thin dielectric with the same width as the microstrip top track and will be used to bridge the gap in the FR-4 prototype. The electrical properties of both microstrip prototypes were measured, using both small cylindrical as well as the rectangular magnets to hold the thin dielectric in place. The microstrip prototype jig with the thin dielectric line being held down by magnets is shown in Fig. 3.3 with the circular magnets and 3.4 with the rectangular magnets.

The measurement results are presented in Figs. 3.5 and 3.6. The circular magnets are the same width as the transmission line and do not seem do have a big influence on the measured results. The rectangular magnets were placed perpendicular to the transmission line, since the short length of the line did not allow them to be put along the direction of the conductive track. The results with the rectangular magnets were not as good as the cylindrical ones, perhaps due to the increased size of the magnet.

For the measurements with the circular magnets the $S_{11}$ is below $-15$ dB from 0.2GHz to 3GHz. For the S12 the value has its lowest value of approximately $-1.1$

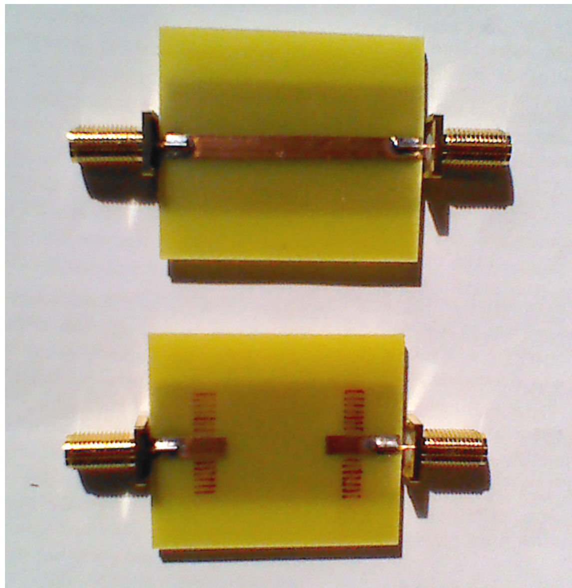

**Figure 3.2** Transition used to test the effect of permanent magnets on the performance of a microstrip line

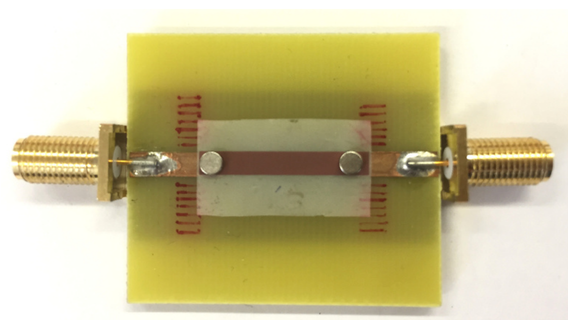

**Figure 3.3** Test jig using circular magnets to hold conductive line in place

dB which means that at least 77% of power is transmitted. The rectangular magnet results didn't perform as well with $S_{11}$ having a maximum of approximately $-8$ dB and for the $S_{12}$ the lowest value was of $-1.5$ dB close to 1.9GHz.

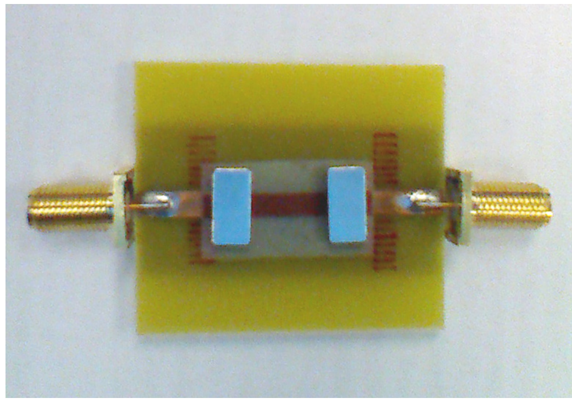

**Figure 3.4** Test jig using rectangular magnets to hold conductive line in place

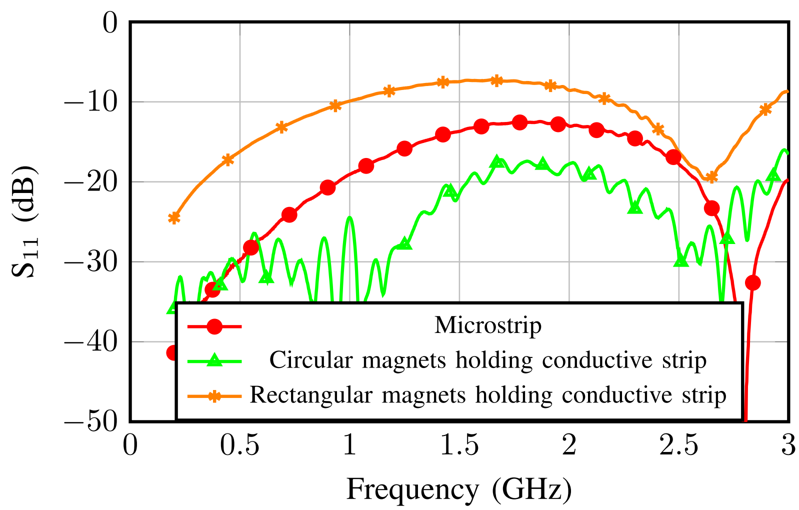


**Figure 3.5** $S_{11}$ results

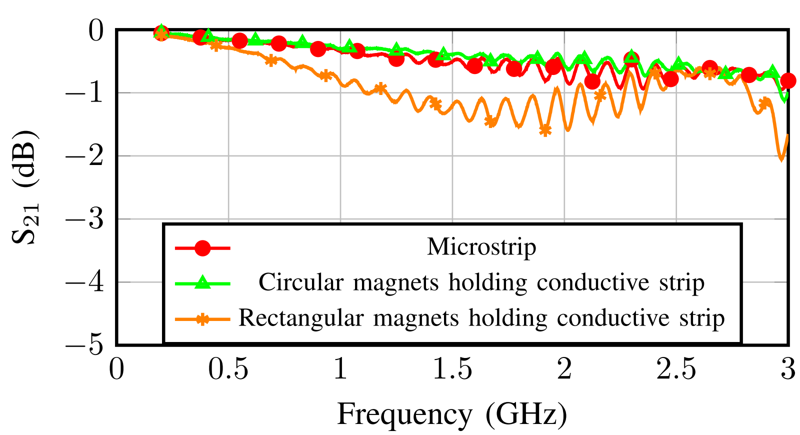


**Figure 3.6** $S_{21}$ results

## 3.3 Simulated Model and Comparison with Measurements

After the measurements shown in the previous chapter, the next step was to simulate the same transition using textile materials and compare with measurements. To simulate conductive thread embroidered in denim, the textile conductive line was modeled in CST MWS as a block of material. The model is a 40 mm long microstrip etched in FR-4 where the conducting line has a 16 mm central gap etched out of the conducting track as show in Fig. 3.7.

The values of the Denim permitivity ($\epsilon_r$) were obtained from [2] and were set as $\epsilon_r = 1.8$, the Denim's thickness was set to 0.45 mm. The magnet's electrical conductivity was obtained from [1] with the value of $0.47 \times 10^6$ S/m. The magnets are placed directly above and below the textile conductive line. This placement is used for the magnets to apply contact force between the conductive thread and the copper line as show in Fig. 3.8.

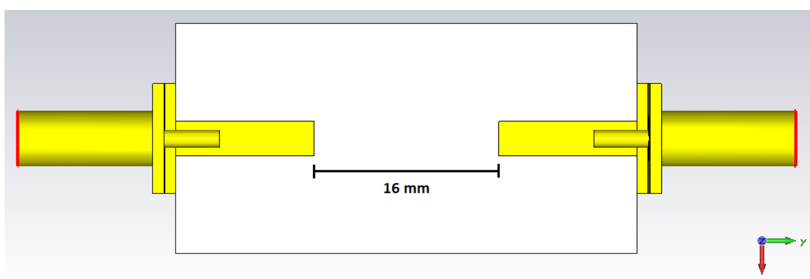


**Figure 3.7** Top view of the microwave transition without textile or magnets

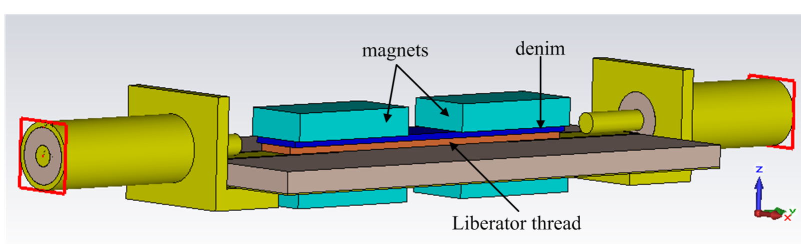


**Figure 3.8** Simulated model with rectangular magnets

The conductive thread used is Liberator™ created by Syscom Advanced Materials. A specification sheet for the thread can be found in the Appendices on Chapter 7. Simulating a textile embroidered microstrip with all the individual physical characteristics of the physical prototype, such as individual strands would be very computational intensive. So the embroidered microstrip was simulated as a rectangular block of material. To simulate the textile microstrip as a block of material the conductivity that was used in CST, was calculated in the following manner. A microstrip line 25 mm long and 3 mm wide was embroidered with a density of 7 lines/mm, in a 3 mm wide section there are 21 lines of thread. With the DC resistance value r of 6.67 Ω/m obtained from the spec sheet, the resistivity $\rho$ was calculated using equation 3.1. Where A is the metalized area of the cross section in each thread in $m^2$ and l the length in meter. Since we already have the value of the resistance per length from the specification sheet, the equation can be simplified.

$$\begin{aligned} R &= \rho \times \frac{l}{A}, \\ \rho &= \frac{R}{l} \times A = r \times A \end{aligned} \tag{3.1}$$

Looking at the specification sheet, one Liberator 20 core yarn has 157.5 $\mu m$ diameter. When metallized the diameter increases to 221 $\mu m$. Calculating the metallized area for outer coating of the yarn gives us a result of approximately $1.88 \times 10^4$ $\mu m^2$ which is $1.88 \times 10^{-8} m^2$. In the embroidered 3mm wide microstrip there are 21 threads side by side. Which means the total metallized area is

$$1.88 \times 10^{-8} m^2 \times 21 = 3.95 \times 10^{-7} m^2 \tag{3.2}$$

Going back to Equation 3.1, where A = $1.62 \times 10^{-7} m^2$ we have

$$\begin{aligned} \rho &= r \times A, \\ \rho &= 6.67 \Omega/m \times 3.95 \times 10^{-7} m^2, \\ \rho &= 2.63 \times 10^{-6} \Omega.m \end{aligned} \tag{3.3}$$

To calculate the value of conductivity

$$\begin{aligned} \sigma &= \frac{1}{\rho}, \\ \sigma &= 3.8 \times 10^5 S/m \end{aligned} \tag{3.4}$$

For the textile prototype, the textile conductive thread was embroidered in denim using under-sewing, this means that the conductive thread is set up on the looper of the embroidery machine as shown in Figure 3.9 in blue. By adjusting the tension of the threads on the embroidery machine it is possible to have the thread from the bobbin remain flat against the fabric. Having the conductive thread remain flat against the fabric instead of being embroidered on the top track that goes through the denim, reduces the resistance and improves the quality of microwave transmission on the prototype. Previous research done in [3] and [4], showed that higher efficiencies were achieved when the conductive threads were embroidered in a direction parallel to the current flow.

The conductive line was then set up in place, Figure 3.10 shows the textile line attached with the rectangular magnets. In this picture, the microstrip line facing the camera is actually non-conductive textile thread, the conductive textile is under it being pressed to the etched copper by the magnets.

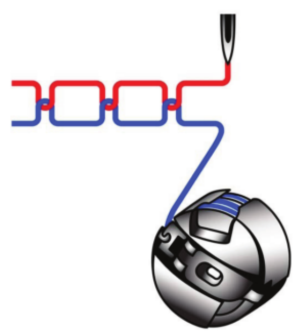

**Figure 3.9** Bobin with top thread and looper thread [5]

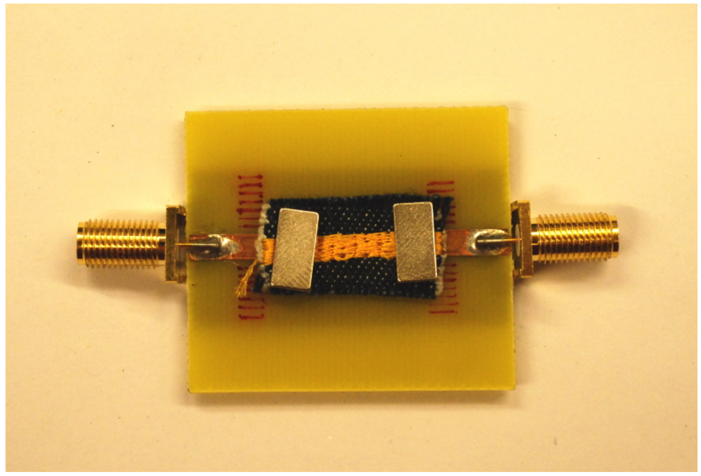

**Figure 3.10** Test jig using rectangular magnets to hold conductive textile line in place

## 3.4 Comparison between measurements and simulated results

Measurements were made using an Anritsu MS4622B VNA, the microstrip gap was covered either with the copper line etched in dielectric or with the conductive thread in denim. In this measurements it was found that the circular magnets do not have enough force to hold the denim in place, and any small movement will displace the textile line. The rectangular magnets however perform quite well in maintaining the denim piece in place.

In Figure 3.11 and Figure 3.12 there is a small difference between the simulated and measured results. It could be due to material differences between the simulated conductive line and real conductive line. There is an improvement when the rectangular magnets are used with the textile conductor embroidered in denim when compared to the etched line in thin dielectric, it could be because the orientation of the magnets is different but mostly due to the increased spacing between the magnet surface and the conductive line due to two layers of fabric.

The value of $S_{12}$ when using the conductive textile remains above $-1.5$ dB which is around 70% power transmitted. Ideally this value should be above $-1$ dB for a good transmission of power.

After these measurements it became apparent that both the magnets and conductive textile thread are feasible for a textile-to-rigid dielectric transition. The next

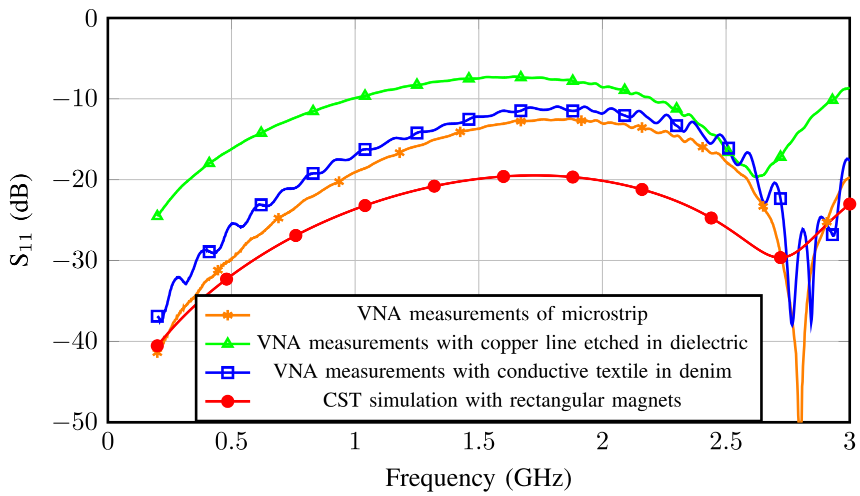


**Figure 3.11** $S_{11}$ results using rectangular magnets

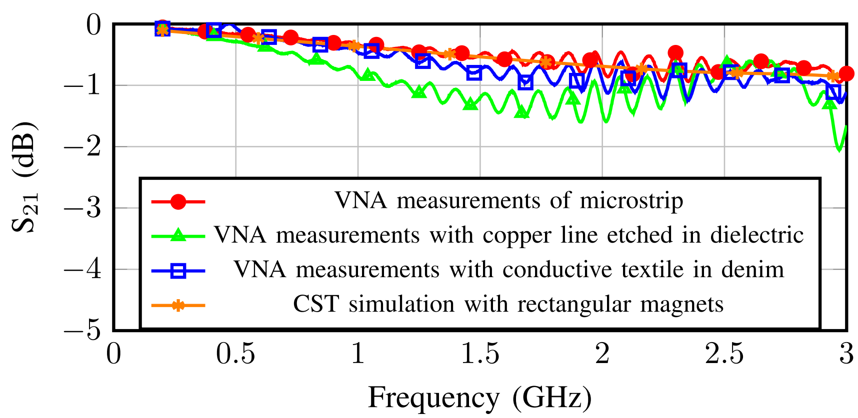


**Figure 3.12** $S_{12}$ results using rectangular magnets

step was to create a fully embroidered transmission line.

## 3.5 Full Textile Transition

Up to this point, the prototype that was being used was only a top conducting track of conductive thread sitting on top of a FR-4 board bridging the gap in a copper track. To measure a full textile microstrip new FR-4 boards were created.

To evaluate a transition between a rigid FR-4 microstrip and a fully textile one, a model was simulated using CST® MWS. The results, which will be presented later demonstrated good RF characteristics and a prototype was embroidered. To test the transition a copper microstrip was etched in a rigid FR-4 dielectric board. This board then had a $16 \times 25$mm square area cut from the central area of the board to accomodate the textile microstrip. Figure 3.13 presents the schematics of the rigid dielectric board, Figure 3.14 the textile microstrip and Figure 3.15 the assembled test jig.

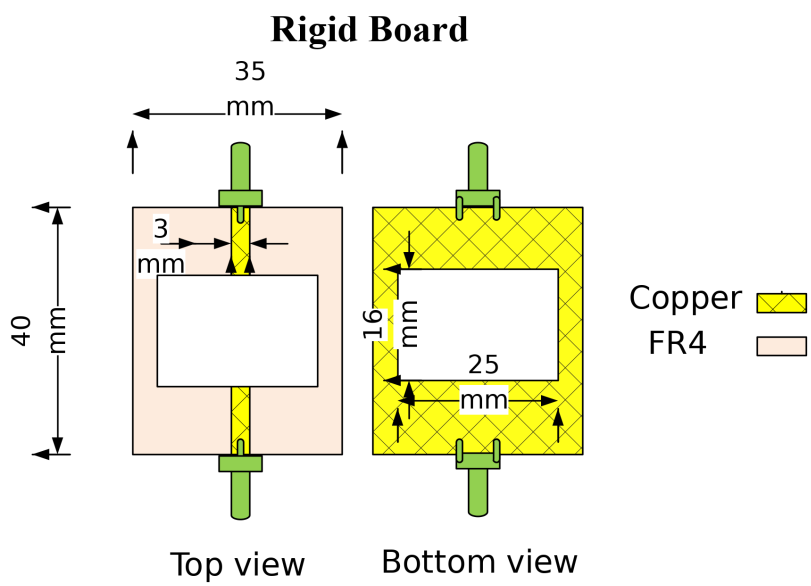


**Figure 3.13** Board prototype used in full textile transition jig

The conductive textile microstrip was embroidered on a top denim layer that was later attached to three extra layers of denim with the goal of having $1.6 \pm 0.1$mm thickness, roughly the same thickness as the FR-4 board. With the added thickness of the conductive line, the textile microstrip was found to be close to 2.6mm thick. As a ground plane for this textile microstrip the conductive textile fabric Nora-Dell [6] was used. The textile microstrip line is 5mm wide while the line etched on FR-4 is

3mm wide with a step transition between the two, both have been designed to have an impedance of 50Ω.

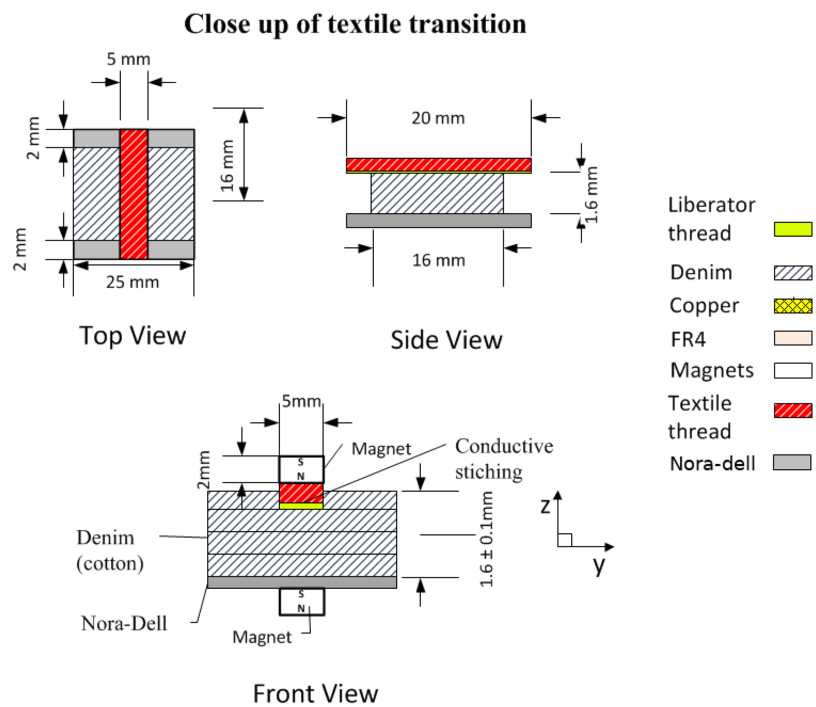


**Figure 3.14** Textile microstrip prototype used in full textile transition jig

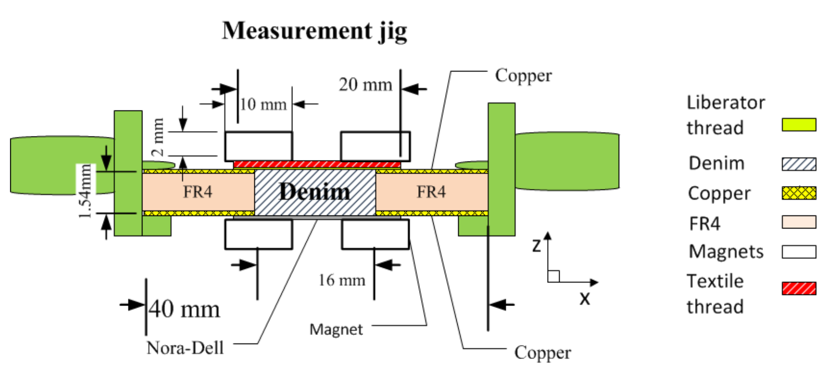


**Figure 3.15** Jig used in the measurements of the fully textile transition

The system was then connected to a Anritsu 37397D Vector Network Analyser via the SMA connectors on the FR-4 board with the textile microstrip bridging the gap. The magnets were tested in two configurations, transverse to the microstrip line and parallel to the microstrip line. The results presented next are the measurements done with the magnets in different configurations, with the FR-4 board without the textile microstrip covering the gap and the CST® simulation results. Measured results with the whole jig sitting on top of a human hand are also presented. The results are shown in 3.16 and 3.17 next to the measured results of the transition presented next.

In Figure 3.16 all of the measurements performed seem to have results that are similar to the CST simulation. The biggest difference is found at higher frequencies, this could be due to the electrical length of the simulated model being slightly different from the constructed prototype. The Reflection Coefficient has a maximum of −13 dB at 2GHz and an acceptable impedance match up to 3 GHz.

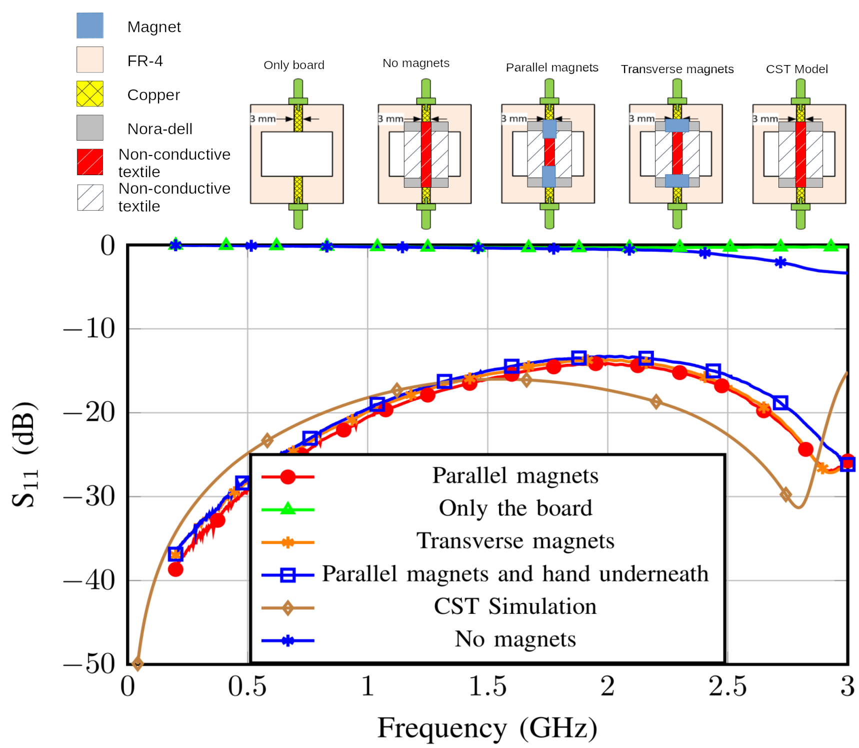


**Figure 3.16** $S_{11}$ results with different jig configurations

In Figure 3.17 the values for the measured $S_{21}$ vary from −0.1 dB at 0.2 GHz up to −0.9 dB at 3 GHz when the textile microstrip with the magnets is used. This demonstrates a good RF connection in the frequencies presented here. In both figures 3.16 and 3.17, the results with the jig sitting on top of a human hand do not have a noticeable difference when compared to the measurements when the hand was not present. This indicates that the body has a very small effect on the transition due to the ground plane.

The structure was also measured without the microstrip covering the gap and with the microstrip in place but without using the magnets. This was done to evaluate whether some power could be transmitted even without the textile bit and to check if the magnets are really necessary to apply contact force and establish a good RF connection. When the microstrip is not present the results for the insertion loss drop to around $-50$ dB which means that virtually no power is being transmitted when the textile microstrip is not used. When the textile bit is put in the gap but the magnets are not used, the insertion loss values are below $-13$ dB which translates to roughly 5% power transmitted. It can be said that in this jig, the magnets are essential to ensure good contact between the copper microstrip and the conductive thread.

The textile microstrip prototype demonstrates to be able to make a good RF connection at these frequencies. The orientation of the magnets seems to not have much effect on the final results. The prototype is also resilient to the effects of close proximity to the body, the results with the hand are very close to the rest of the measurements. It can also be said that the magnets are essential for the structure to have a good electrical connection. The next section covers measurements of an antenna when using a regular SMA connector and while using the textile interconnect.

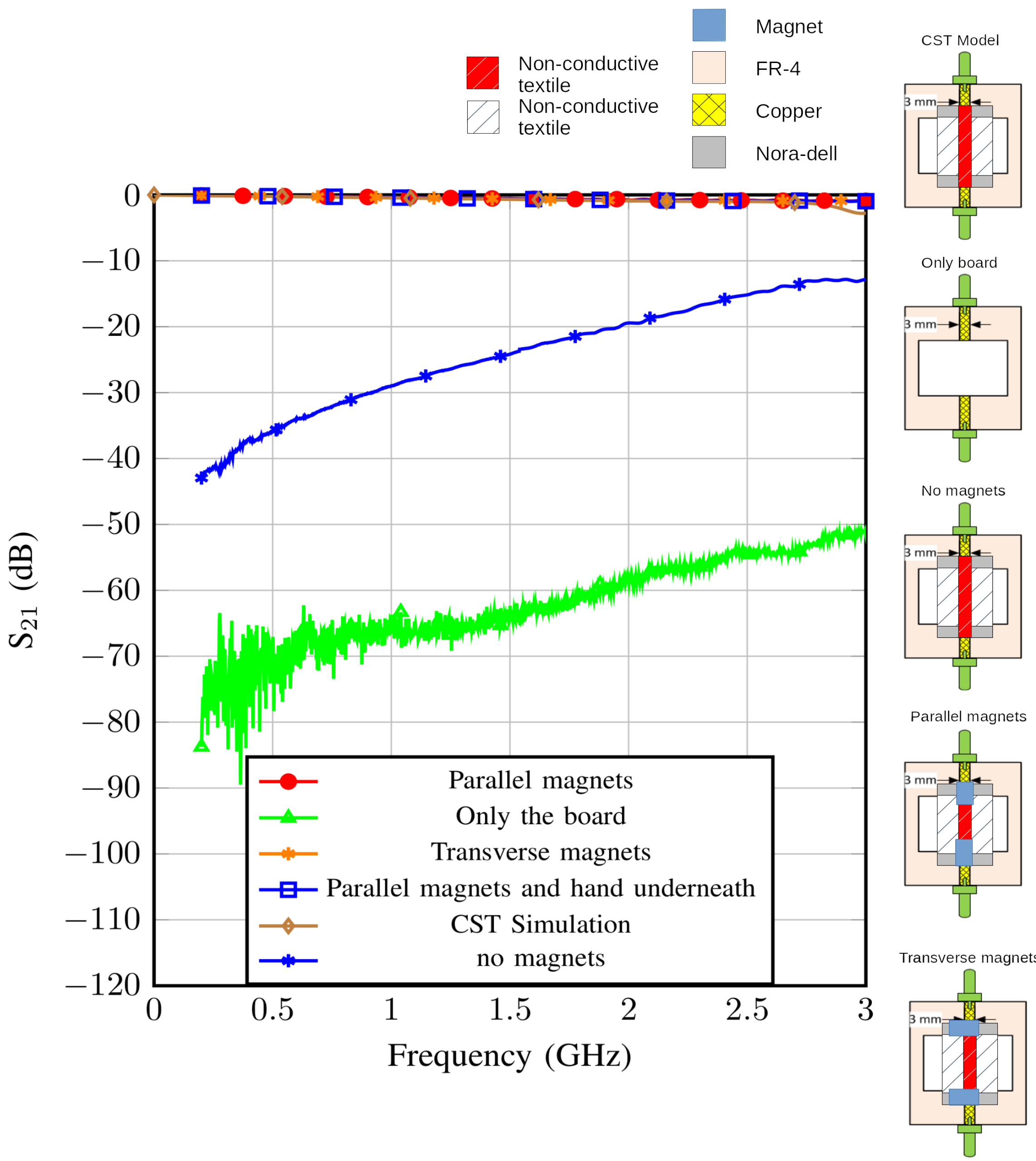


**Figure 3.17** $S_{21}$ results with different jig configurations

## 3.6 Testing with Textile Antenna and Repeatability Measurements

After the measurements with the fully textile transition, a textile antenna was connected to a VNA using the textile connector developed as shown in Figure 3.18. The connector differs from the previous one in that only one side of the textile is attached to a FR-4 part, using the other side to attach to the antenna. This antenna [7] is an inverted IFA, a comparison between the measurements with and SMA and the textile connector was done.

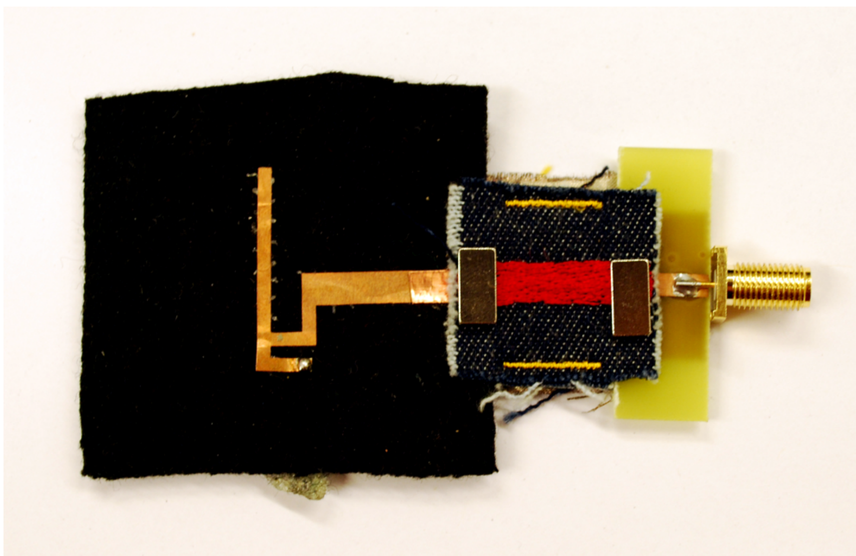

**Figure 3.18** Jig used when connecting the textile antenna to the VNA

In [7] the $S_{11}$ result for this textile antenna is $-30$ dB when using a rigid SMA. The results that were obtained on the measurement day had some difference, this could be due to some problems in the solder of the SMA to the textile antenna. The measured results are presented in Figure 3.19, it is shown that when using the textile connector the obtained value of $S_{11}$ was approximately $-30$ dB at the resonant frequency. The measurement shows that the textile connector does not change the resonance of the antenna but has slightly increased the bandwidth of the system. This could be due to the extra added length of the feeding line.

A repeatability measurement was done by attaching and removing the connection from the antenna ten times. In Fig. 3.20 the results of ten different measurements are presented. There are slight variations in the results but that is to be expected. The

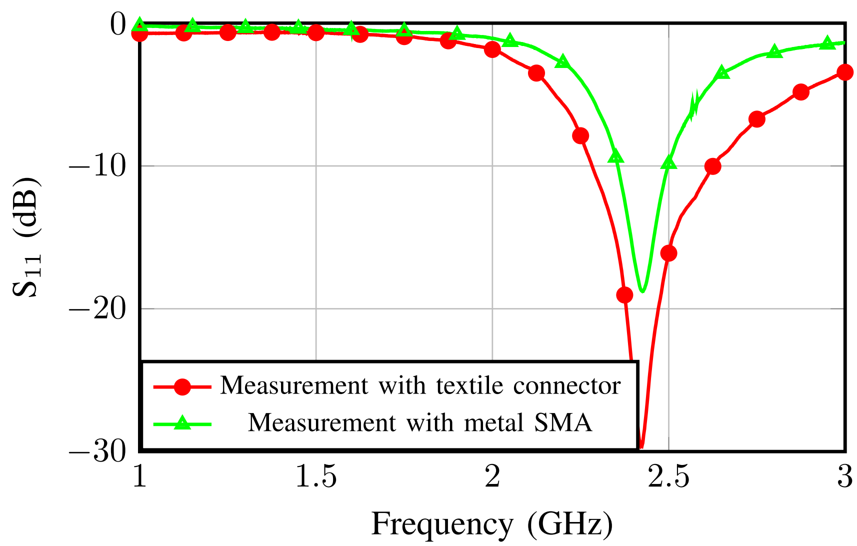


**Figure 3.19** $S_{11}$ results with SMA connector and using textile connector

biggest variation is $S_{11}$ of −17 dB in the first measurement and $S_{11}$ of −24 dB for the third measurement. This is due to small changes in the positions of the magnets or slight misalignments between the feeding microstrip lines.

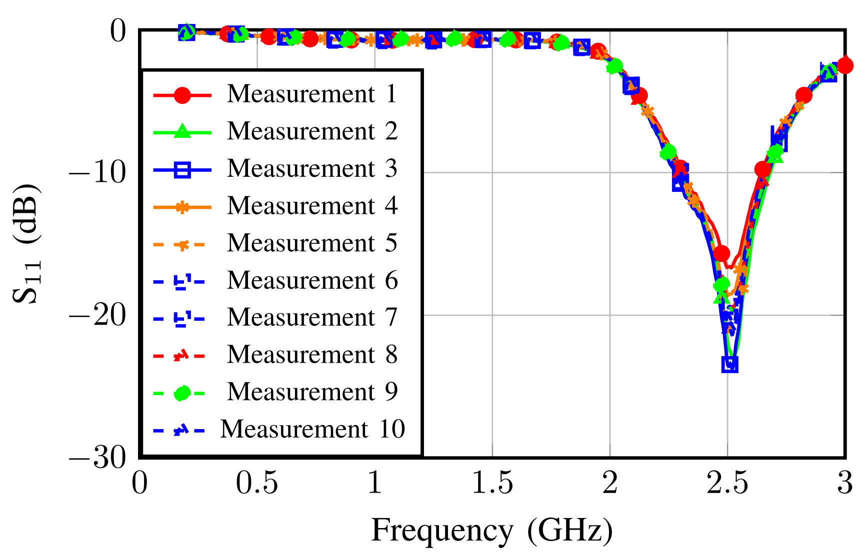


**Figure 3.20** $S_{11}$ results for ten different measurements

The interconnect was attached and roughly aligned with the antenna feeding line. As presented with the repeatability measurement, the interconnect shows resilience to errors related to the connection. There seems to be no detuning and only a slight change in the $S_{11}$ value for the resonant frequency. This is an important factor in a system that requires frequent attachment and removal of electronic components.

## 3.7 Textile Microstrip Characterization

### 3.7.1 Different Textile Lengths

As presented in the previous chapter 3.6, the textile microstrip had good results when measured on its own. It also did not seem to change the measured antenna $S_{11}$ results by too much, so the next course of action is to characterize the textile transition.

For the first step three new FR-4 boards were made, one with a short gap of 1.6cm, another with a long gap of 5cm and a microstrip board without gap. Two textile microstrips are also embroidered to cover these gaps in the rigid boards. Making two measurements with different lengths of textile microstrip, the effect of the textile on the transmission line could be obtained. The three boards can be seen in Fig.3.21, all of them have a length of 9 cm and the top conductor is 3 mm wide.

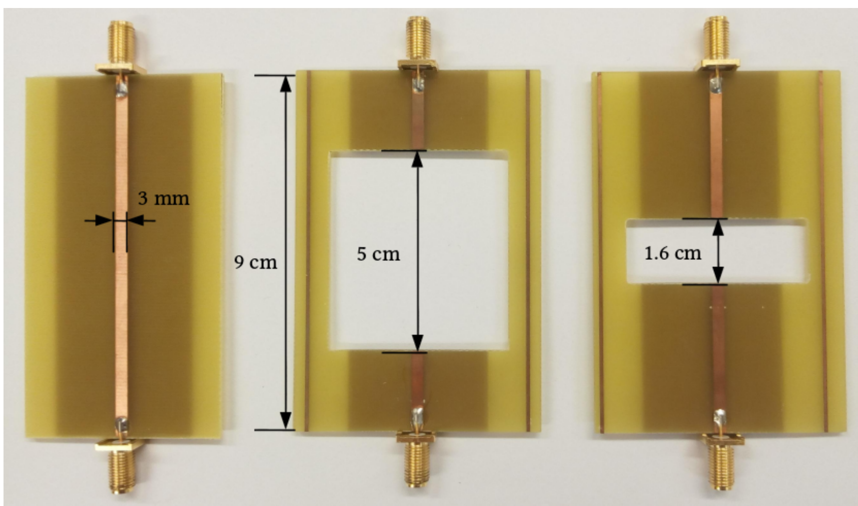


**Figure 3.21** Different sized FR-4 boards used to characterize textile connection

For the textile transmission lines to be held in place by magnets, they need to be longer than the gaps in the rigid dieletric. This is so that there's extra fabric above and below the gap for the magnets to hold in place. With this in mind, the textile transmission used to bridge the 5cm gap is 6.5cm long, and the textile line used on the 1.6cm line is 3cm long. Since denim is quite lossy, differences are to be expected between long and short textile lines with 6.5cm and 3 cm respectively. The results from this measurement are shown in Figs. 3.22 and 3.23. The measurement where the long textile microstrip is bridging the gap has much higher losses than when a short length is used. The biggest difference in $S_{21}$ is around 1.43 dB at 2.15 GHz between the short and long textile prototype. The drop in power can be due to some reflections due to material differences between denim and FR-4 and to denim's lossy properties. These reflection could be creating a standing wave in the textile part which is radiating. The length of the long textile microstrip is 65mm which is approximately $\lambda/2$ of 2.3GHz which coincides with the centre frequency at which our loss of transmitted power is highest.

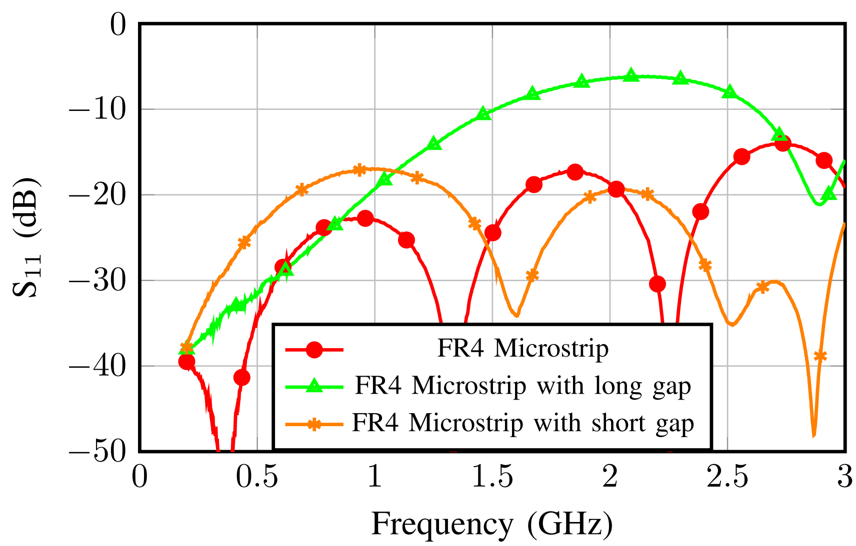


**Figure 3.22** $S_{11}$ results for the three different microstrips

With the results for the full FR-4 board with the two textile transitions, the effect of the textile microstrip was to be obtained. However, more important than the effect of a predetermined length of textile microstrip was the effect of the connection between textile and copper. With the prototypes presented here the effect of the difference in length of the textile microstrip could be observed. Despite this, in order to de-embed and measure the effect of the textile to copper connection new prototypes were created to use de-embedding theory. The new prototypes were required because each part of the system had to be measured individually, as will be explained later in the de-embedding chapter. The FR-4 board prototype was adapted for these new measurements, by using only the short length of FR-4 that connects the textile to the SMA connector. The textile microstrip has the same dimensions but two prototypes

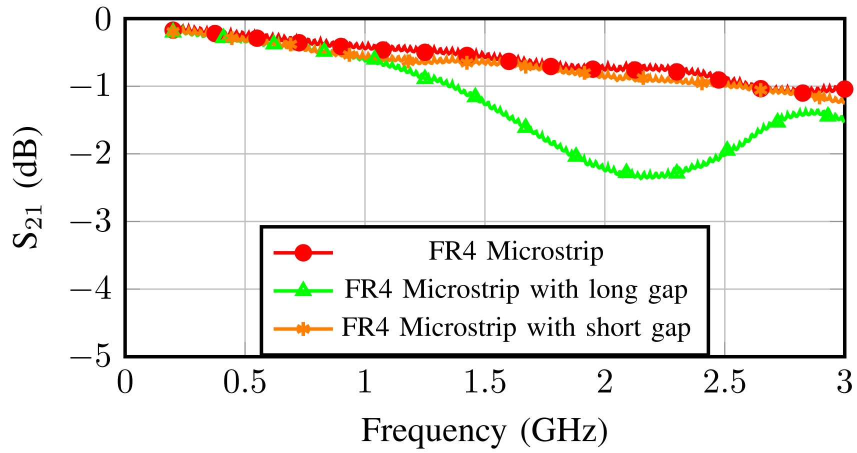


**Figure 3.23** $S_{11}$ results for the three different microstrips

are now embroidered as shown in Fig.3.24. One prototype will have SMA connectors soldered to both ends and the other prototype will have only one side soldered to a SMA. This second prototype is the one that will be used to connect to a VNA and have a full measurement of a textile to rigid dieletric transition.

The SMA adapters were first soldered to a Nora-Dell backed textile microstrip. The solder worked but it proved extremely difficult due to heat related problems. Nora-dell begins to deteriorate with the heat and copper tape was thought of to simplify the soldering procedure.

Two FR-4 microstrips were also created, Fig.3.25. The prototype on the left is used to connect to the textile microstrip with one SMA, to have a measurement of the full system shown in Fig3.26.

These prototypes were created to individually measure each part of the system, with the $ABCD$ parameters for each device de-embedding is possible as will be explained in the next chapter.

**Figure 3.24** Two prototypes of the embroidered microstrip. One with soldered SMA at end and the other with open an open end to attach to FR-4 adapter

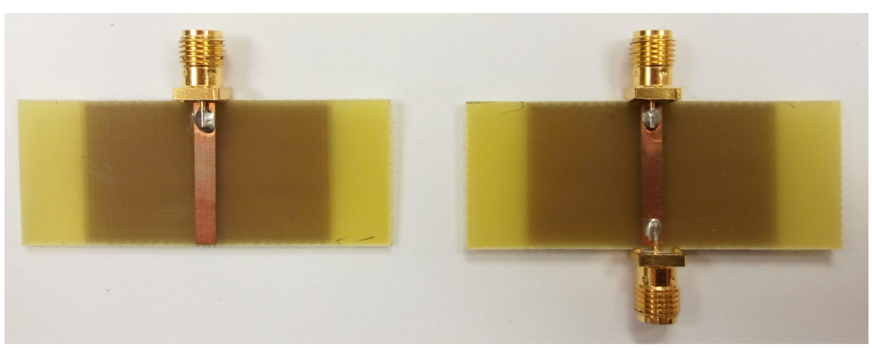

**Figure 3.25** FR-4 adapters used for de-embedding

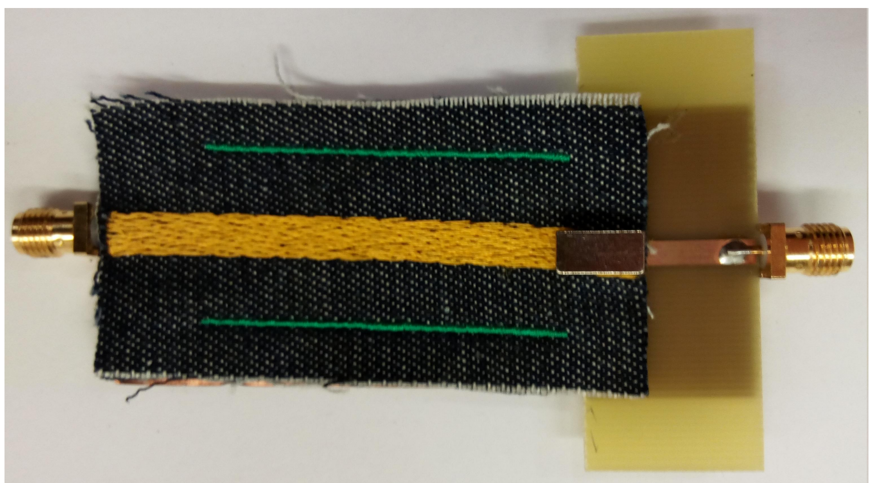

**Figure 3.26** Textile to FR-4 transition for the structure shown in Fig. 3.15

### 3.7.2 De-embedding theory

De-embedding is the act of removing some part of the system that is currently being measured for the results. There are various ways to characterize a microwave network, $Z, S$ and $Y$ parameters can be used for an arbitrary number of ports in a network. However, most microwave networks are composed of cascaded connections between two or more two-port networks [8]. For this type of network, $ABCD$ parameters were used to define an $ABCD$ matrix for each two-port network. In this case the $ABCD$ parameters were obtained from S parameters, the conversion table can be found on Table 4.2.

Complex devices can be modelled as two-port networks models as shown in Fig. 3.27, which are represented by four external variables: $V_1$, $I_1$ which are the voltage and current at the input port and $V_2$, $I_2$ voltage and current at the output port. Take into account that in Fig. 3.27 $I_2$ is the current flowing out of port 2. A two-port network can also be thought of as a black box, modelled by the relationships between the four variables $V_1$, $V_2$, $I_1$ and $I_2$.

port network.bb port network.bb

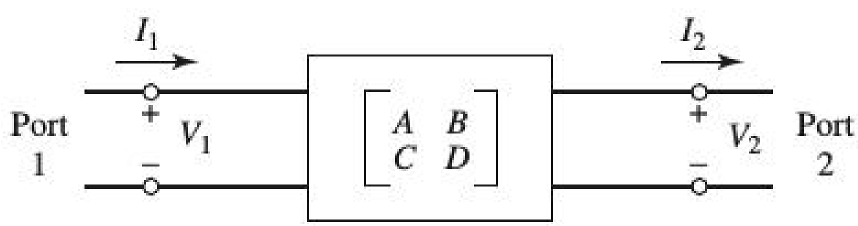


**Figure 3.27** A two-port network, from Pozar [8] et al.

The $ABCD$ matrix is defined in terms of voltages and currents as the following:

$$\begin{aligned} V_1 &= AV_2 + BI_2, \\ I_1 &= CV_2 + DI_2, \end{aligned} \tag{3.5}$$

Of when using the matrix form as:

$$\begin{bmatrix} V_1 \\ I_1 \end{bmatrix} = \begin{bmatrix} A & B \\ C & D \end{bmatrix} \begin{bmatrix} V_2 \\ I_2 \end{bmatrix} \tag{3.6}$$

Using $ABCD$ parameters is very useful because it simplifies the analyses of complex systems. Since each device can be modelled by a two-port network, a series of

| ABCD Parameters | S Parameters |
|---|---|
| A | $\frac{(1+S_{11})(1-S_{22})+S_{12}S_{21}}{2S_{21}}$ |
| B | $Z_0\frac{(1+S_{11})(1+S_{22})-S_{12}S_{21}}{2S_{21}}$ |
| C | $\frac{1}{Z_0}\frac{(1-S_{11})(1-S_{22})-S_{12}S_{21}}{2S_{21}}$ |
| D | $\frac{(1-S_{11})(1+S_{22})+S_{12}S_{21}}{2S_{21}}$ |

**Table 3.1** S parameter to *ABCD* parameter conversion table from Pozar et al. [8]

devices connected together can be modelled by a cascade of their individual two-port networks as shown in Fig. 3.28. In this case, the *ABCD* parameters of the combined network are obtained by matrix multiplication of each individual two-port network.

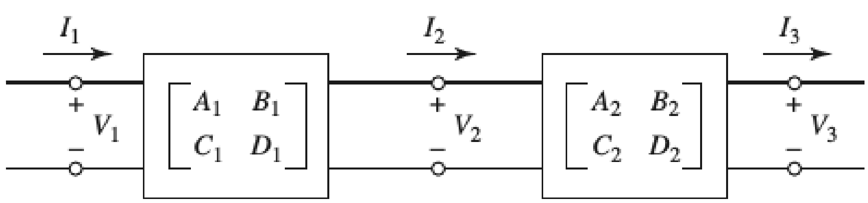


**Figure 3.28** A cascade connection of two-port networks, from Pozar [8] et al.

The cascade connection of the two networks in Fig. 3.28 can be represented in matrix form as:

$$\begin{bmatrix} V_1 \\ I_1 \end{bmatrix} = \begin{bmatrix} A_1 & B_1 \\ C_1 & D_1 \end{bmatrix} \begin{bmatrix} A_2 & B_2 \\ C_2 & D_2 \end{bmatrix} \begin{bmatrix} V_3 \\ I_3 \end{bmatrix} \tag{3.7}$$

This theory is used to de-embed individual parts of a system. By having the *ABCD* parameters of a device, using matrix multiplication theory the effect of the device on the network can be removed.

### 3.7.3 De-embedding and Results

To apply this theory to the prototypes presented in the previous chapter, each individual device was measured with a VNA to obtain its S parameters. From the S parameters, $ABCD$ parameters were obtained using Table. 4.2. These measurements provide us with the $ABCD$ matrices of each device on the system. When the microstrip with both SMAs from Fig. 3.24 was measured, its S parameters were obtained and then converted to ABCD parameters, obtaining the matrix in Eq. 4.1. The SMAs were de-embeded by moving the VNA's measurement plane forward, this is possible because the SMA connectors have well known parameters and can be easily de-embeded.

$$\begin{bmatrix} A & B \\ C & D \end{bmatrix}_{textile\_microstrip} \tag{3.8}$$

The reason that de-embedding is necessary is to obtain the effect of the transition from textile to copper. That transition is the small length where the conductive textile sits on top of the copper microstrip. In Fig. 3.29 this transition is the one directly under the magnet. This small length is considered as a device in the system, this is so that it can be modeled as a two-port network and extract its parametes with de-embedding theory.

To help visualise the cascade connection of the devices in our textile adapter shown in Fig 3.26, a composite figure has been created. The adapter is considered to have three devices, the textile microstrip, the textile to FR-4 connection and the FR-4 microstrip. Since the SMA connector effect has been removed by the measurement in the VNA, these are not accounted for. The cascade connection of these two-port networks can be shown mathematically as the multiplication of each two-port network $ABCD$ parameter matrix, as shown in equation 4.2.

$$\begin{aligned} \begin{bmatrix} A & B \\ C & D \end{bmatrix}_{adapter} = \begin{bmatrix} A & B \\ C & D \end{bmatrix}_{textile\_microstrip} \times \begin{bmatrix} A & B \\ C & D \end{bmatrix}_{textile\_connection} \\ \times \begin{bmatrix} A & B \\ C & D \end{bmatrix}_{fr4\_part} \end{aligned} \tag{3.9}$$

This brings us up to the composite figure, Fig.3.29. In this figure the labels of the devices have been superimposed on the prototype. The label 'adapter' is what has been designated as the $ABCD$ parameters of the whole system measurement, 'textile_microstrip' is the label that refers to the measurement of the textile microstrip, 'Fr4_part' is the label for the individual measurement of the FR-4 microstrip and 'textile_connection' is the label assigned to the two-port network that is the textile to copper transition.

To extract the parameters for the textile to copper transition, Equation 4.3 will be rearranged into:

$$\begin{bmatrix} A & B \\ C & D \end{bmatrix}_{textile\_connection} = \begin{bmatrix} A & B \\ C & D \end{bmatrix}^{-1}_{textile\_microstrip} \times \begin{bmatrix} A & B \\ C & D \end{bmatrix}_{adapter} \times \begin{bmatrix} A & B \\ C & D \end{bmatrix}^{-1}_{fr4\_part} \tag{3.10}$$

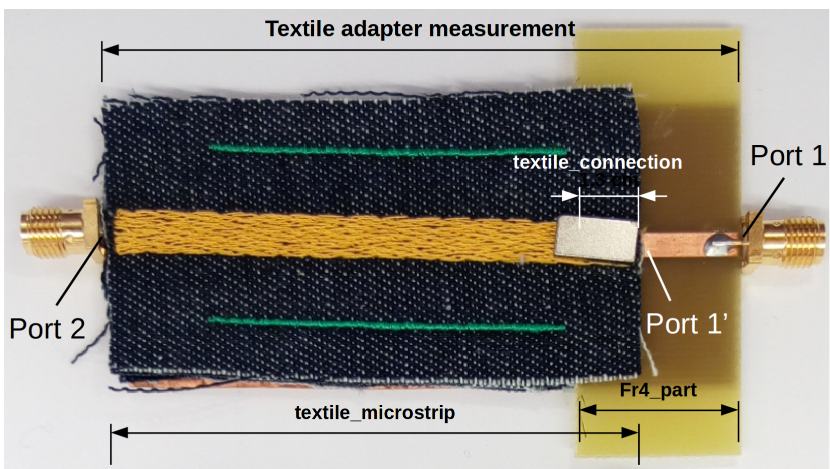


**Figure 3.29** Textile to FR-4 transition with $ABCD$ parameters displayed for each device.

The individual measurements for the textile microstrip, FR-4 microstrip and adapter are presented in Figures 3.30a and 3.30b. The measurements of the textile microstrip and FR-4 microstip were made using prototypes with the same length, and the measurements were done between Port 1' and Port 2. For the textile adapter the measured system is slightly longer in length, the port was moved further out as it was measured from Port 1 to Port 2.

The results for the textile microstrip and copper microstrip are very similar, with $S_{21}$ results above $-1$ dB throught the frequency range as shown in Fig. 3.30b. The

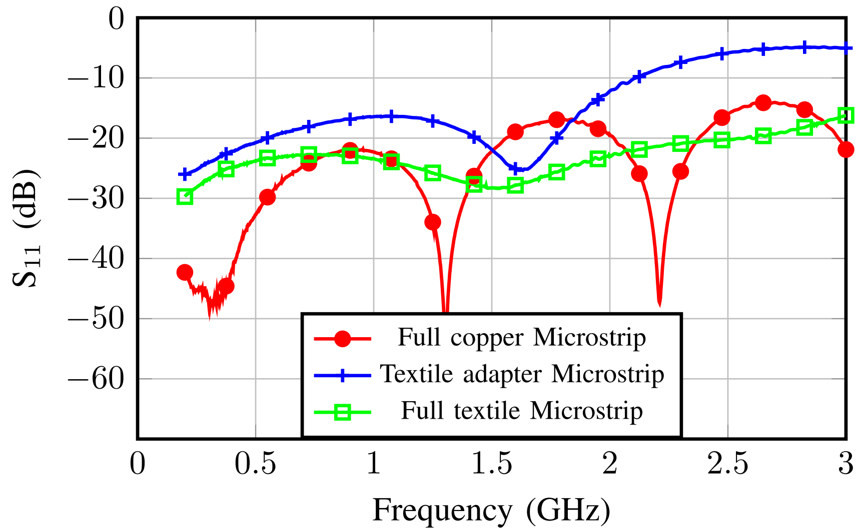


**Figure 3.30a** $S_{11}$ Comparison between FR-4 microstrip, textile microstrip and textile adapter

measurement with the adapter has a clear loss of power after 2 GHz down to −3 dB at 3 GHz. From the $S_{11}$ measurements the adapter model seems to have high losses at higher frequencies. In previous studies using a much shorter transmission line [9] this drop in power was not observed, even thought two textile to copper transitions were being used. This loss in power is most probably due to the sudden dielectric change from Denim $\epsilon_r \approx 1.8$ and FR-4 $\epsilon_r \approx 4.3$ which creates reflections. If comparing to [9] the difference can be attributed to the increased length of the lossy textile transmission line.

As for the de-embeded result of the textile to copper transition shown in Fig. 3.31 it has very good power transmission up to 2 GHz which then degrades to −2 dB at 3 GHz. It seems that this specific adapter is useable for frequencies up to 2 GHz without much deterioration of the signal. By doing the de-embeding it is also possible to insert the effects the transition has on another system, for example to connect a textile antenna. By cascading the two-port network parameters of the system with the two-port network parameters of an antenna, the effect of the connection can be predicted.

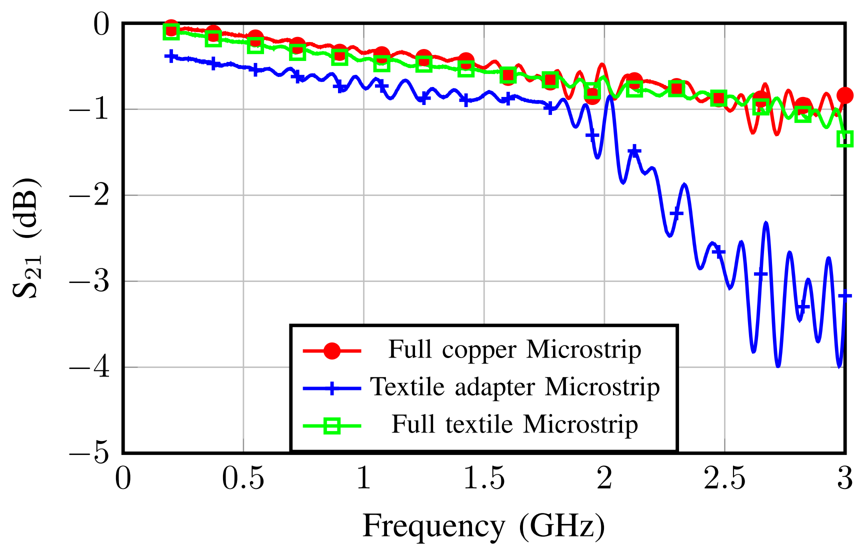


**Figure 3.30b** $S_{21}$ Comparison between FR-4 microstrip, textile microstrip and textile adapter

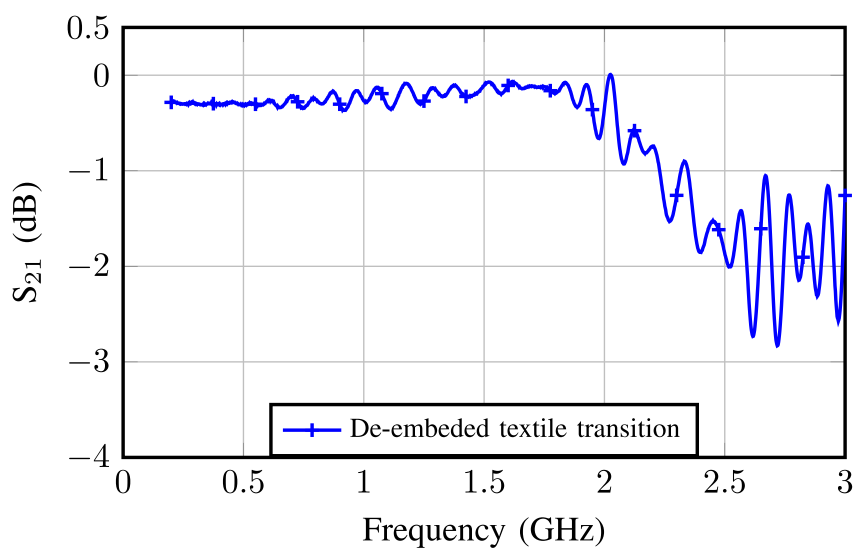


**Figure 3.31** $S_{21}$ values for the de-embeded textile connection

## 3.8 Conclusions

In this chapter the introduction of the textile connector was made. The early prototypes were a proof of concept to test out if the textile transition using magnets would work. The obtained results were promising and more work was done to create the full textile transition. It was apparent that the magnets could indeed be used to apply contact force on a textile-to-copper transition, and such magnets would not have a negative effect on the results. A measurement with a textile antenna was done and as the results revealed, the usage of the textile connector did not have a negative impact on $S_{11}$ measurements when using that specific antenna. This created the need to characterize the connector so that its effects could be predicted when used in a system with an antenna.

The longest part of this work was the characterization of the connector. By looking into de-embedding theory, it was found that it could be useful in characterizing this connector. As has been shown in the previous section, the connector was successfully characterized and the effect it has on a system can be inferred. However this is only valid for the specific connection in question. If one were to change the length of the textile transition, the results would most definitely be different. With a few different standard interconnects it could be possible to predict the effect these would have on other systems and use them in other research. Removable textile connects could benefit the wearable textile research area. When testing the effect of washing or environmental effects on textile systems, the interconnect can be removed and will not be affected by these tests.

# References

[1] "Characteristics of NdFeB Magnets,", http://www.ndfeb-info.com/characteristics.aspx, accessed: 21/11/2014.

[2] A. Tsolis, W. G. Whittow, A. A. Alexandridis, and J. C. Vardaxoglou, "Embroidery and related manufacturing techniques for wearable antennas: challenges and opportunities," Electronics **3,** 314–338 (2014).

[3] T. Acti, S. Zhang, A. Chauraya, W. Whittow, R. Seager, T. Dias, and Y. Vardaxoglou, "High performance flexible fabric electronics for megahertz frequency communications," In *2011 Loughborough Antennas Propagation Conference*, pp. 1–4 (2011).

[4] R. Seager, S. Zhang, A. Chauraya, W. Whittow, Y. Vardaxoglou, T. Acti, and T. Dias, "Effect of the fabrication parameters on the performance of embroidered antennas," IET Microwaves, Antennas Propagation **7,** 1174–1181 (2013).

[5] T. Acti, S. Zhang, A. Chauraya, W. Whittow, R. Seager, T. Dias, and Y. Vardaxoglou, "High performance flexible fabric electronics for megahertz frequency communications," In *Antennas and Propagation Conference (LAPC), 2011 Loughborough*, pp. 1–4 (2011).

[6] "Nora Dell-CR Conductive Metallized Nylon Fabric,", http://www.shieldextrading.net/pdfs/NoraDell%20CR.pdf, accessed: 21/11/2014.

[7] A. Paraskevopoulos, A. Alexandridis, T. Zervos, A. Michalopoulou, F. Lazarakis, and J. Vardaxoglou, "Modelling of dynamic on-body channels using different types of wearable antennas," In *Antennas and Propagation (EuCAP), 2014 8th European Conference on*, pp. 852–856 (2014).

[8] D. M. Pozar, *Microwave Engineering, 4th Edition* (Wiley Global Education, 2011).

[9] D. S. Fonseca, R. D. Seager, and J. A. Flint, "Textile-to-rigid microstrip transition using permanent magnets," Electronics Letters **51,** 709–710 (2015).

# Chapter 4

# Textile Grounded Co-planar Waveguide Characterization

## 4.1 Introduction

This chapter presents another type of textile to FR-4 transition, this time using Grounded Coplanar Waveguide, it is referenced in this chapter as CPW. The chapter begins with a short introduction on CPW and follow on to presenting the simulation of the CPW model. In section 4.3 the CPW model simulation model is presented, the software AWR Microwafe Office was used to simulate this model. Afterwards on section 4.4 the detailed embroidery process of the textile CPW prototype is shown. In section 4.5 the results of each individual part of the simulated model and measured prototype are presented and compared to one another. The last section 4.6 is similar to the section in the last chapter 3.7, where the characterization of each individual part of the system is characterized and de-embedded.

## 4.2 Coplanar Waveguides

Similar to microstrip transmission lines, coplanar waveguides can also be thought of as a flattened coaxial cable. It is different from microstrip because it has the ground plane on the same layer, the top layer has a central conductor and the ground plane on each side, which is the most common CPW design. Usually, CPW lines do not need a ground plane if the dielectric is thick enough for the majority of the EM fields to not leave the substrate. However, since this design is to be used in a wearable system, it can not be too thick so a Grounded CPW model is used. The main difference between classic CPW and grounded CPW is the use of a ground plane in the bottom layer of the CPW. In this case it will help shield the transmission line from the effects of close proximity to the body.

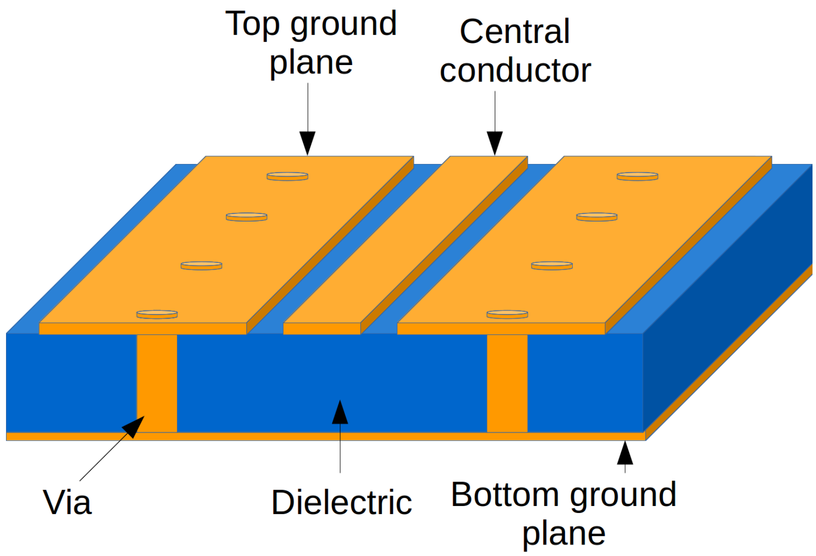


**Figure 4.1** Grounded coplanar waveguide, with via showing through dielectric

## 4.3 Simulated Model

A Grounded Co-Planar Waveguide was the second type of transmission line tested as a connection between textile and rigid circuitry. The design began by creating a model in AWR Microwave Office with the correct dimensions and the simulating it using AWR Analyst. Analyst is National Instruments AWR Design environment 3D EM solver [1]. It is a fast and accurate solver that can simulate more than one dielectric substrate in the same model. A tool that comes with AWR software called TXLine was used to obtain the correct physical dimension for a 50 Ω line. The FR-4 values used were $\epsilon_r = 4.3$ and loss tangent $\delta = 0.02$. For Denim the values were obtained from [2], $\epsilon_r = 1.8$ and tangent $\delta = 0.07$. With such a big difference in dielectric constants, the dimensions for a 50 Ω coplanar waveguide will be very different depending on dielectric. Consequently the short length of FR-4 is tapered, to make a smoother transition between FR-4 dielectric and Denim dielectric.

Due to the fabrication process, mainly the embroidery machine and conductive textile thread properties, some limits were imposed to the model. The gap G between the central conductor and side ground planes was set to 1 *mm*, it is very difficult to create a gap smaller than this when using Liberator 20, as the thread tends to fray and some strands of thread might bridge the gap creating a short circuit.

Figures 4.2 and 4.3 show the top and 3D view of the simulated model, the box around the design is the boundary used by the software. The model is composed of two parts, the left side with $L_2$ length is the FR4 adapter while the right side is the textile model.

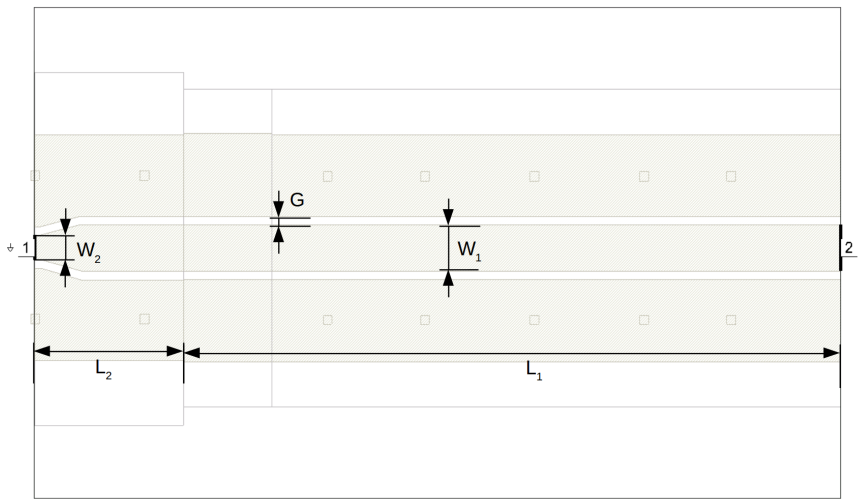


**Figure 4.2** Top view of CPW model in AWR Microwave Office

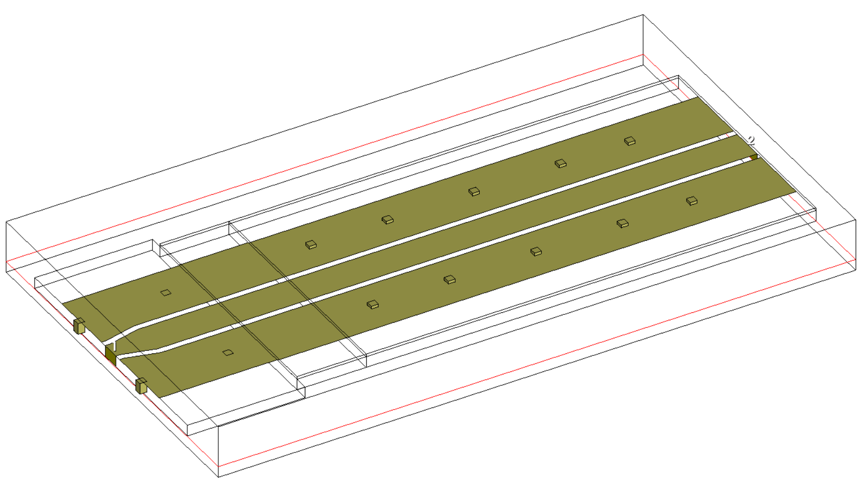

**Figure 4.3** 3D view of CPW model in AWR Microwave Office

In Table 4.1 the dimensions $W_1$ and $W_2$ are the different widths for the central conducting line on Denim and FR-4 respectively. The height between top ground plane and central conductor remains the same.

| CPW Dimensions | |
|---|---|
| G | 1 mm |
| $W_1$ | 5 mm |
| $W_2$ | 2.7 mm |
| H | 1.6 mm |
| $L_1$ | 65 mm |
| $L_2$ | 17 mm |

**Table 4.1** Dimensions of simulated CPW model

This design is harder to do in textile than the microstrip. If the distance between the bottom ground plane and the central conductor is smaller than gap between side ground planes and central conductor, the circuit behaves as a microstrip line and not a grounded coplanar waveguide [3]. In the end, the height H was set to 1.6 *mm* for two reasons. First it is the average thickness of the FR-4 dielectric that we have used previously, secondly it takes two layers of denim to get to approximately that thickness and any thicker than that makes the embroidery design very difficult.

The FR-4 part was tapered to accommodate for the textile part. The textile part has to be placed on top of the FR-4 board and if the dimensions of the textile and rigid board are not the same, there will be a short circuit from the textile central conductor touching the FR4 side ground planes

## 4.4 Construction and embroidery of prototype

The FR-4 adapter was constructed in the workshop and vias were soldered manually using copper wire. For the textile prototype, Liberator 20 thread was used both on the looper as well as the top thread to create the vias that connect the top ground planes with the bottom ground plane. For the top central conductor and side ground planes, Liberator was used on the looper with non-conductive thread as the top thread. For the ground plane on the textile prototype, Nora-dell was used.

The embroidered prototype was designed in Brothers PE Design Next software [4] and can be seen in Fig. 4.4. The model has been zoomed on so that the detail is easier to see.

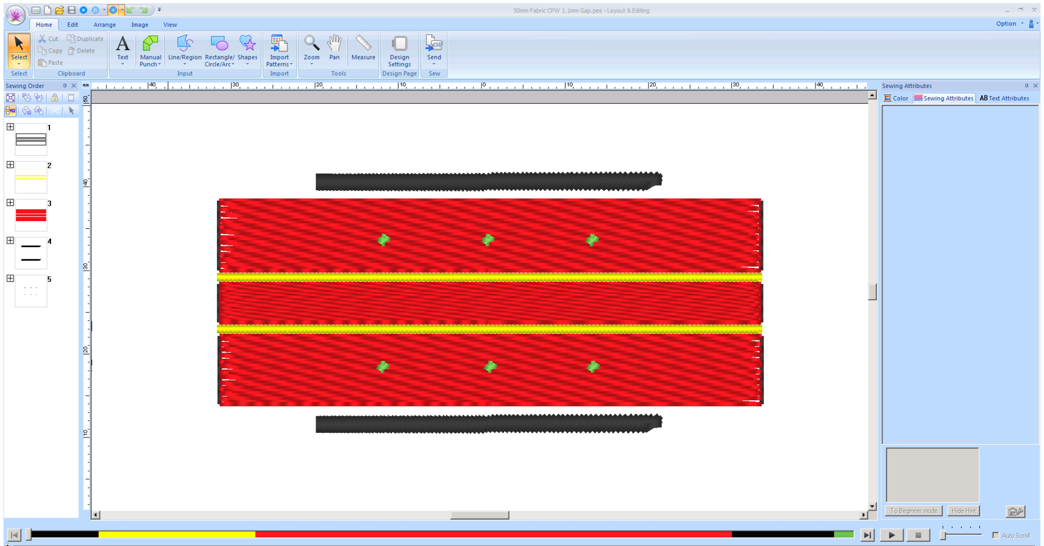

**Figure 4.4** Embroidered model in PE Design Next software

To overcome the problem of the conductive thread fraying, an extra line is embroidered. Instead of having a simple gap between the central conductor and side ground planes, the first thing that gets embroidered is a non-conductive thread to fill the 1 *mm* wide gap as shown in Fig. 4.5. After this, the looper thread is changed with Liberator 20 and the central conductor is embroidered, Fig. 4.6. When the central conductor is embroidered, the prototype must be removed from the embroidery machine to trim any fraying strands of conductive thread. If this is not done before embroidering the side ground planes, strands of thread will bridge the gap and create a short circuit. The next step is to embroider both side ground planes and verify again that no threads are connecting the central conductor with side planes, Fig. 4.7. The easiest way to do this, is to use a multimeter and check whether there is a connection over the gap.

All of this is embroidered on the top layer of denim, while the whole prototype uses two or three layers of denim, depending on the fabric thickness, to have the desired height. To continue the fabrication process an extra layer of Denim is needed as well as the bottom layer of Nora-dell. To prevent wasting expensive material such as Nora-dell, only a small portion of it is cut into shape and attached to the bottom of the lower Denim layer. It can be held there by some strong tape but the best way to attach it temporarily is to use staples. The staples will make sure that the Nora-dell will stay in place until it gets secured by the embroidery process, this can be seen in

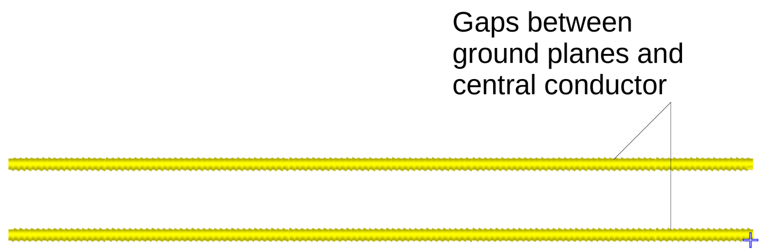


**Figure 4.5** First step of embroidery process

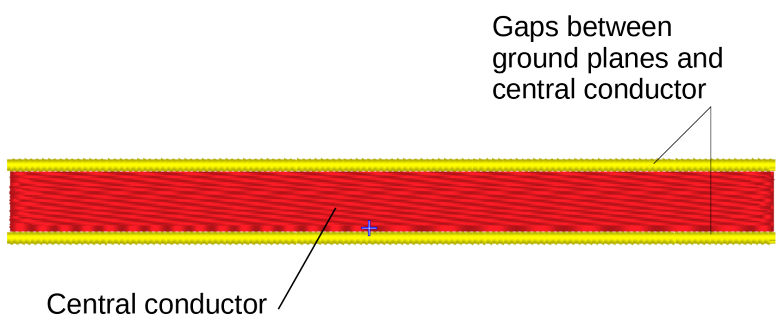


**Figure 4.6** Second step of embroidery process

Fig. 4.8.

The last two steps are to embroider the textile vias, shown in green in Fig. 4.9 and two lines of non-conductive thread to secure everything together shown in black in the same Figure. The embroidered prototype is shown in Fig. 4.10, here the coaxial cables were soldered to the textile line to measure it on the VNA.

An exploded view of the prototype is presented in Fig. 4.11. As is shown, the conductive thread stays between the top layer of Denim and the bottom layer. The conductive vias connect the top and bottom ground planes.

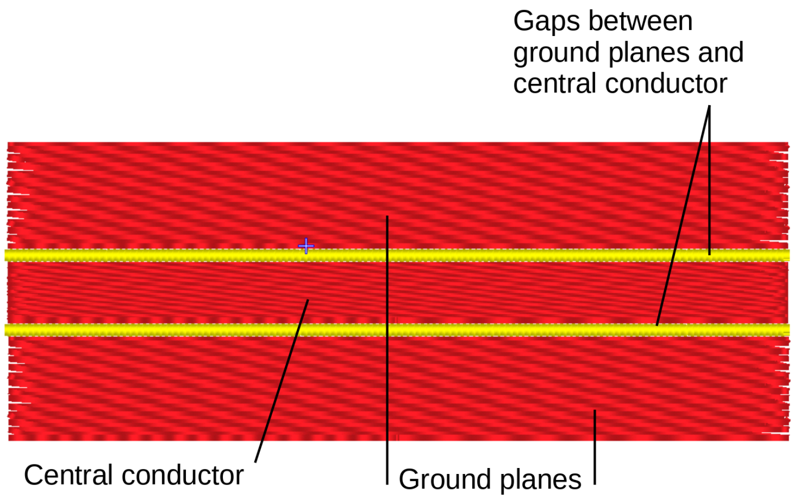


**Figure 4.7** Third step of embroidery process

**Figure 4.8** Staples temporarily holding Nora-Dell until it gets secured by the embroidery

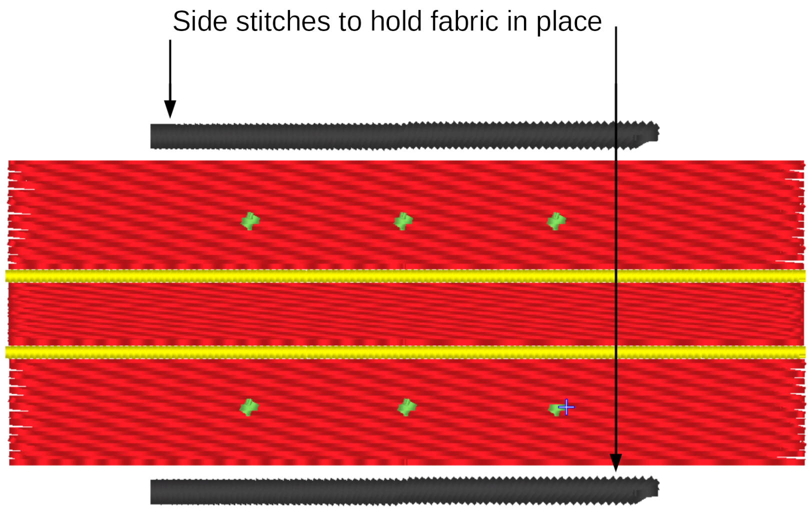


**Figure 4.9** Final step of embroidery process

**Figure 4.10** CPW embroidered prototype with coaxial SMA for measurement

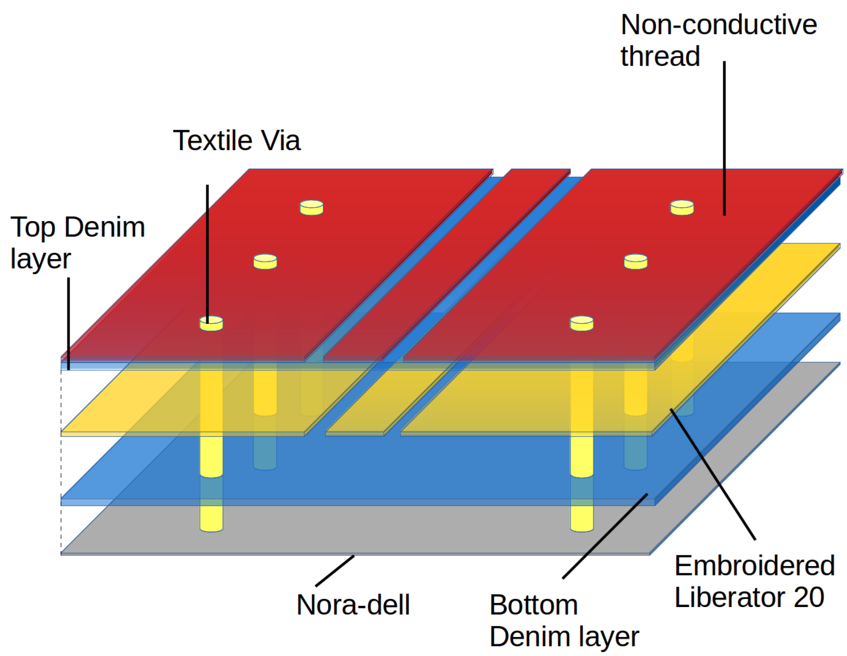


**Figure 4.11** Exploded view of the textile CPW prototype

## 4.5 Measurement and Simulation Results

In this section the results of simulations and measurements will be presented. The prototype was measured using an Anritsu 37397D VNA. The calibration setup used the calibration kit Agilent 85033D and was calibrated for the frequency range of 0.2 to 3 GHz. When measured on the VNA, the measurement plane was moved forward as to remove the effect of the coaxial SMA connectors.

Each individual part of the system was measured as well as the complete system. This follows the same logic used in the previous chapter 3 and the results will be used for the de-embedding procedure. The simulated results will be compared with the measurements. Some differences are expected in the textile line due to the nature of the embroidery. For the FR-4 board very similar results are expected because the prototype can be accurately created.

The textile CPW is the device on the system that bridges the connection from textile to FR-4, as such it has been designed on textile as a 50Ω grounded co-planar waveguide. Due to the different materials used, Denim and FR-4, the physical dimensions for a 50Ω transmission line will vary. The connection between textile and FR-4 will have a smooth transition to minimize the reflections. This transition was made on the FR-4 part of the system since it is easier to create than on the textile side.

Some problems were encountered when de-embedding the textile connection. These problems were related to parallel-plate modes on the side ground planes [5] and will be explained in the next sections. The prototypes had to be re-made and a comparison of the results is presented in the following sub-sections.

### 4.5.1 CPW Textile line results

A top view of the model simulated in Microwave Office is shown in Fig. 4.12. In Figures 4.13 and 4.14, S parameter results for the textile CPW are presented, with simulation and measured results shown together.

There are differences in the results for the textile CPW line when comparing the measurement with the simulations. At lower frequencies the simulated model seems to have higher reflections than the measurement of the embroidered prototype. This could be due to material and model differences. Since Denim has a wide range of thicknesses and densities, the value of $\epsilon_r = 1.8$ is an approximation. When looking at the $S_{21}$ results in Fig. 4.14 there is also a small difference. In the prototype measured

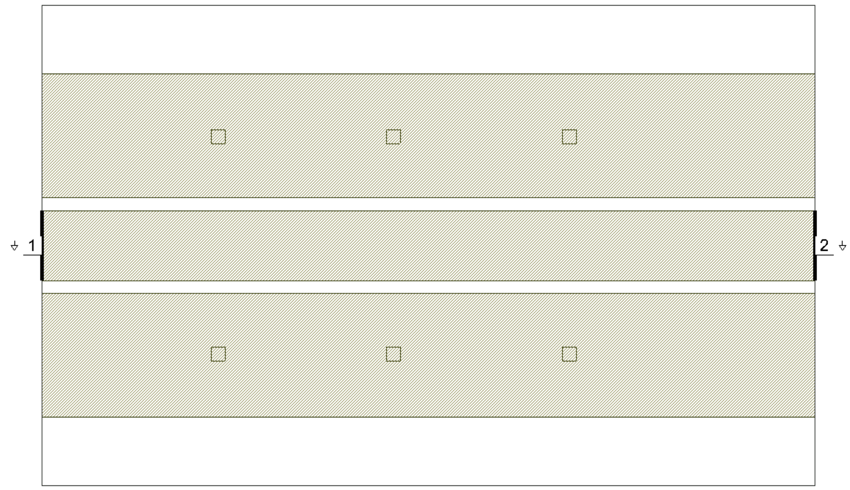


**Figure 4.12** Top view of Simulated textile model

with the VNA, there is a higher transfer of power when compared with the simulated model. But the change in power transfer related to frequency seems to follow the same pattern.

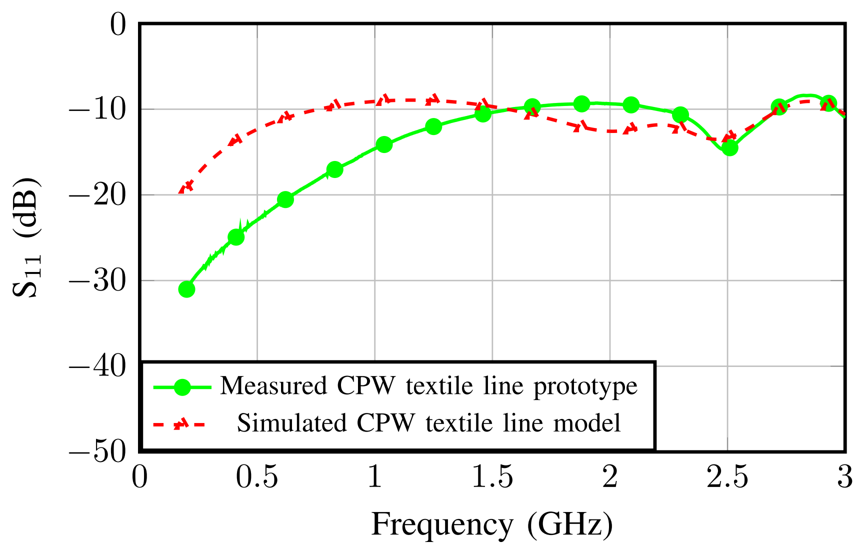


**Figure 4.13** $S_{11}$ results for simulated and measured textile CPW

The drop in transmitted power after 2 GHz is problematic and after some work, a new simulation model was built to check whether this drop in power was connected to the parallel-plate modes on the side planes as referenced earlier. According to [5], ground planes of grounded coplanar waveguides can behave like overmoded patch

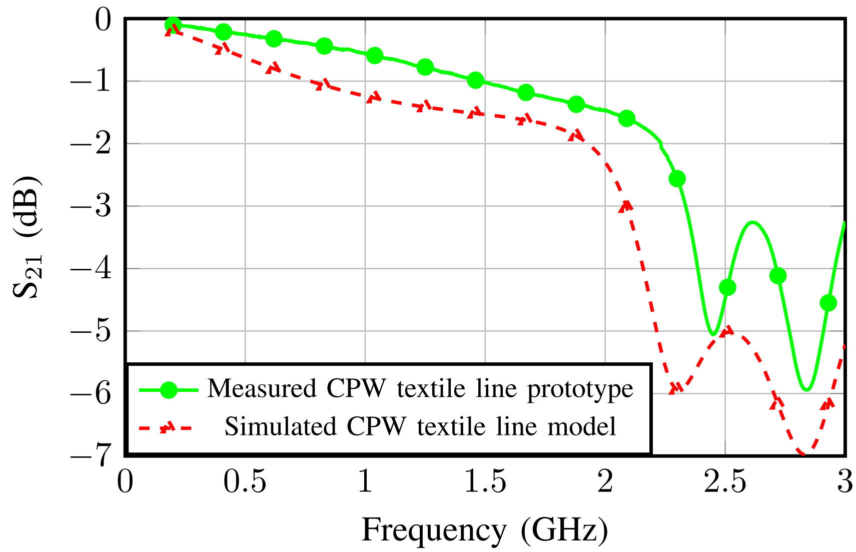


**Figure 4.14** $S_{21}$ results for simulated and measured textile CPW

antennas that support parallel-plate modes and resonate. These parallel-plate modes are excited at the gap of the CPW line, so in order to supress them this is where extra vias had to go. The new model was simulated in Microwave Office with extra vias added on the sides. The new model is shown in Fig. 4.15. The simulations results indicate that the extra vias work in eliminating the drop in power. So a new textile prototype was also embroidered and measured. The new measurement results can be seen in Figs. 4.17 and 4.16.

The drop in transmitted power that was present in the previous figure is no longer present. This shows that there was a problem with the ground planes in the model. By adding the extra vias, these modes were suppressed and the resonaces eliminated. The effect of eliminating these resonances is presented in more detail in the next chapter, where three iterations of vias are added and the results presented.

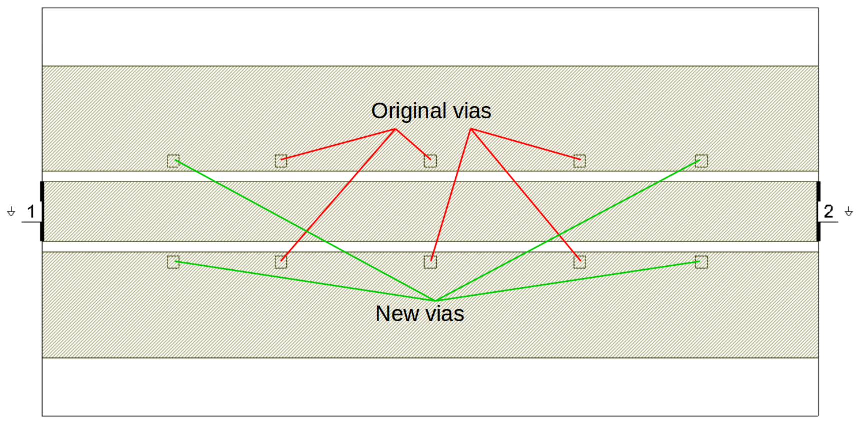


**Figure 4.15** Top view of Simulated textile model with increased number of vias

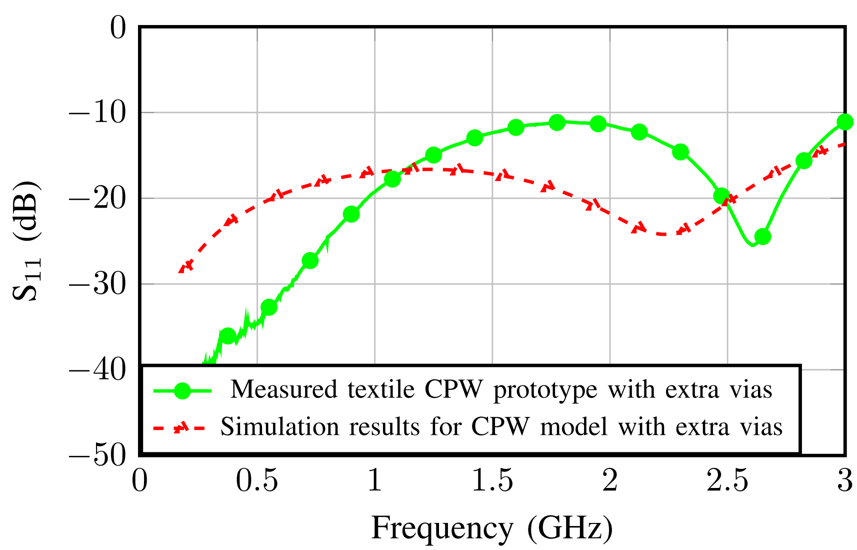


**Figure 4.16** $S_{11}$ results for the textile CPW model with more vias

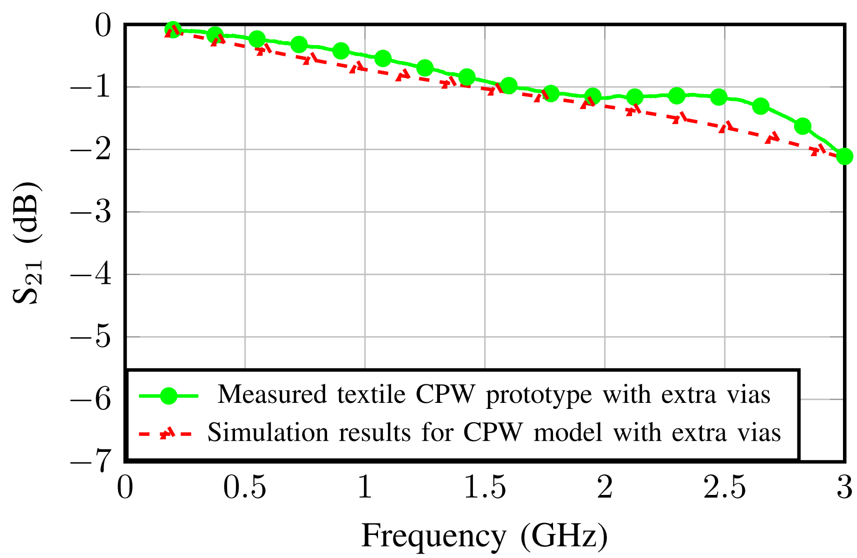


**Figure 4.17** $S_{21}$ results for the textile CPW model with more vias

### 4.5.2 FR-4 board results

When looking at the FR-4 results, Figures 4.19 and 4.20, the results for simulation and measurement seem to be very similar. This is due to the fact that the dimensions of the measured and simulated model are very accurate due to the construction procedure, the value for $\epsilon_r = 4.3$ also does not vary so much with the material. A top view of the model is shown in Fig. 4.18.

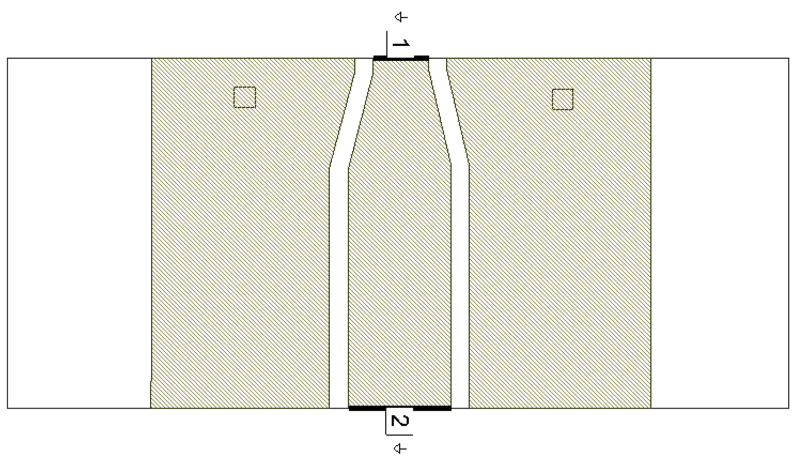


**Figure 4.18** Top view of Simulated FR-4 part model

The drop in power in Fig. 4.20 has a small shift in frequency. Since the facilities at our lab do not have automated via construction, the holes had to be drilled manually as well as the vias had to be soldered manually. After changing the location of the vias in the simulation, the frequency which has the drop in power would also shift. The frequency shift could come from slight differences on via location on the fabricated prototype.

When looking at the results in Fig. 4.21 the results for $S_{11}$ and $S_{22}$ are different. At 2 GHz the value of $S_{22}$ increases which indicates that there are reflections coming back to port 2. On the other hand, the value for $S_{11}$ decreases which seems do indicate that from port 1 there are less reflections at 2 GHz. However, the results for $S_{12}$ and $S_{21}$ are the same, with loss of transmitted power at 2 GHz.

After some extra research in the literature it was found that what could be happening was due to the side ground planes in our design. As presented in [5] the ground planes in conductor backed CPW can behave as over-moded patch antennas, supporting parallel-plate modes and resonate. This can explain the loss in power shown in Figs. 4.20 and 4.22.

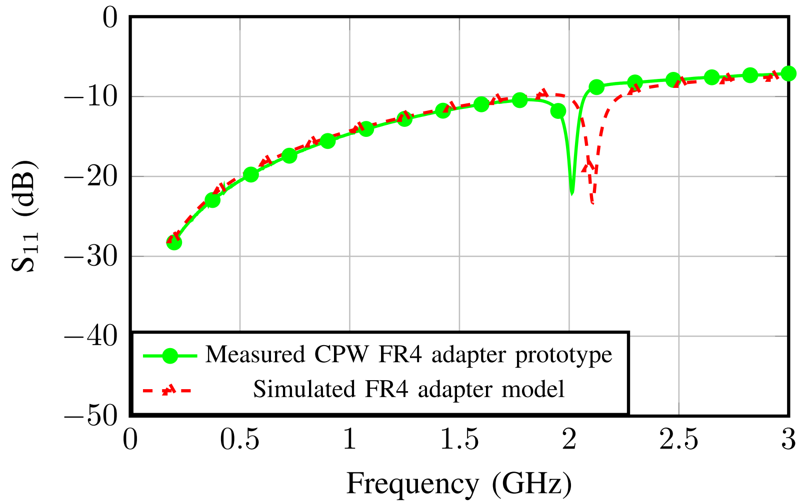


**Figure 4.19** $S_{11}$ results for simulated and measured FR-4 CPW part

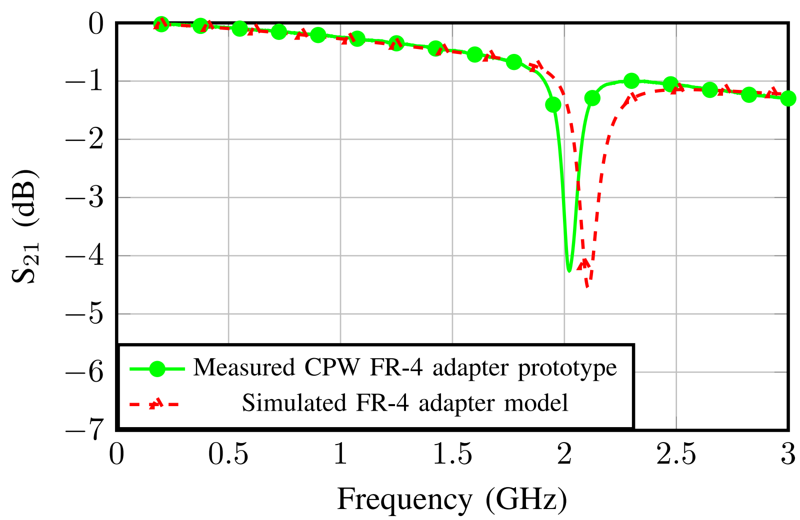


**Figure 4.20** $S_{21}$ results for simulated and measured FR-4 CPW part

To try to remove this resonance from the results, new simulations were made with different locations for the vias as well as extra added vias. Three iterations of the model with different via locations were simulated. For the first iteration the original vias are moved 2 mm on the $x$ axis Fig. 4.23. On the second iteration the original vias stay in the same location and a new set of vias is added Fig. 4.24, these new vias are 4 mm away from the original vias. The third iteration is similar to the second iteration, using two sets of vias but the second set of vias is 6 mm away from the original vias Fig. 4.25.

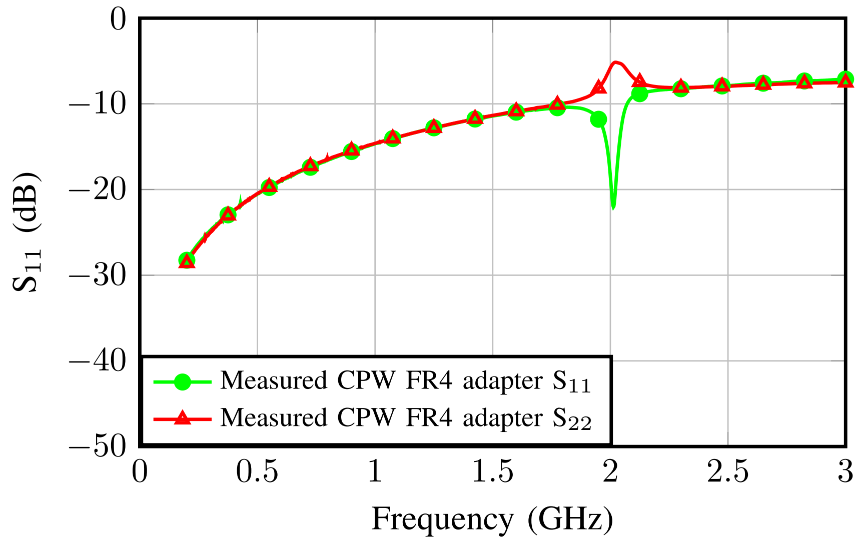


**Figure 4.21** $S_{11}$ and $S_{22}$ results of FR-4 board

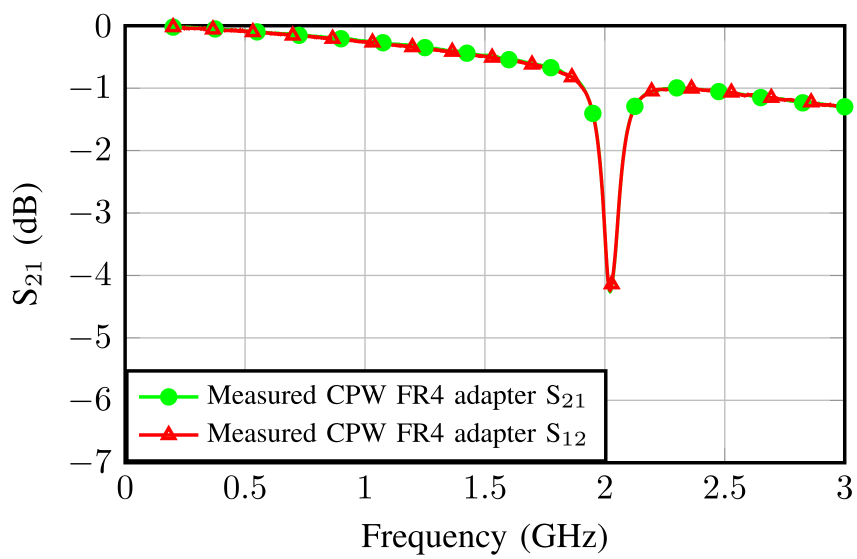


**Figure 4.22** $S_{21}$ and $S_{12}$ results of FR-4 board

The results of these simulations can be seen in Figures 4.26 and 4.27. It seems that as the extra via is added, the resonance shifts in frequency. When the extra via is moved further away, in the third iteration, the resonance is outside the desired frequency range of 3 GHz. According to [5] if the vias are not near the gap between conductor and ground plane, the substrate modes are not fully suppressed but only shift the resonant frequencies of the ground planes. This can be why there are still high reflections at higher frequencies, as the vias could be closer to the gap.

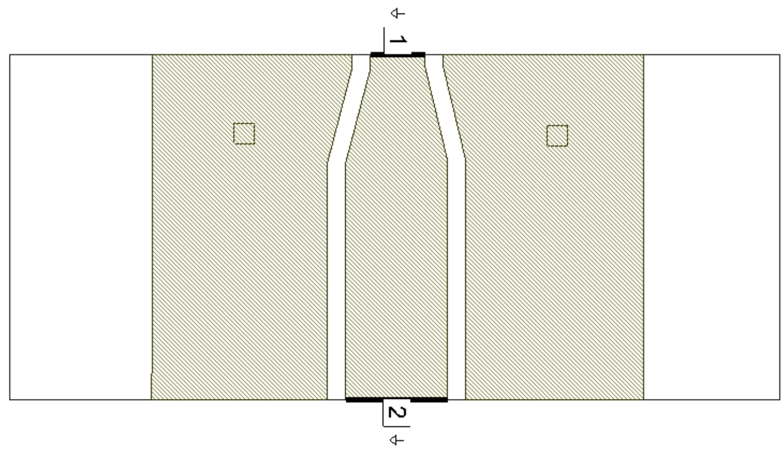


**Figure 4.23** First iteration of vias on the FR-4 board

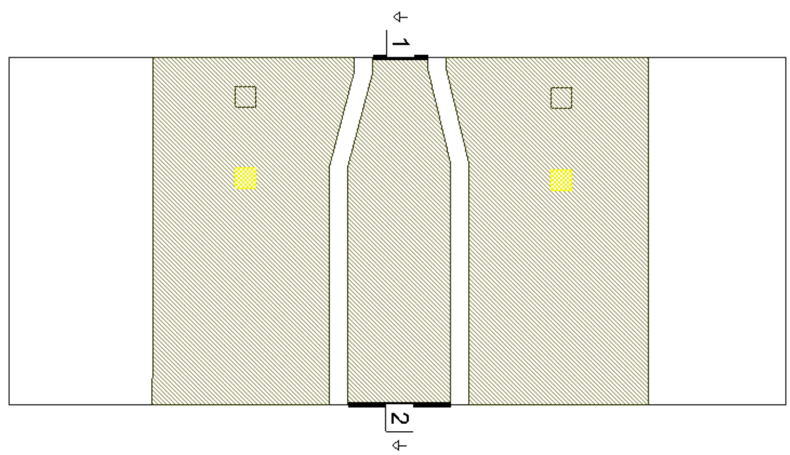


**Figure 4.24** Second iteration of vias on the FR-4 board

By adding extra vias the resonances were removed for the desired frequencies. These resonances on the individual parts of the system were creating problems when all the parts of the system were measured together. By joining the short FR-4 CPW adapters and the textile line, the lengths of the ground plane changed. This meant that the resonances would shift in frequency due to different electrical length of the radiating ground planes. This will be explained further in the following chapter.

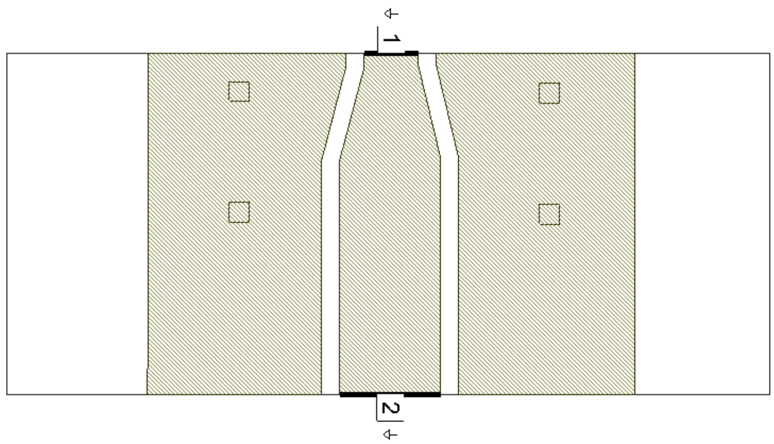


**Figure 4.25** Third iteration of vias on the FR-4 board

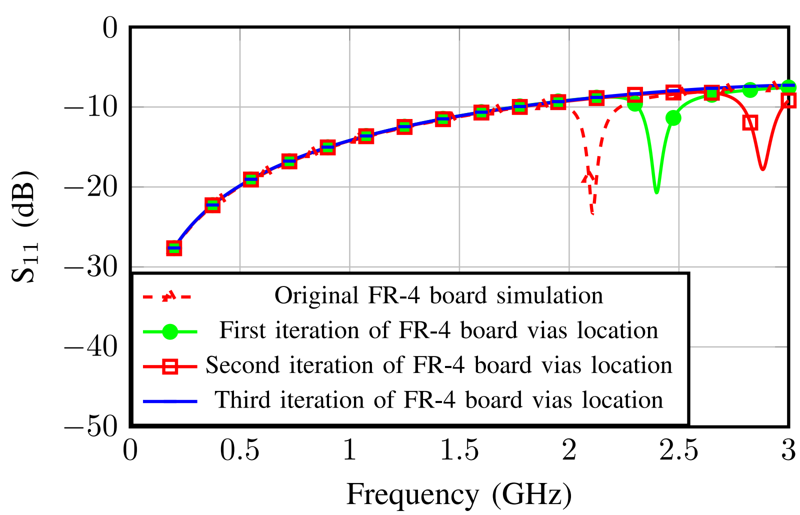


**Figure 4.26** $S_{11}$ results for simulated models of the FR-4 board with different via configuration

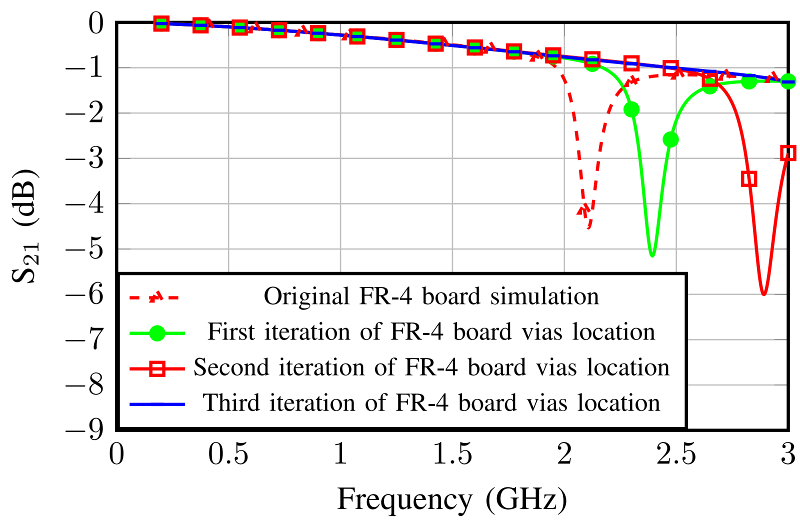


**Figure 4.27** $S_{21}$ results for simulated models of the FR-4 board with different via configuration

### 4.5.3 Full CPW adapter system results

In this subsection the results for the entire system are presented. Following the previous section's organization, results of the simulated model will be compared with measurements performed in the lab. Both models are shown, in Fig. 4.28 the prototype that was fabricated is presented and in Fig. 4.29 the simulated model is also presented. There are some differences between simulated and build prototype where the textile part connects to the FR-4. In the simulation it was not possible to model the overlap of the textile over the rigid board. When simulating the whole system, the textile CPW line is adjacent and connected to the rigid board instead of overlapping it. Due to this, the total length of the whole simulated system is slightly longer than the measured prototype.

In Figures 4.30 and 4.31 the results for the whole system are presented. This is the complete measurement of the CPW FR-4 part attached to the textile CPW. The results of the simulated system are slightly different than the real measurements. This difference is evident in Fig. 4.31, as the drop of transmitted power at 2.5 GHz is much smaller in the simulation. As was explained before, the simulated model is slightly different from the constructed prototype. On the constructed prototype, when measuring the whole system, the top and bottom layers of the textile CPW go above and below the rigid FR-4 board. On the simulations the two parts of the system are simply connected side-by-side.

**Figure 4.28** Test structure of the full system, with embroidered and FR-4 parts attached by magnets

The loss in power in the $S_{21}$ plot, Fig. 4.31, is also partly due to unwanted modes in the side ground planes as well as what looks like poor impedance match. These

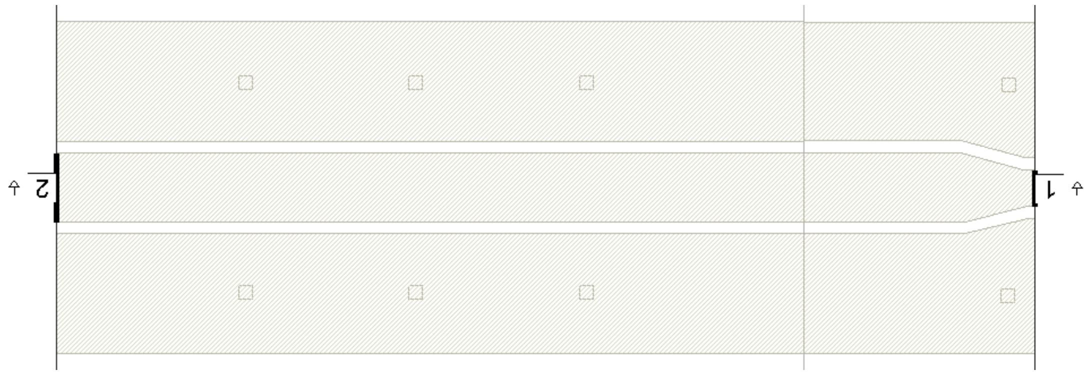


**Figure 4.29** Model of the simulated full system

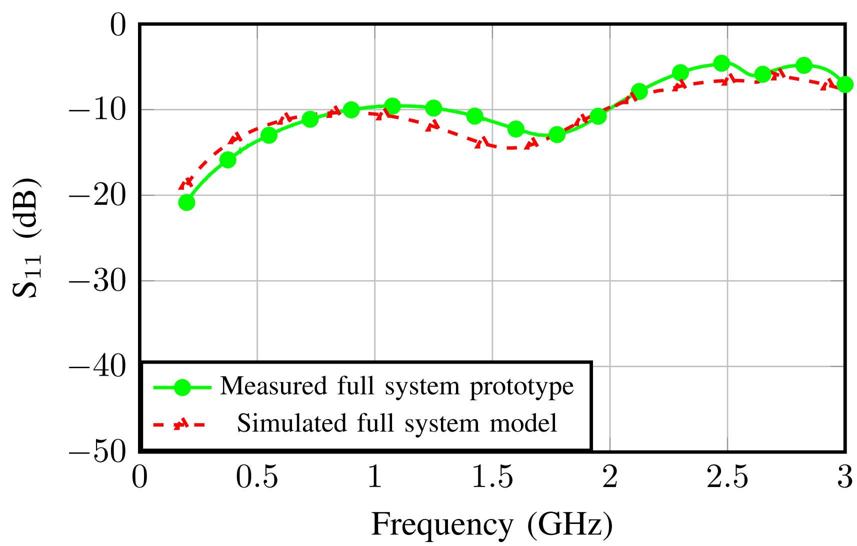


**Figure 4.30** $S_{11}$ results for simulated and measured CPW adapter system

whole system measurements were performed before the new models with extra vias were created. When using the new models presented in the previous sections, the drop is power caused the the parallel-plate modes is less accentuated. Comparisons between simulation and measured results will also be presented.

When each device of the system was measured individually, the extra added vias removed the unwanted modes. However, it seems that when all the devices are measured in the full system some loss in power is still present. Figures 4.32 and 4.33 show a comparison between simulated and measured results when using the models with extra vias.

This drop in power must be due to the design itself, the switch from textile and FR-4 and its associated impedance mismatch. There is a big difference between

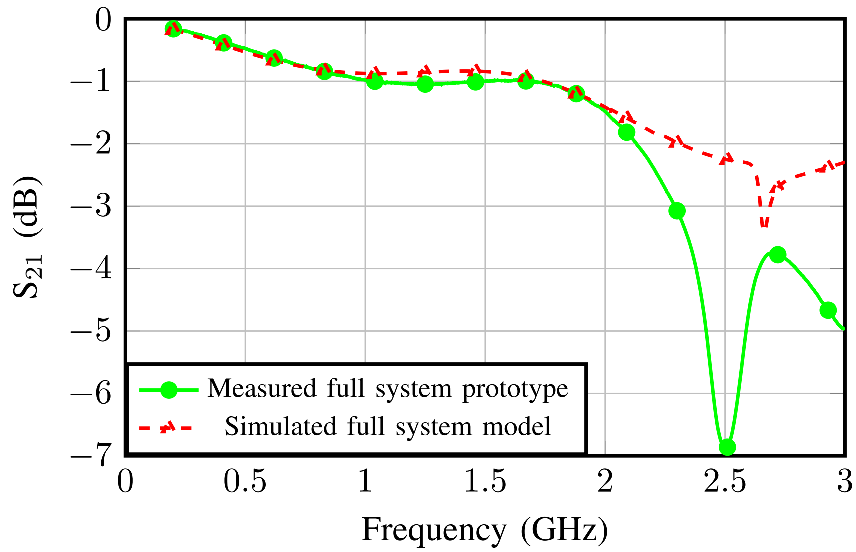


**Figure 4.31** $S_{21}$ results for simulated and measured CPW adapter system

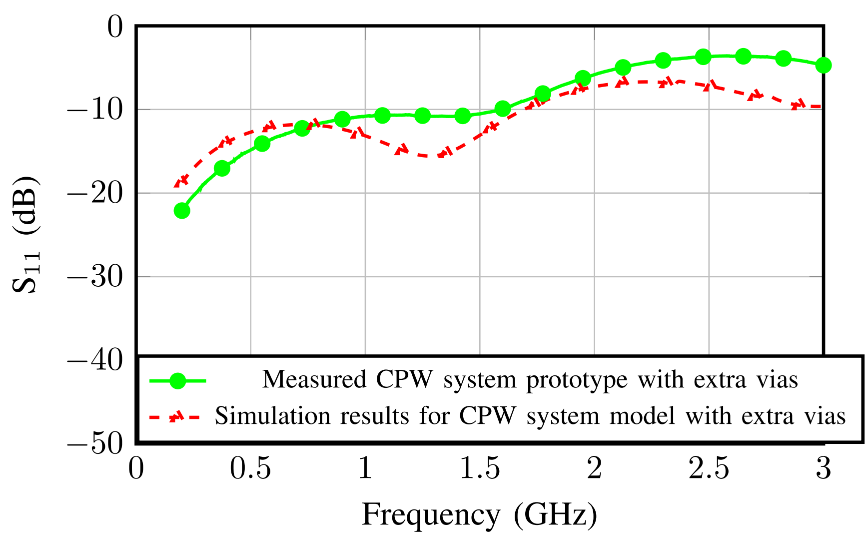


**Figure 4.32** $S_{11}$ results for simulated and measured CPW adapter system with new elements with extra vias

simulated and measured results at higher frequencies. This could indicate material differences between the two.

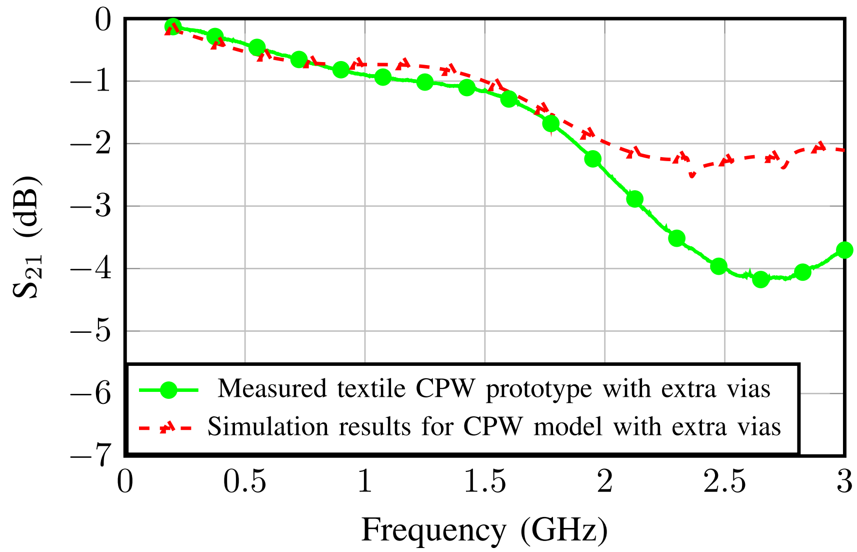


**Figure 4.33** $S_{21}$ results for simulated and measured CPW adapter system with new elements with extra vias

## 4.6 De-embedding

The de-embedding method used is the same as used with the microstrip model in the previous chapter. Each individual device was measured with a VNA to obtain its S parameters, which has been done in the previous sections with results also presented. From the S parameters, ABCD parameters were obtained by using Table 4.2 and a two-port network ABCD parameter matrix is generated for each device as in Eq. 4.1.

$$\begin{bmatrix} A & B \\ C & D \end{bmatrix}_{textile\_CPW} \tag{4.1}$$

The entire system is composed of three devices. The textile cpw, the textile to FR-4 transition and the FR-4 board. Each of these devices has a two-port network associated with them and the whole system is modelled as a cascade connection of these two-port networks as shown in Equation 4.2.

$$\begin{aligned} \begin{bmatrix} A & B \\ C & D \end{bmatrix}_{adapter} = \begin{bmatrix} A & B \\ C & D \end{bmatrix}_{textile\_cpw} \times \begin{bmatrix} A & B \\ C & D \end{bmatrix}_{textile\_connection} \\ \times \begin{bmatrix} A & B \\ C & D \end{bmatrix}_{fr4\_part} \end{aligned} \tag{4.2}$$

| ABCD Parameters | S Parameters |
|---|---|
| A | $\dfrac{(1+S_{11})(1-S_{22})+S_{12}S_{21}}{2S_{21}}$ |
| B | $Z_0\dfrac{(1+S_{11})(1+S_{22})-S_{12}S_{21}}{2S_{21}}$ |
| C | $\dfrac{1}{Z_0}\dfrac{(1-S_{11})(1-S_{22})-S_{12}S_{21}}{2S_{21}}$ |
| D | $\dfrac{(1-S_{11})(1+S_{22})+S_{12}S_{21}}{2S_{21}}$ |

**Table 4.2** S parameter to $ABCD$ parameter conversion table from Pozar et al. [6]

To help visualise the cascade connection of the devices in our textile adapter, a composite figure has been created Fig 4.34. The adapter is considered to have three devices, the textile CPW, the textile to FR-4 connection and the FR-4 CPW. Since the SMA connector effect has been removed by the measurement in the VNA, these are not accounted for. The de-embedding process is being used to extract the effect of the connection between textile and copper, in our system we call it textile_connection. This connection is directly under the magnet in this figure.

The measurement of the textile CPW was done between Port 1' and Port 2. For the textile adapter the measured system is slightly longer in length, the port was moved further out as it was measured from Port 1 to Port 2.

From Equation 4.2 and using simple matrix algebra, we obtain Equation 4.3. With this new equation we can obtain the ABCD parameters for the textile to fr-4 transition. The results for the transition are presented in the next section.

$$\begin{aligned}\begin{bmatrix} A & B \\ C & D \end{bmatrix}_{textile\_connection} &= \begin{bmatrix} A & B \\ C & D \end{bmatrix}^{-1}_{textile\_cpw} \times \begin{bmatrix} A & B \\ C & D \end{bmatrix}_{adapter} \\ &\times \begin{bmatrix} A & B \\ C & D \end{bmatrix}^{-1}_{fr4\_part}\end{aligned} \tag{4.3}$$

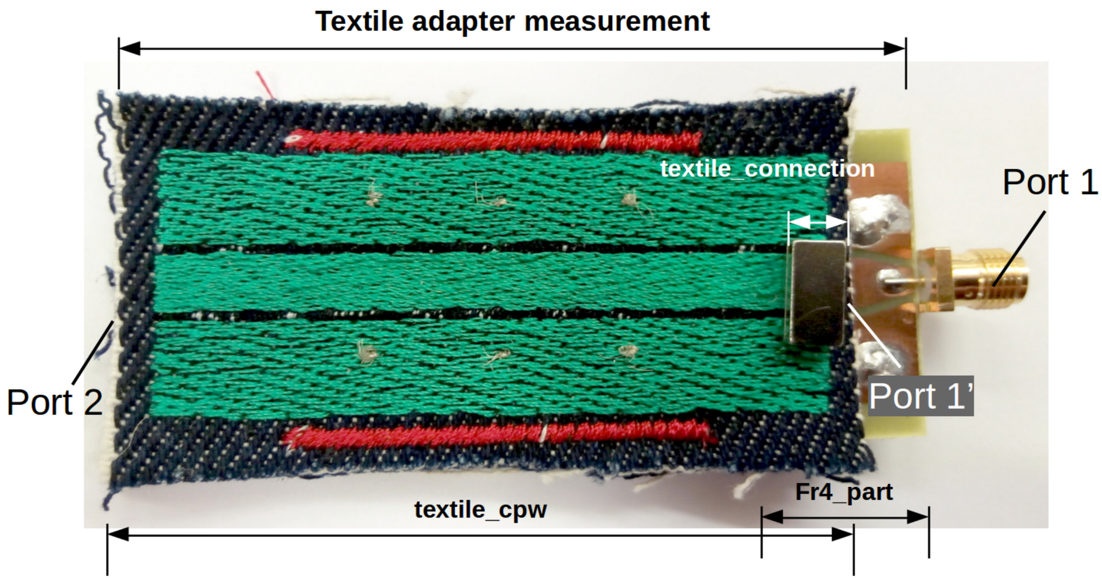


**Figure 4.34** CPW adapter system with all devices connected and ABCD parameters displayed for each device

### 4.6.1 De-embedding Results

As was previously demonstrated, the original models had problems with unwanted modes created by resonating side ground planes. The results for the de-embedding of these original models will also be presented here to demonstrate why the algorithm failed to perform in that case.

After extracting the $ABCD$ parameters from Equation 4.3, the $ACBD$ matrix is converted into a S-parameter matrix. When looking at the de-embedded results in Figs. 4.35 and 4.36, $S_{11}$ and $S_{21}$ values go above 0 dB in some frequencies. This is the effect of the unwanted modes when each individual device in the system was measured. In the $S_{21}$ plot the values go above 0 at 2 GHz and around 2.7 GHz. It is not a surprise that these frequencies are the same that were problematic in the FR-4 board and textile line respectively.

However as shown in the previous section Fig. 4.31 when all the devices of the system are measured together, the drop in power at 2 GHz is no longer present. This is probably due to the change in dimensions when the FR-4 board and the textile line are attached together. When the whole system is measured, the unwanted modes do not seem to exist at 2 GHz and seem to be attenuated at around 2.7 GHz.

This explains why the extracted S-parameters for the textile connection seem to behave as an amplifier. Since there is a drop in power on the single device measure-

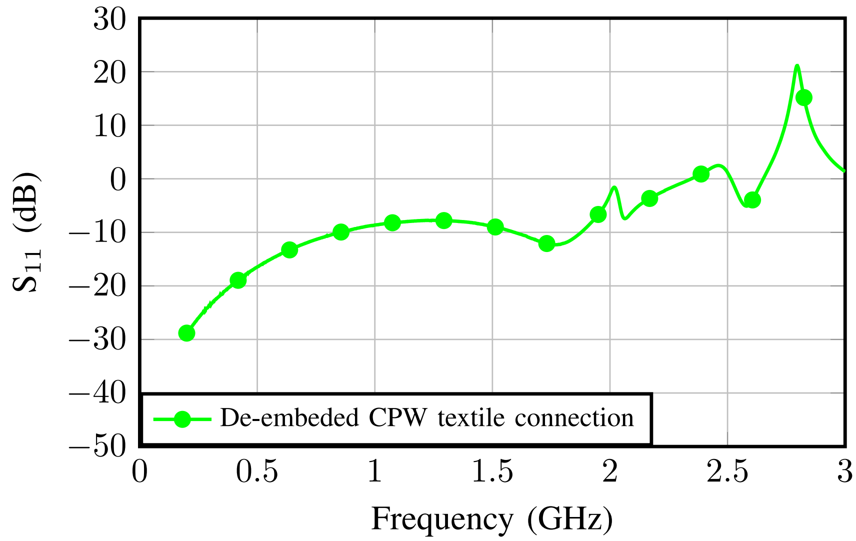


**Figure 4.35** $S_{11}$ results of de-embedded textile connection

ments but it disappears on the whole system measurement, the algorithm extracts this as an amplification.

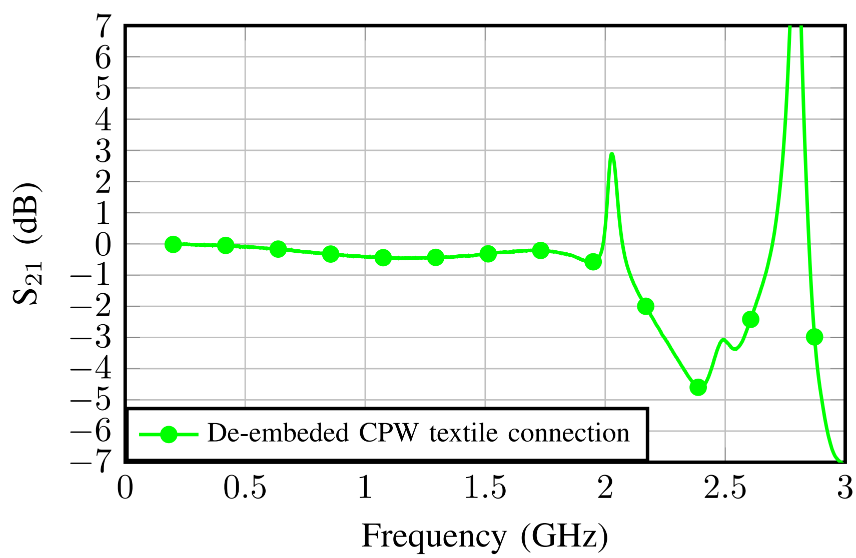


**Figure 4.36** $S_{21}$ results of de-embedded textile connection

However, when looking at the results from the devices with the extra vias, Figures 4.37 and 4.38, the results no longer show this value of S-parameters above $0dB$. The system has reasonable results up to 2 GHz but higher than that and reflections become a problem. These reflections come from an impedance mismatch on the FR-4 board due to the tapper. Similar to the results obtained on the microstrip model, the transition from denim to FR-4 dielectric can also be causing reflections.

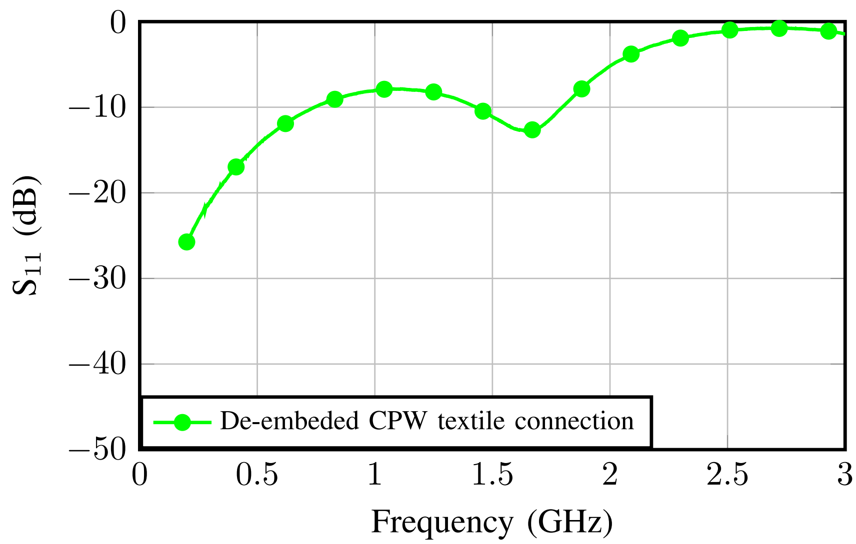


**Figure 4.37** $S_{11}$ results of de-embedded textile connection with added vias

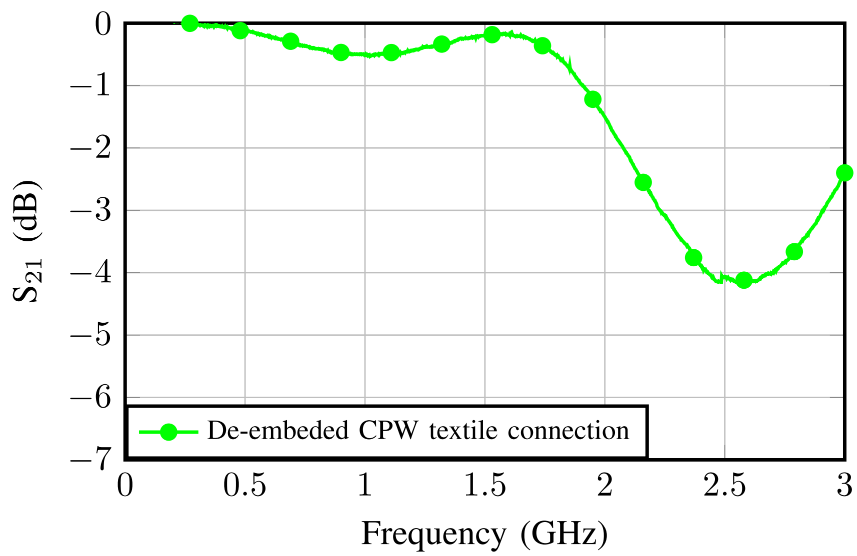


**Figure 4.38** $S_{21}$ results of de-embedded textile connection with added vias

## 4.7 Conclusion

In this chapter a reusable textile grounded CPW connector has been presented. As with the microstrip model it requires no permanent connection on the textile side. For frequencies up to 2 GHz this model has reasonable insertion loss of $-2$ dB. These results could be improved by reducing the length of textile which is very lossy. It was found that the models suffered from unwanted parallel-plate modes in the side ground planes which were radiating. By introducing extra vias in the textile CPW, these modes were suppressed and the resonance removed. On the FR-4 model, the vias could have been created closer to the gap between conductor and ground plane. Perhaps it would have improved the results at higher frequencies. After the de-embedding procedure, the effect of the textile to FR-4 connection was extracted. From the results, we can see that the $S_{11}$ reflections increase a lot after 2 GHz to almost full reflection at 3 GHz. The same happens with the $S_{21}$ values after 2 GHz, the power transferred from Port 1 to Port 2 has a steep drop up to 3 GHz. These high reflections and low power transfer is most likely due to bad impedance matching. In these models there are two factors that could create a bad impedance match. The first one is the difference between the denim dielectric and the FR-4 dielectric. The second factor is the sudden change in dielectric which can also lead to reflections. These could be more accentuated at higher frequencies due to the shift in $\epsilon_r$ at higher frequencies.

This chapter demonstrates the possibility of using CPW fed systems in textile. However due to the difficulty of manufacture using embroidered Liberator 20, perhaps a different thread could be tested.

## References

[1] N. I. N. AWR, "National Instruments NI AWR Design Environment 3D FEM Electromagnetic (EM) Analysis,", 2017.

[2] A. Tsolis, W. G. Whittow, A. A. Alexandridis, and J. C. Vardaxoglou, "Embroidery and related manufacturing techniques for wearable antennas: challenges and opportunities," Electronics **3,** 314–338 (2014).

[3] M. Riaziat, R. Majidi-Ahy, and I. J. Feng, "Propagation modes and dispersion characteristics of coplanar waveguides," IEEE Transactions on Microwave Theory and Techniques **38,** 245–251 (1990).

[4] Brother, "Brother PE Design Next software,", 2017.

[5] W. H. Haydl, "On the use of vias in conductor-backed coplanar circuits," IEEE Transactions on Microwave Theory and Techniques **50,** 1571–1577 (2002).

[6] D. M. Pozar, *Microwave Engineering, 4th Edition* (Wiley Global Education, 2011).

# Chapter 5

# Different embroidery filling designs and effects on results

## 5.1 Introduction

In this chapter, results for the microstrip system with the textile part embroidered using different methods will be presented. In the previous microstrip chapter 3.5, the embroidered prototype used a common embroidery meshing where the lines are embroidered along the direction of the microstrip. It also used a linear density of 5 lines/mm on all the prototypes. Some work has been done in [1] where different types of stitching direction and density parameters are studied to evaluate the effects on embroidered antennas efficiency. The motivation to try different embroidery meshes is to try and reduce the amount of conductive thread used, as well as to see the effects of these embroidery patterns. The microstrip model was chosen because it is simpler to create than the CPW model. The dimensions remained the same as the previous prototype.

## 5.2 Microstrip with gradient filling

Two prototypes were created using gradient filling, which we will call microstrip **A** and microstrip **B**. What this means is that there is higher thread density on the outside of the microstrip conductor than on the centre. Brother's embroidery software has the option to use this filling, which was set up with the same original 5 lines/mm and then the gradient was adjusted. For the gradient filling, only the top conductor was embroidered with the gradient. The ground plane remains the same as before, using a sheet of Nora-Dell.

The schematic in Fig. 5.1 illustrates how the gradient filling was used. It follows from the theory [2] that in microstrip lines, the current mostly travels on the edges of the copper line due to the skin effect. Note that due to the nature of the Liberator thread, the embroidered prototype will not look like separate threads as seen in the presented figure. Since the liberator threads fray during embroidery, there will be bridging connections between adjacent threads. The individual threads however, will be more noticeable on the middle of the central conductor.

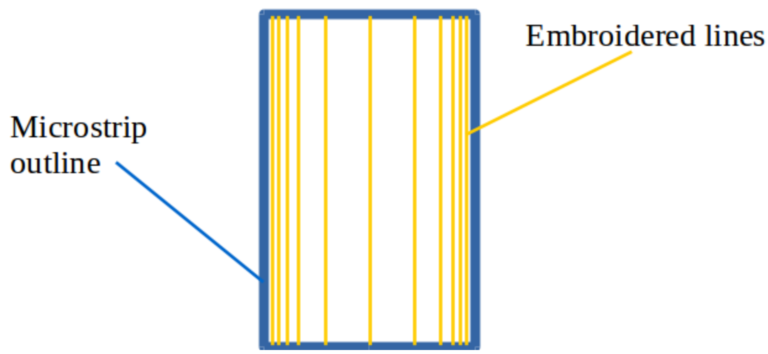


**Figure 5.1** Mock-up of microstrip prototype with gradient embroidery

By using the gradient filling, the amount of thread used was reduced. On the original textile prototype, the central conductor had 504 stitches with a stitch spacing of 2 mm which is around 1 meter of thread.

For the microstrip with the gradient filling A, the settings used in the embroidery software are shown in Fig. 5.2. The prototype has a stitch count of 266 stitches with the same 2 mm stitch spacing which uses around 0.53 m of thread. This is a 53% reduction in thread amount. I could not reduce the amount of thread any more or during embroidery it would consist of only a couple of conductive thread lines.

For the microstrip B prototype, the gradient filling used is shown in Fig 5.3. It has 300 stitches that uses 0.6 m of thread, which when compared to the original prototype is a 59% reduction in thread.

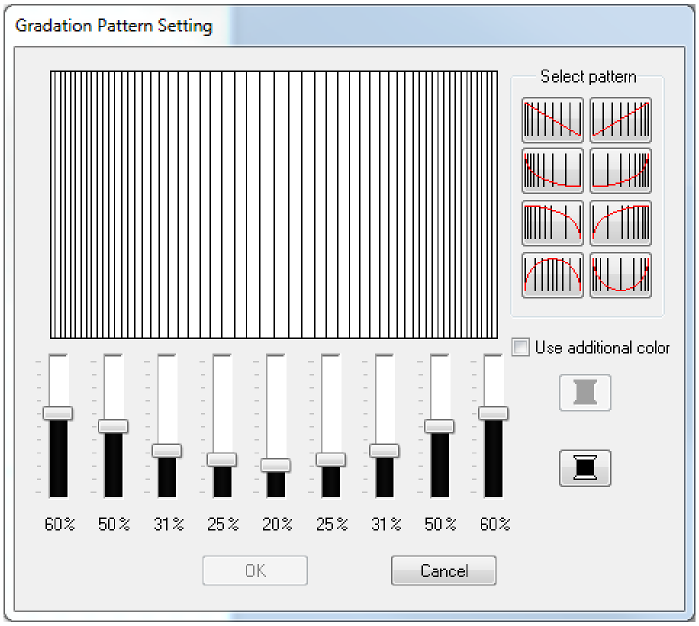


**Figure 5.2** Gradient used on the microstrip A

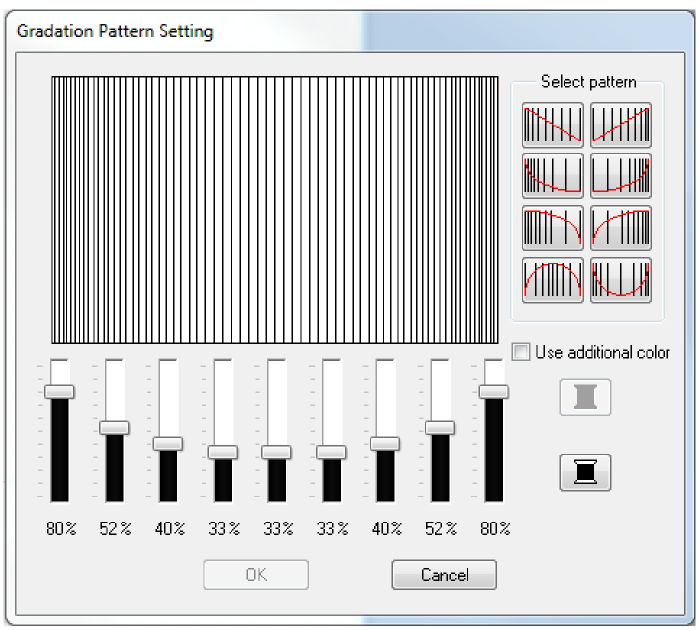


**Figure 5.3** Gradient used on the microstrip B

### 5.2.1 Results for textile microstrip A

The gradient values were set in Brother's embroidery software. For the prototype using gradient **A**, the gradient follows the values presented in Fig. 5.2.

The prototype with the gradient filling was measured individually as well as in the textile adapter system. To measure the textile line individually, coaxial SMAs were soldered to the textile part as demonstrated in the previous chapter.

In Fig. 5.4 a comparison of $S_{11}$ values between the prototype embroidered with the gradient pattern A and the original textile prototype are presented. On the prototype with the gradient pattern, reflections are much higher in most of the measured frequency band. However when comparing the results for the $S_{21}$ measurements in Fig. 5.5, the results are much more similar. The prototype with the gradient filling has a slight drop in power transfer of around −1.4 dB at 2 GHz.

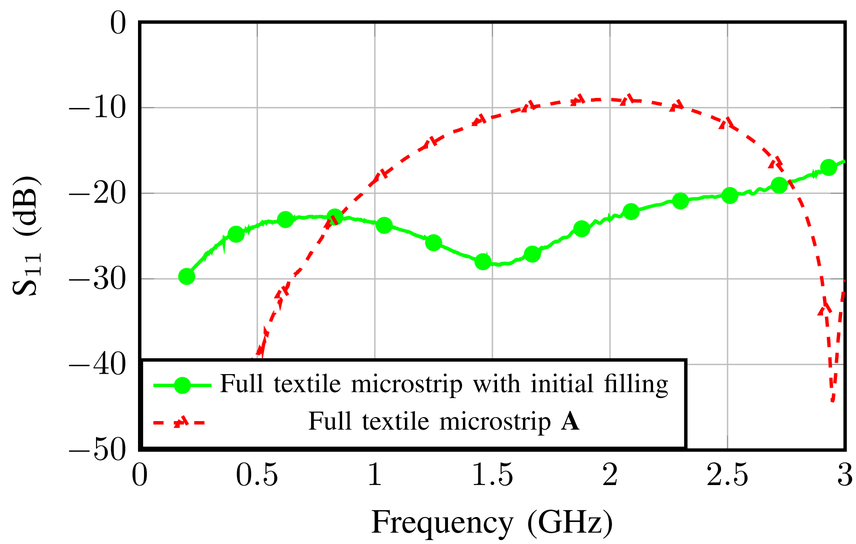


**Figure 5.4** Comparison of $S_{11}$ values between the textile microstrip **A** and original textile microstrip

Presented in Fig. 5.6 is the radiated and reflected power loss for the microstrip with gradient pattern A and the original prototype. The results are quite similar in both prototypes.

In order to check why the reflections are so high for the microstrip with gradient A, Zin was calculated for both microstrip prototypes. It was assumed that the impedance of the VNA was 50Ω. By using equation 5.1, $Z_{in}$ was calculated and the result is shown in Fig. 5.7. From 0.8GHz to 2.7GHz the input impedance of the transmission

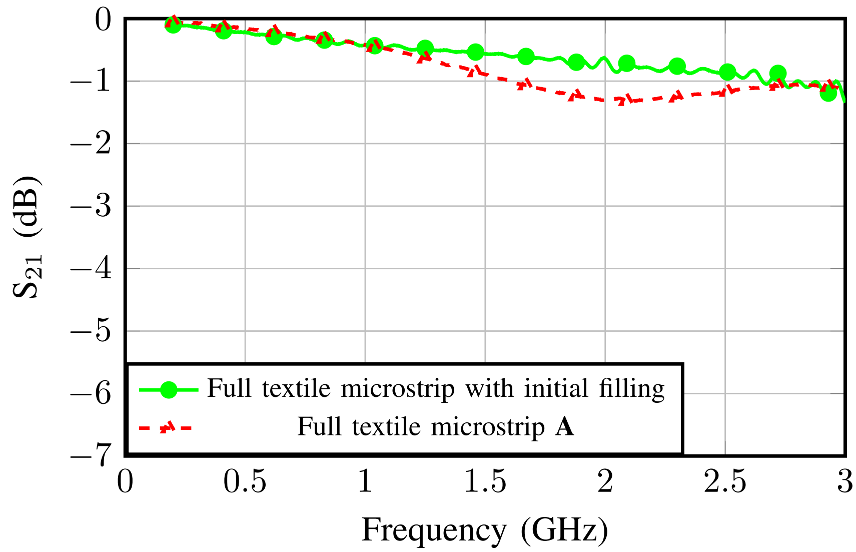


**Figure 5.5** Comparison of $S_{21}$ values between the textile microstrip **A** and original textile microstrip

line deviates a lot from the desired 50Ω. Since $Z_{in}$ was obtained from $S_{11}$, the highest impedance mismatch is at 2GHz

$$Z_{in} = 50 * \frac{1 + S_{11}}{1 - S_{11}} \tag{5.1}$$

The next step was to measure it as part of the textile adapter system. These results are shown next. In Figures 5.9 and 5.11 the measured results of the system are presented when using the original textile microstrip, as well as when using the textile microstrip **A**.

Looking at the plots it seems that when used in the textile adapter system, the differences between using the original microstrip and microstrip **A** are very small. The fact that the FR-4 board is being used seems to negate some of the difference between the original textile prototype and the prototypes with the gradient filling. This could be due to the way the SMAs were soldered on the conductive textile in the previous measurement. In Fig. 5.10 is the design of the microstrip with gradient **A** as it was designed in the embroidery software. The black lines are the embroidered threads and the red lines were not embroidered. As can be seen, at the ends of the microstrip the wires only travel along the direction of the conductor and don't have a perpendicular connection with the threads on the sides. When the connector is soldered to the centre of the conductor, it only makes a good electrical connection

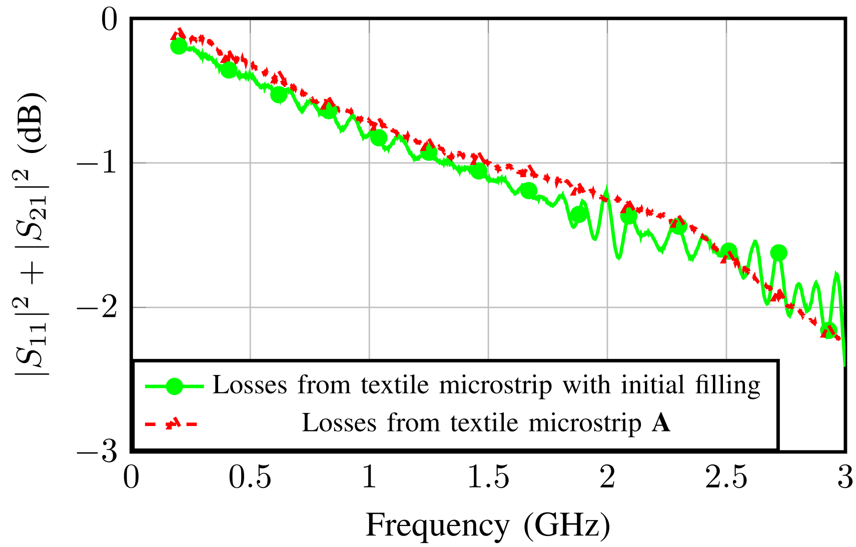


**Figure 5.6** Comparison losses between the textile microstrip **A** and original textile microstrip

with the threads in the centre. This is where the thread density is smaller. However, when the FR-4 adaptor is used, the embroidered conductor is pressed against the copper conductor as in Fig. 5.8. This means that all of the threads along the width of the textile conductor connect to a flat copper line. This increases the quality of the connection and that can be seen in the results.

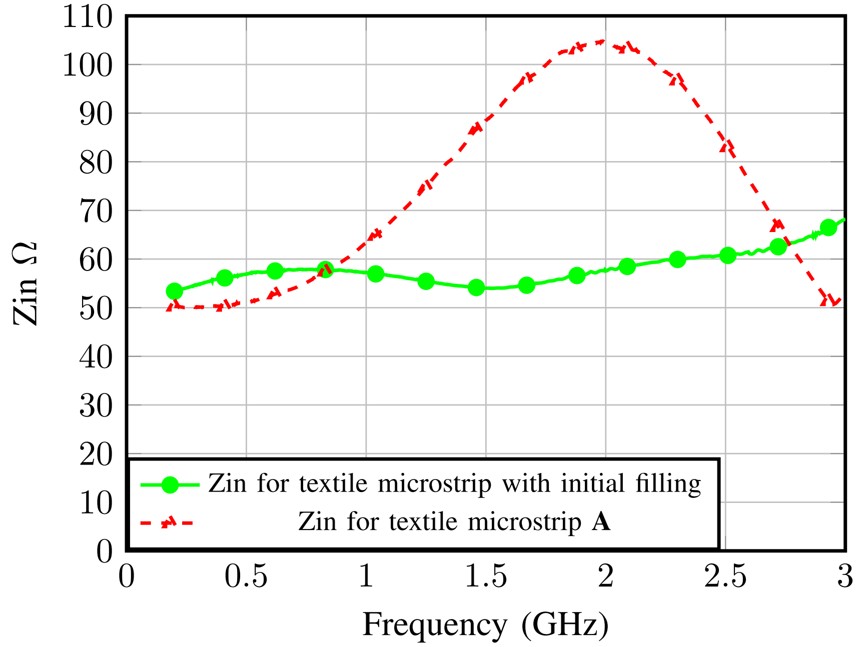


**Figure 5.7** $Z_{in}$ of textile microstrip **A** and original textile microstrip

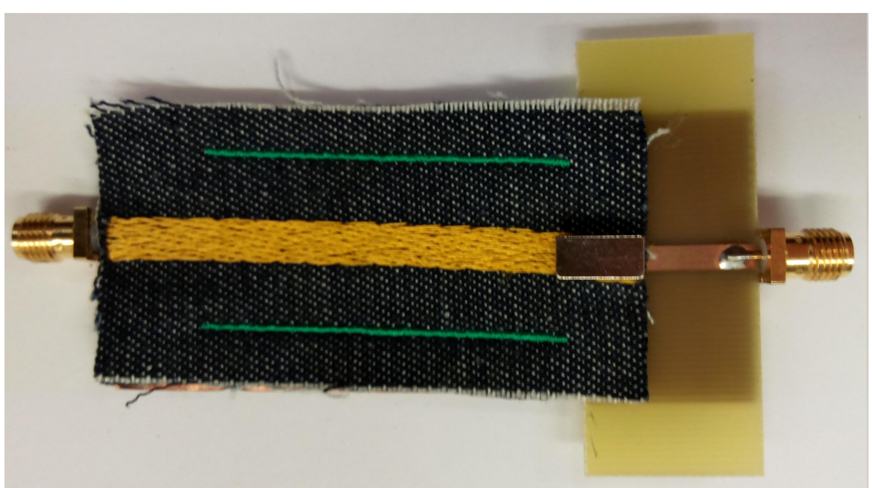

**Figure 5.8** Textile to FR-4 transition

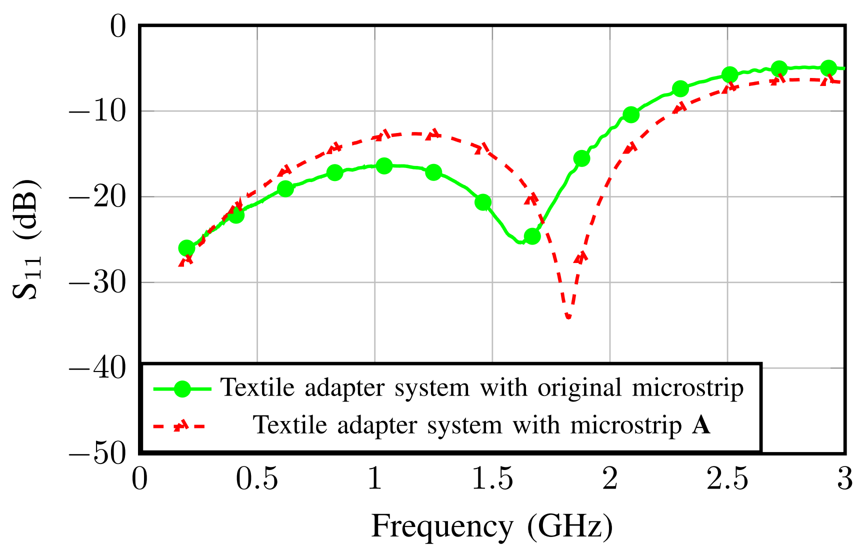


**Figure 5.9** Comparison of $S_{11}$ values between the textile microstrip **A** and original textile microstrip when used in the textile adapter system

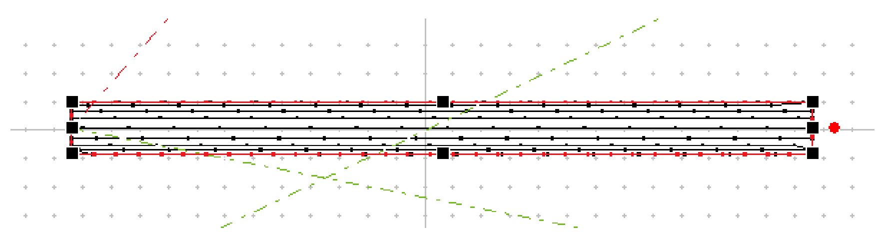

**Figure 5.10** Microstrip with gradient **A** design in Brother's embroidery software

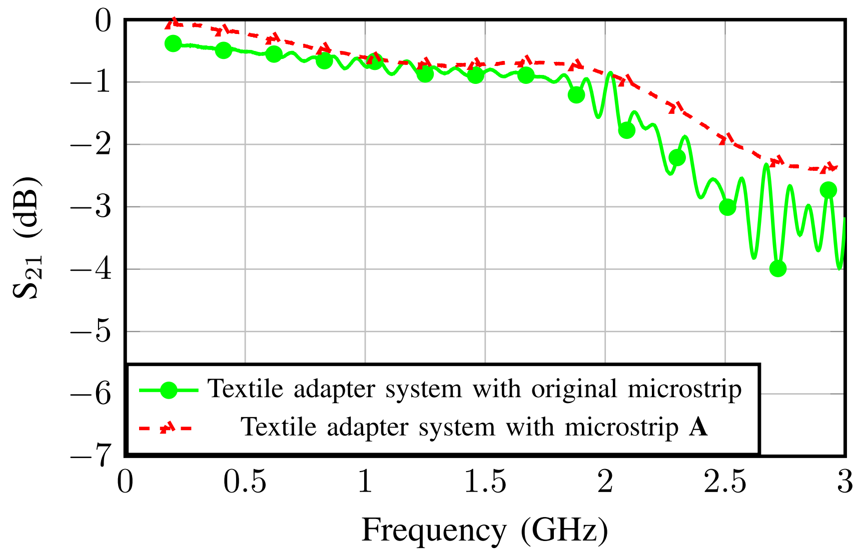


**Figure 5.11** Comparison of $S_{21}$ values between the textile microstrip **A** and original textile microstrip when used in the textile adapter system

### 5.2.2 Results for textile microstrip B

For the textile microstrip B prototype, the gradient filling was increased. This was done to see how much the performance would be affected by an increase in conductive thread.

Figure 5.12 shows the $S_{11}$ results for microstrip B compared with the original textile prototype. With the increase in conductive thread used, the results start to approximate the original textile thread. There are still increased reflections on the measurements with microstrip B. The $S_{21}$ values are almost the same as the original textile thread, as can be seen in Fig. 5.13.

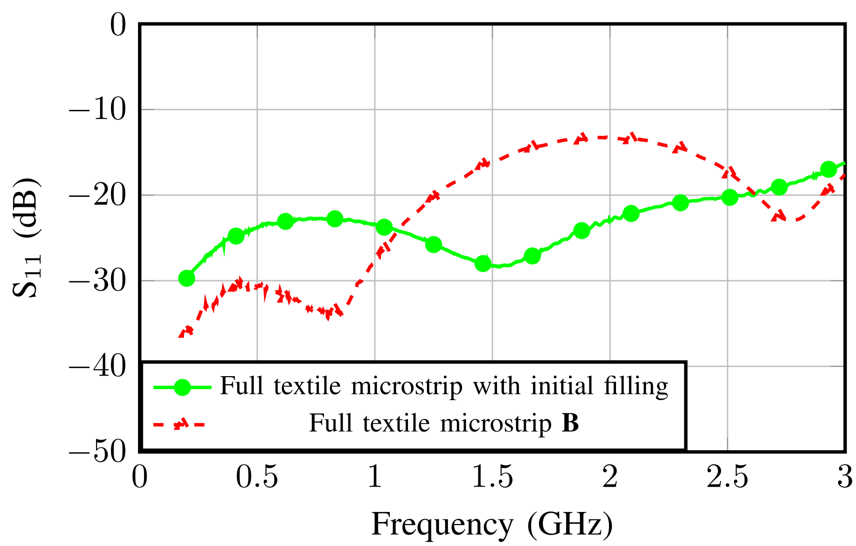


**Figure 5.12** Comparison of $S_{11}$ values between the textile microstrip **B** and original textile microstrip

As for the measurements when using it on the textile adapter, these can be found in Figures 5.14 and 5.15. As with the previous prototype it seems that when using the textile prototype with the gradient filling, the performance of the system increases. However this is more likely due to the measurement itself. As the textile microstrip is flexible, the original prototype might have been measured in a less than ideal position.

As it was shown in the past two chapters, using the gradient filled transmission line in the whole system mitigates some of the problems seen when individual measurements were performed.

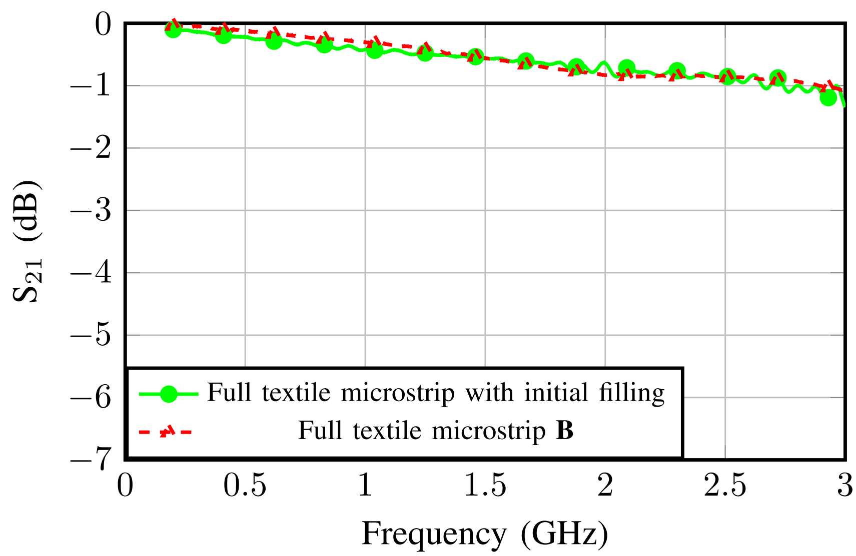


**Figure 5.13** Comparison of $S_{21}$ values between the textile microstrip **B** and original textile microstrip

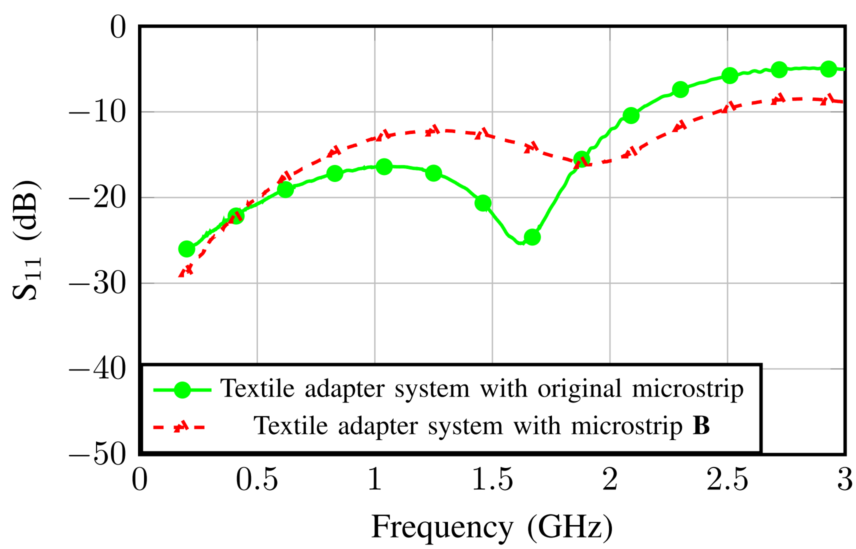


**Figure 5.14** Comparison of $S_{11}$ values between the textile microstrip **B** and original textile microstrip when used in the textile adapter system

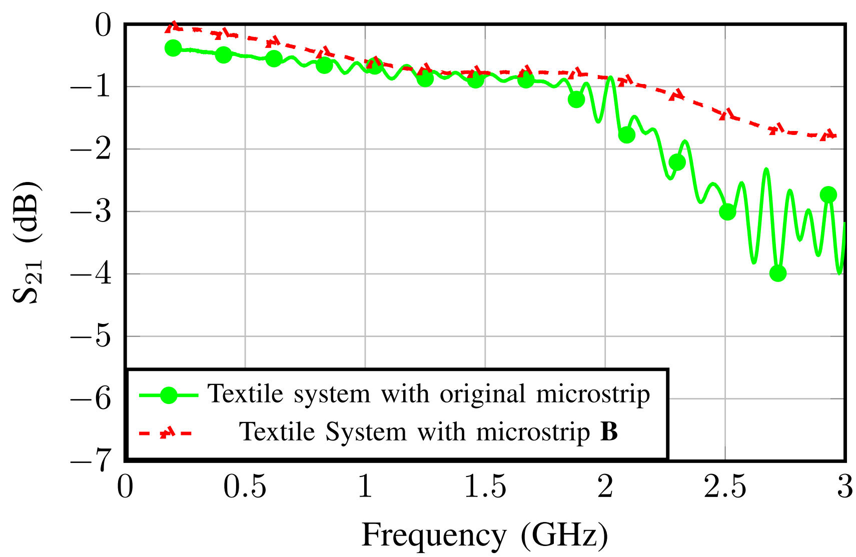


**Figure 5.15** Comparison of $S_{21}$ values between the textile microstrip **B** and original textile microstrip when used in the textile adapter system

### 5.2.3 De-embedded results for gradient filling connections

Now the de-embedded results of the textile to copper transition will be presented. These are the results for the microstrip prototypes with the gradient filling pattern. The de-embedding process is the same as in previous chapters. The results for the gradient filling prototypes, will be presented along with the de-embedded results for the original textile microstrip connection.

The results for the de-embedded textile to FR-4 connection are shown in Figures 5.16 and 5.17. The connection with Model B, with its higher thread count has less reflections from 1.5 GHz up to 3 GHz when compared to the prototype with gradient A. In both plots all the prototypes share higher reflections and less power transfer at higher frequencies. This is usually associated with power being radiated.

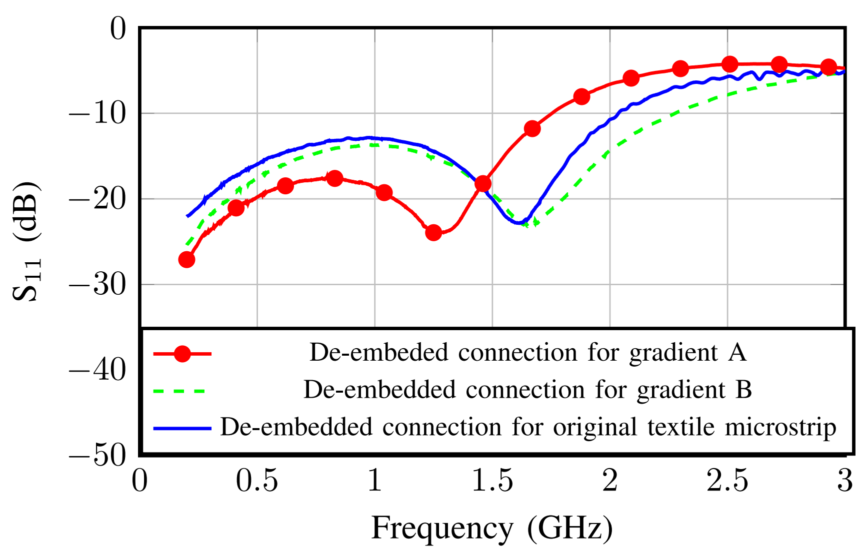


**Figure 5.16** De-embedded $S_{11}$ values for both microstrip prototypes with gradient filling

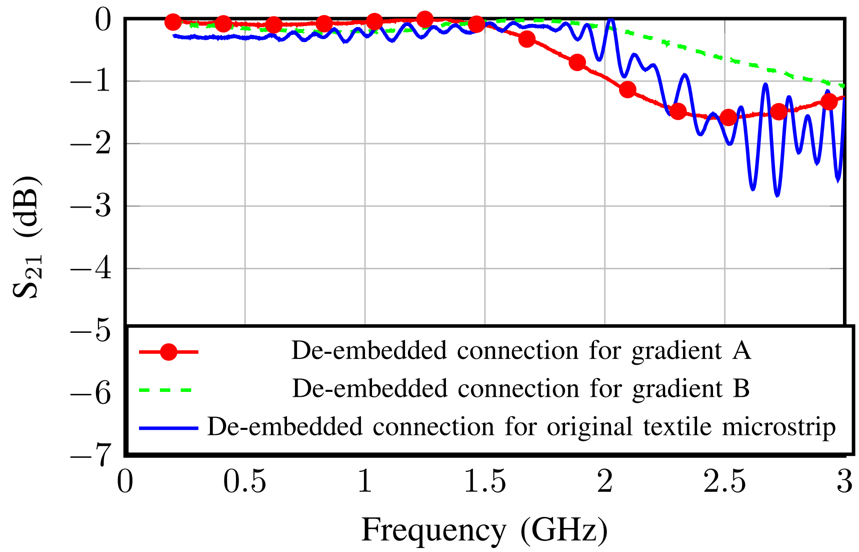


**Figure 5.17** De-embedded $S_{21}$ values for both microstrip prototypes with gradient filling

### 5.2.4 Conclusions of gradient filling study

By using a gradient filling on the central conductor of the microstrip prototype, a smaller ammount of conductive thread was used. The results show that when measured individually and using soldered coaxial SMA's, the results are worse than the original prototype. However, when attached to the FR-4 board and measured as the textile adapter. The results are slightly worse in lower frequencies, but after around 1.7 GHz for model A and 2 GHz for model B the results look better.

This shows that by reducing the amount of material used by using this gradient filling, not much performance is lost when the textile microstrip prototypes are used in the whole system.

More prototypes could be done with smaller intervals in terms of gradient differences. Then a more complex plot could be made to demonstrate the change in models as in Figures 5.18 and 5.19.

Studying gradient fillings that are able to make a good RF connections is very important in the textile wearable research area. The conductive threads used in wearable research are usually quite expensive. By lowering the production costs while having good performance can make this area more attractive for future research.

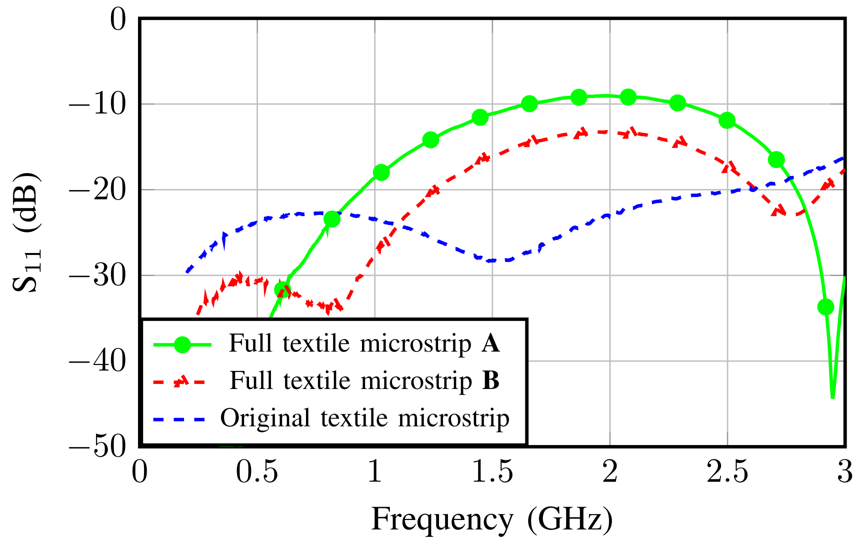


**Figure 5.18** Comparison of $S_{11}$ values between the textile microstrip **A** and **B**

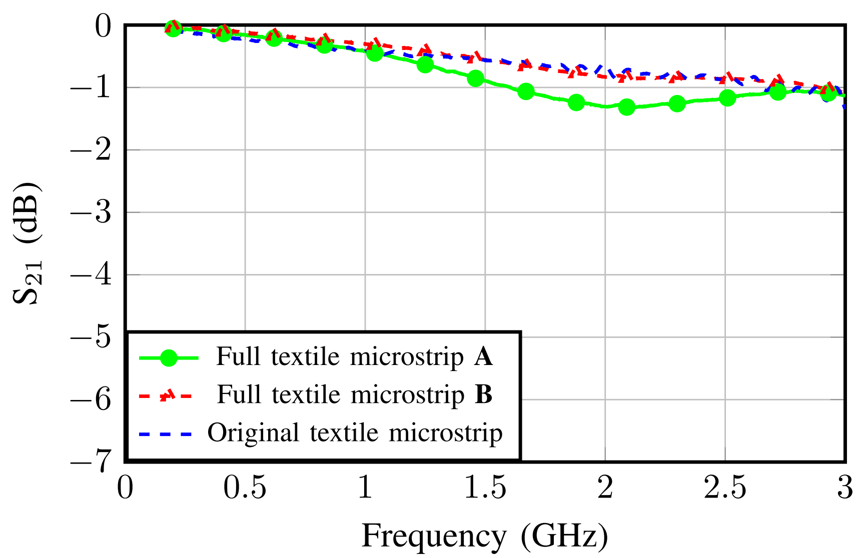


**Figure 5.19** Comparison of $S_{21}$ values between the textile microstrip **A** and **B**

## 5.3 Microstrip with triangular filling

Another embroidery filling that was used is a triangular filling. The idea for this filling comes from the work made in conjunction with an undergraduate student's project that focuses on infinite lattice structure of resistors based on [3]. To create this type of filling pattern, a different approach had to be made. Brother's embroidery software just wasn't up to the task of creating a custom pattern. At first it was thought that the embroidery files could be directly edited for this purpose, however the files use a proprietary binary file format '.pes' that cannot be edited outside of Brother's embroidery software. To get around this, an open source software called Embroidermodder [4] was used. What was used from this software was the libembroidery library, this library handles the conversion between different embroidery software file formats. The library was used to convert the '.pes' files to '.csv' files to understand how these binary file format worked.

Matlab was used to make an algorithm that creates and exports a .csv file containing the stitching pattern. Then, the '.csv' file is converted back to '.pes' and opened by the embroidery machine. In Fig. 5.20 a small example of what an embroidery file looks like when converted to '.csv' format is presented. Each stitch is composed of X and Y coordinates. On the top there is a header with general notes. After that on the third "paragraph" its where the software reads the dimensions of the frame as well as stitch count. On the bottom is where the stitch information is read, in this example only 3 stitches are shown.

In Fig. 5.21 the mesh is represented in Matlab. It looks as if the triangles are deformed but this is due to the offset introduced to reduce problems that appeared during the embroidery process. While on the first Matlab model the meshing was designed so that each adjacent triangle vertices stitching was done at the same coordinates, once embroidered this was no longer the case. Due to the fabric stretching and the machine accuracy, what happened was that the vertices of adjacent triangles would be slightly displaced and no electrical connection would be made. To circumvent this, it was thought that a small offset of the vertices could counteract what was happening.

To better understand the offset that was introduced to reduce the displacement effect of the vertices, both stitching designs will be presented. Originally the stitching steps followed Fig. 5.22, in the figure the blue stars represent the point where the needle does a stitch. These stitches are numbered in order of stitching, with the

```
"#","Embroidermodder 2 CSV Embroidery File"
"#","http://embroidermodder.github.io"

"#","General Notes:"
"#","This file can be read by Excel or LibreOffice as CSV (Comma Separated Value) or with a text editor."
"#","Lines beginning with # are comments."
"#","Lines beginning with > are variables: [VAR NAME], [VAR VALUE]"
"#","Lines beginning with $ are threads: [THREAD NUMBER], [RED], [GREEN], [BLUE], [DESCRIPTION], [CATALOG NUMBER]"
"#","Lines beginning with * are stitch entries: [STITCH TYPE], [X], [Y]"

"#","Stitch Entry Notes:"
"#","STITCH instructs the machine to move to the position [X][Y] and then make a stitch."
"#","JUMP instructs the machine to move to the position [X][Y] without making a stitch."
"#","TRIM instructs the machine to cut the thread before moving to the position [X][Y] without making a stitch."
"#","COLOR instructs the machine to stop temporarily so that the user can change to a different color thread before resuming."
"#","END instructs the machine that the design is completed and there are no further instructions."
"#","UNKNOWN encompasses instructions that may not be supported currently."
"#","[X] and [Y] are absolute coordinates in millimeters (mm)."

"#","[VAR NAME]","[VAR VALUE]"
">","STITCH COUNT:","757"
">","THREAD COUNT:","3"
">","EXTENTS LEFT:","-11.400000"
">","EXTENTS TOP:","-0.000000"
">","EXTENTS RIGHT:","11.200000"
">","EXTENTS BOTTOM:","65.000000"
">","EXTENTS WIDTH:","22.600000"
">","EXTENTS HEIGHT:","65.000000"

"#","[THREAD NUMBER]","[RED]","[GREEN]","[BLUE]","[DESCRIPTION]","[CATALOG NUMBER]"
"$","1","0","0","0","Black",""
"$","2","112","188","31","Lime Green",""
"$","3","237","23","31","Red",""

"#","[STITCH TYPE]","[X]","[Y]"
"*","JUMP","0.000000","-0.000000"
"*","STITCH","-0.300000","-0.000000"
"*","STITCH","-0.600000","-0.000000"
"*","STITCH","-0.900000","-0.000000"
```

**Figure 5.20** Example of a csv file for an embroidery design

arrows providing a visual cue to the stitching path.

On Fig. 5.23 the offset can be seen as the blue stars do not connect on the same spot. As was described before, due to the nature of the materials and embroidery process the stitches that had coordinates on the same vertices would not be stitched exactly at the same position. The offset was introduced to create an overlap to ensure that the conductive thread made an electrical connection. The offset is sometimes horizontal on the $X$ axis but other times there is also a displacement on the $Y$ axis.

This stitching method was applied to the microstrip. Figure 5.24 shows the top side of the textile microstrip. It is easy to see the triangular pattern that is seen in green, which is the non-conductive thread. The conductive Liberator 20 is on the bottom side of the denim.

On the other side of the prototype, Fig 5.25 the ground plane was also embroidered using the triangular mesh. However, triangles with bigger sides were used in the ground plane. The white tape was used to hold the Liberator 20 strands in place, while they were soldered to the coaxial SMA. The same was done on the sides of the prototype. With no more stitches to hold it in place, the Liberator 20 thread would eventually start to get loose.

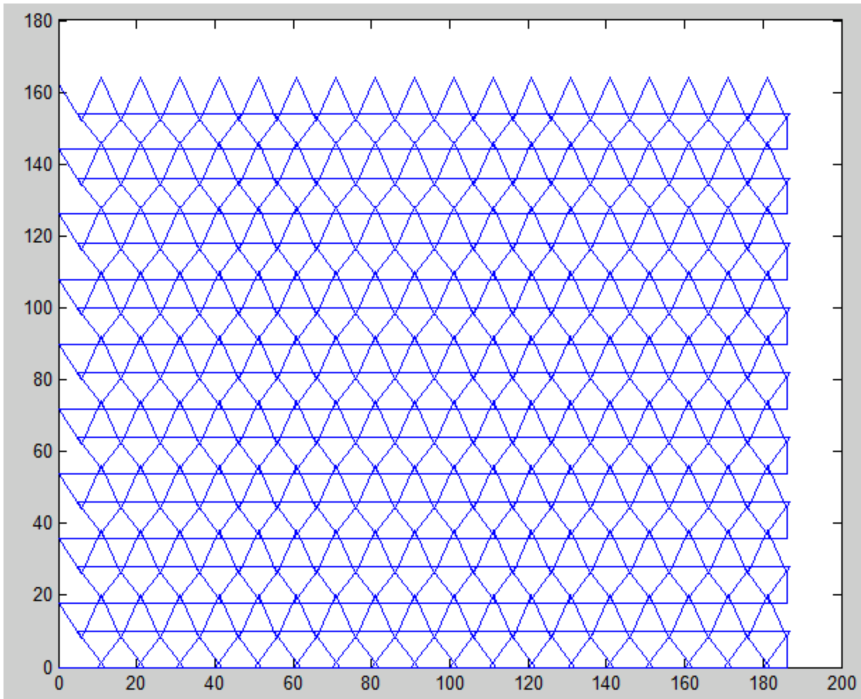


**Figure 5.21** Triangular mesh with offset in Matlab

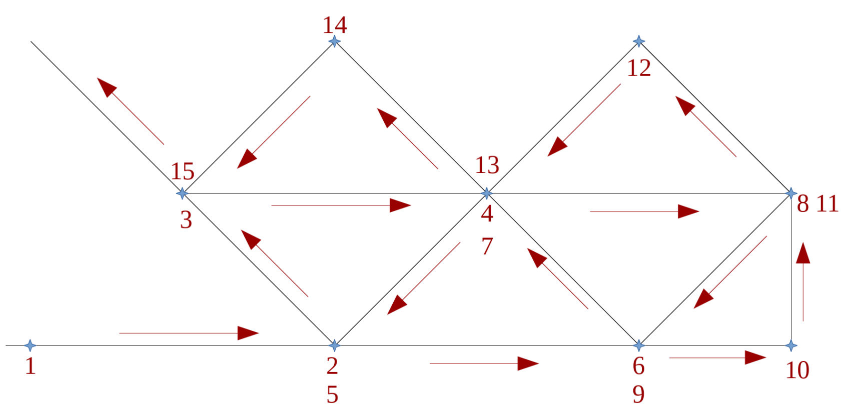


**Figure 5.22** Original stitching steps for triangular mesh

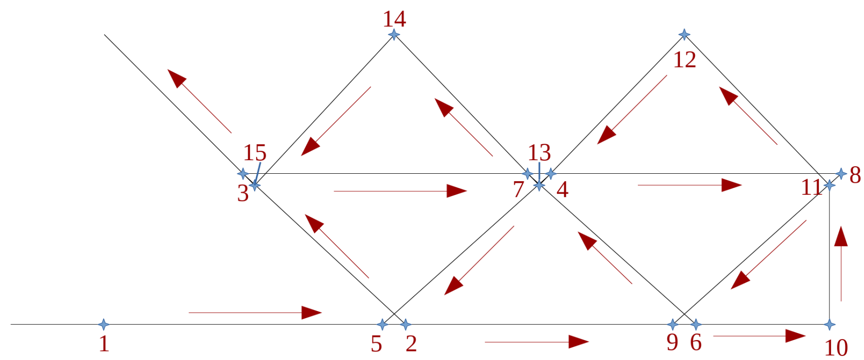


**Figure 5.23** Stitching steps for triangular mesh with offset

**Figure 5.24** Top view of textile microstrip with triangular meshing

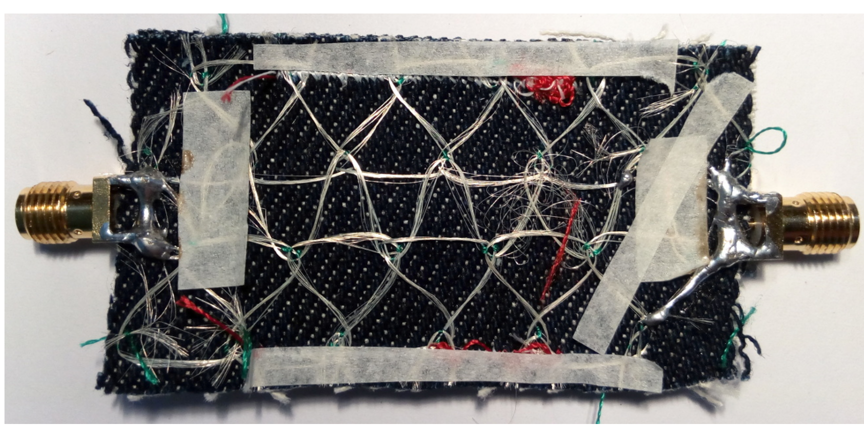

**Figure 5.25** Bottom view of textile microstrip with triangular meshing

### 5.3.1 Results using triangular filling

These measurements follow the same principle as the previous ones. The microstrip prototype was measured by itself, with coaxial SMA's soldered to it. It was also measured attached to the FR-4 board in the textile adapter system.

Instead of only one, perhaps two prototypes should have been created for a better understanding of the results. One with only the central conductor embroidered using the triangle mesh, with a normal Nora-Dell ground plane. The second prototype would be the one that was measured. This would have helped in demonstrating the effect of using the triangular mesh only on the central conductor. While the prototype that was created, has the effect of both ground-plane and conductor embroidered in this fashion.

Another problem with this prototype is the ground plane. In the other prototypes the ground plane is made of a sheet of Nora-dell, which is conductive on both sides. This is why it is possible to attach the textile transmission line to the FR-4 adapter with magnets. In Figure. 5.26 two jigs for the different prototypes are presented. The bottom prototype uses Nora-dell while the top prototype uses the embroidered ground plane. The thickness between the two textile transmission lines should be similar since Nora-dell is a very thin sheet of fabric.

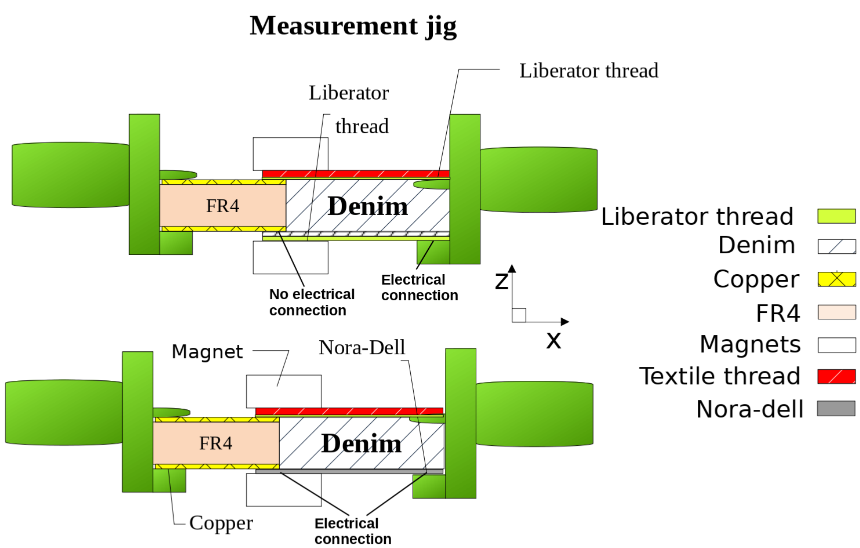


**Figure 5.26** Side by side differences between embroidered ground plane and Nora-dell ground plane

In this model, the ground plane was embroidered on the bottom side to have the correct thickness and to be able to solder the coaxial SMA connectors. This makes the ground plane conductive only on the bottom side of the denim layer. If the ground plane had been embroidered on the top side of the bottom layer of denim. It would still work when attached to the FR-4 board on one side and attached to a load using the magnets on the other side, but wouldn't be able to solder connectors to it for characterization.

The model as it is can not be easily connected to the FR-4 board, the conductive Liberator 20 is on the opposite side on denim that makes contact with the copper. For this to work, a small amount of copper tape was cut the same width of the model and attached to the ground plane. This way an electrical connection between the embroidered ground plane and the copper ground plane was made.

In Figures 5.27 and 5.28, the comparison between the original textile microstrip and the microstrip with the triangular mesh is presented. For the $S_{11}$ results, the values for the triangular mesh prototype are almost 10 dB higher showing high reflections. As for the $S_{21}$ results, the power transfer is 1 dB lower almost throughout the entire frequency range.

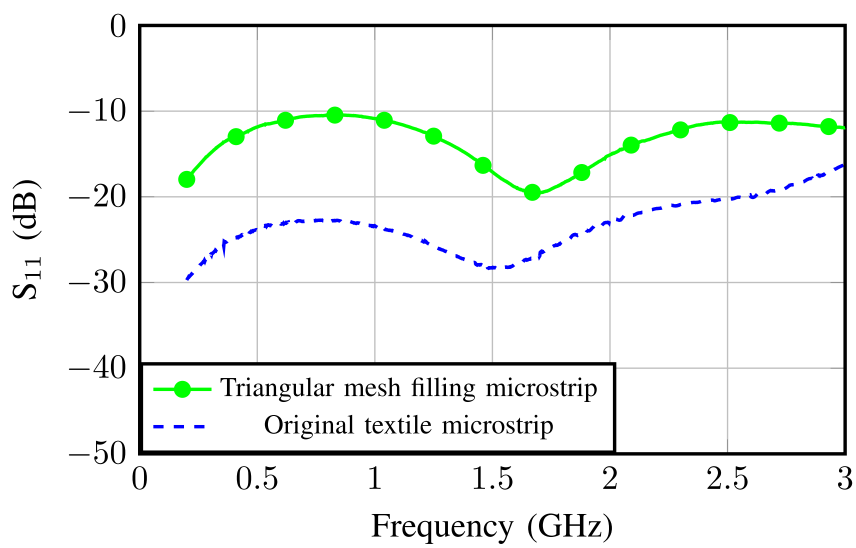


**Figure 5.27** Comparison of $S_{11}$ results between the original microstrip and the microstrip embroidered with the triangular filling

When measuring this prototype attached to the FR-4 adapter the results are not so good. Figure 5.29 shows the values of $S_{11}$ of both textile microstrips when attached to the FR-4 board. The values for $S_{11}$ are above −10 dB in almost the entire frequency range. The power transferred is also low, Fig 5.30, with a maximum of −1 dB at 0.6 GHz and dropping to −4 dB at 0.2, 1.8 and 3 GHz.

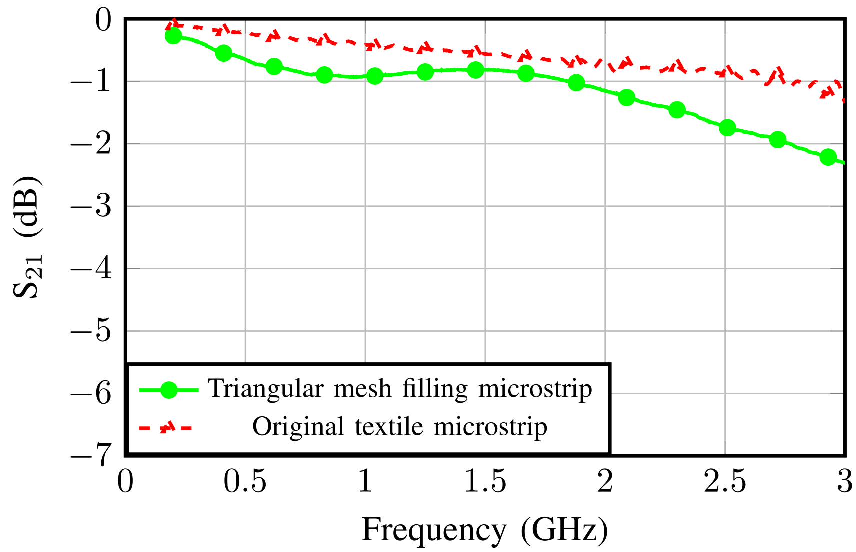


**Figure 5.28** Comparison of $S_{21}$ results between the original microstrip and the microstrip embroidered with the triangular filling

In conclusion, a full triangular mesh does not seem like a good filling pattern for a textile microstrip line. Perhaps if the ground plane was a sheet of Nora-dell like the original prototype, better results could be obtained. Perhaps if the central microstrip conductor was the only part of the prototype with this filling, the results would improve. In this case the alternative filling pattern did not provide good results. But this type of research can be very helpful in the area of textile wearable electronics.

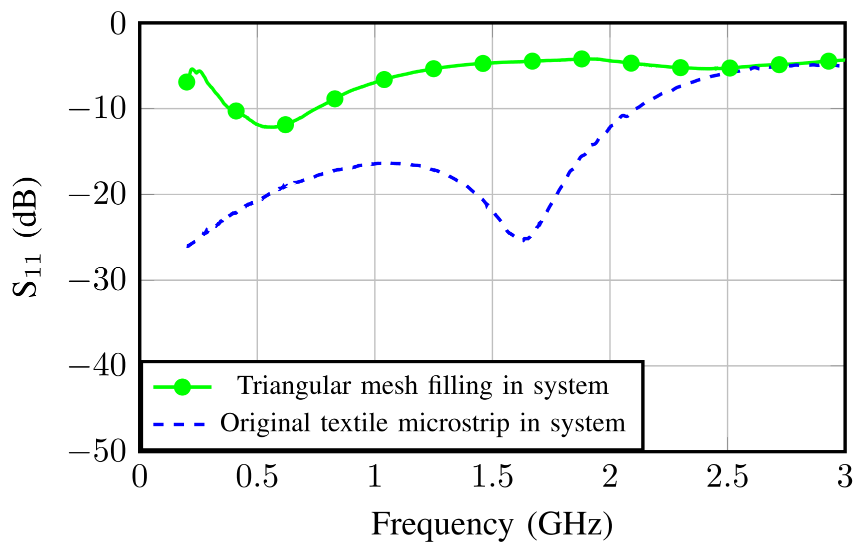


**Figure 5.29** Comparison of $S_{11}$ results between the original microstrip and the microstrip embroidered with the triangular filling attached to FR-4 board

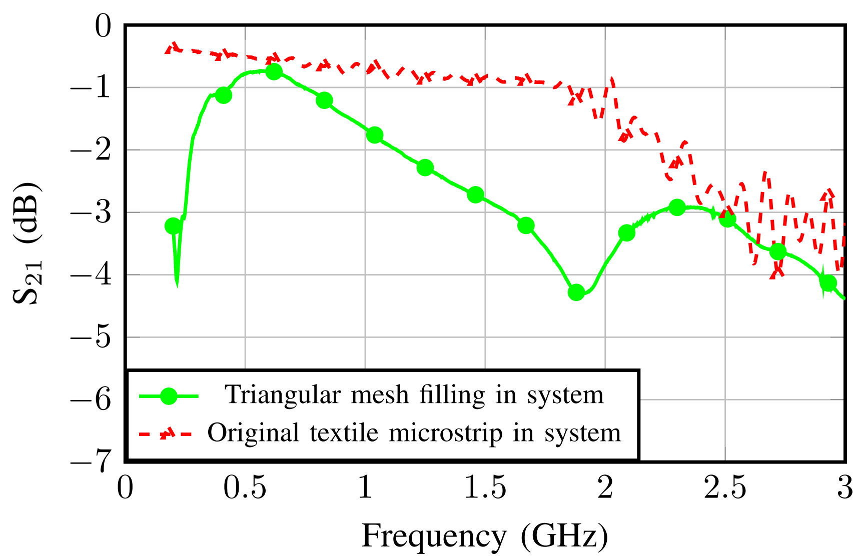


**Figure 5.30** Comparison of $S_{21}$ results between the original microstrip and the microstrip embroidered with the triangular filling attached to FR-4 board

## 5.4 Construction of higher-mode textile patch antenna with embroidered vias

In this section the contruction method used to build the wearable antenna presented in [5] will be presented. An original model consisting of a copper sheet and metallic vias with a felt dielectric was developed by a colleague. This model was probe fed which meant that when measured with a phantom, it would be difficult to mount due to the cables being between the antenna and the body and made the model rigid due to the copper sheet. It was evident that the model could benefit from a full textile construction. A side-by-side image of both antennas is presented in Fig. 5.31.

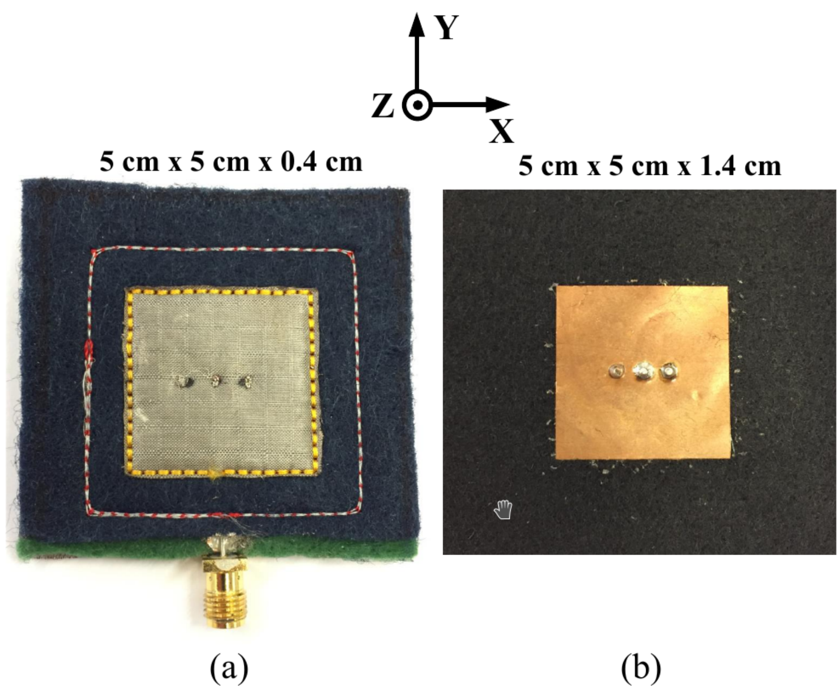


**Figure 5.31** (a) Full textile antenna fabricated with embroidery machine, (b) Textile antenna using rigid copper sheet and metallic vias, from A. Paraskevopoulos et al [5]

### 5.4.1 Fabric materials

The materials used were Nora-Dell [6] and Liberator-20 [7]. Nora-Dell is a conductive metallised nylon fabric coated with nickel and silver which forms a highly conducting flexible sheet. For a patch antenna like this one, where the radiating patch is a simple square, Nora-Dell proved very useful. Since it is already a conductive sheet, it was only necessary to measure and cut a square of this material. However, the square that was cut had to be larger than the dimensions required. This was done so that there is extra material to be held in the felt dielectric before it was embroidered and cut to the correct size. Liberator-20 was the conductive thread used to embroider the vias that connect the top patch to the microstrip line and ground plane. Felt was used as a dielectric for both the transmission line and the antenna, with permittivity and loss tangent measured in a split-post dielectric resonator. For the 1mm felt, $\epsilon_r = 1.2$ and $\tan\delta = 0.0013$ was measured, while for the 2.9mm felt dielectric $\epsilon_r = 1.185$ and $\tan\delta = 0.0012$.

In Fig. 5.31 the dimensions of the full textile model are presented.

### 5.4.2 Embroidery process

In this design there are three major components that have to be embroidered. The central via that connects the top patch to the feeding microstrip and the two side vias that connect to the ground plane. The distance between the vias must be kept at 4mm as shown in Fig. 5.33 as this distance directly influences the antenna impedance matching as well as the proper excitation of the desired $TM_{21}$ mode. The via diameter can also influence the performance of the antenna and should have 1.3mm diameter. A few models for the vias were tested, these are shown in Fig. 5.32. The via models were tested to see which would give the exact diameter and distance between the embroidered vias, they are embroidered using Liberator-20 thread. For the first three models the sewing method was set to satin stitch, with line density starting at 2 to 3 lines/mm and finally 4.5 lines/mm. The last three models had the sewing method set to concentric circle stitch and the density was set to 2, 2.5 and 3 lines/mm. After testing and measuring, the sixth model was chosen to be embroidered in the HMMPA antenna.

To embroider the model three major steps were taken. The first step was stitch the central via through the Noda-Dell and dielectric to the microstrip line. This creates the first via that also holds the patch and the feeding microstrip in place for the remainder of the process. As its shown in Fig. 5.34 by embroidering the central conductor through to the feeding via, the bottom side of the stitch will be in direct contact with the ground plane. To prevent this, a small patch of masking tape was used to cover the bottom side of the stitch under the feeding microstrip. The second

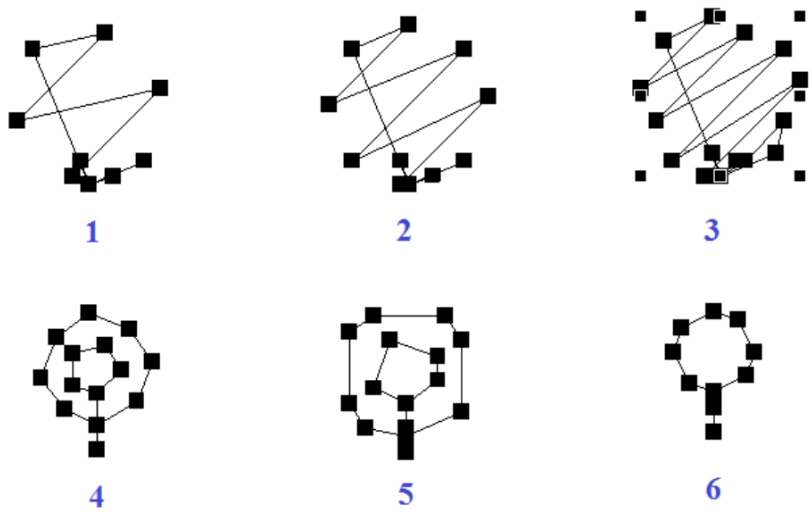


**Figure 5.32** Via models with different stitching methods and density, from A. Paraskevopoulos et al [5]

step is to attach another Nora-dell square to the bottom of the design to act as a ground plane and stitch the side vias to connect it to the top patch. The last step was to secure the whole design in place. The yellow line as seen in Fig. 5.31 was used to hold the top patch in place, it was stitched with the desired dimensions for the top radiating patch. The red and yellow line square that can be seen around the design was used to hold the ground plane in place. Both this threads were non-conductive.

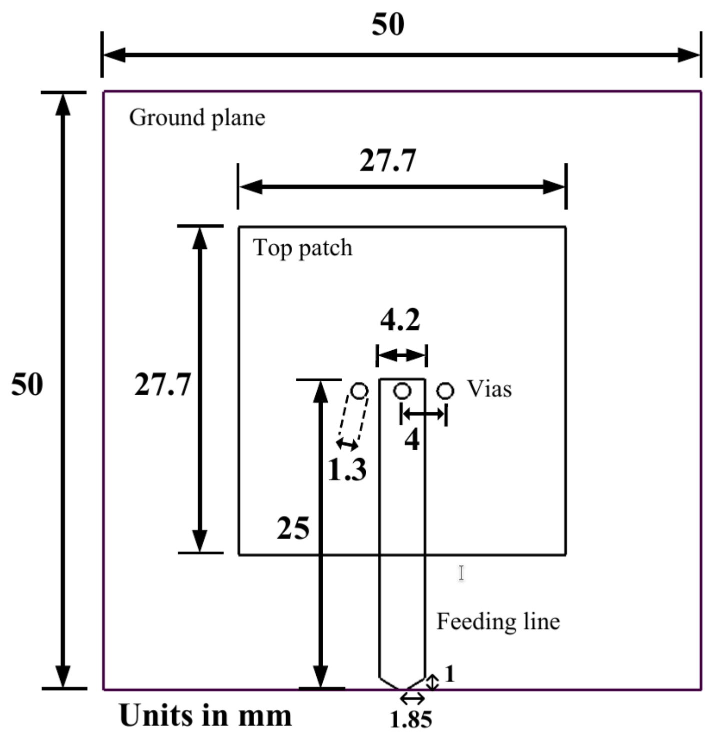


**Figure 5.33** Textile HMMPA antenna dimensions, from A. Paraskevopoulos et al [5]

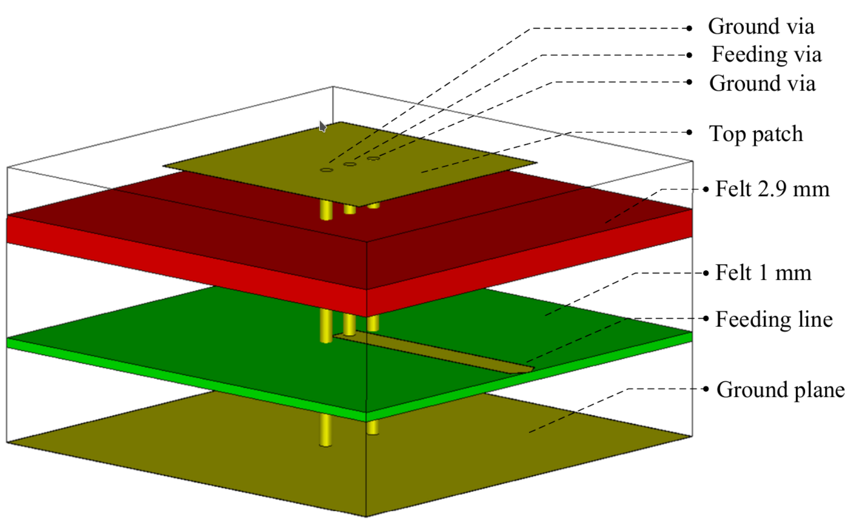


**Figure 5.34** Exploded view of the textile antenna, from A. Paraskevopoulos et al [5]

### 5.4.3 Free space and on-body results

The impedance mismatch performance for the textile HMMPA antenna was measured in free space and on the SAM phantom. As shown in Fig 5.35 the $S_{11} = -21.3$ dB at 2.4 GHz in free space while there was a slight detuning when placed on-body with $S_{11}$ $= -22$ dB at 2.44 GHz. In comparison, the copper HMMPA presented $S_{11} = -21.6$ dB at 2.45 GHz in free space while $S_{11} = -22.3$ dB at 2.46 GHz on-body showing negligible detuning. As far as the $-10$ dB bandwidth (BW) is concerned, the textile antenna presented a three times larger BW of 150 MHz ranging from 2.36 GHz to 2.51 GHz instead of 50 MHz for the copper antenna. In both cases, the BW is large enough to cover the entire 2.4 GHz ISM band (2.4 - 2.485 GHz).

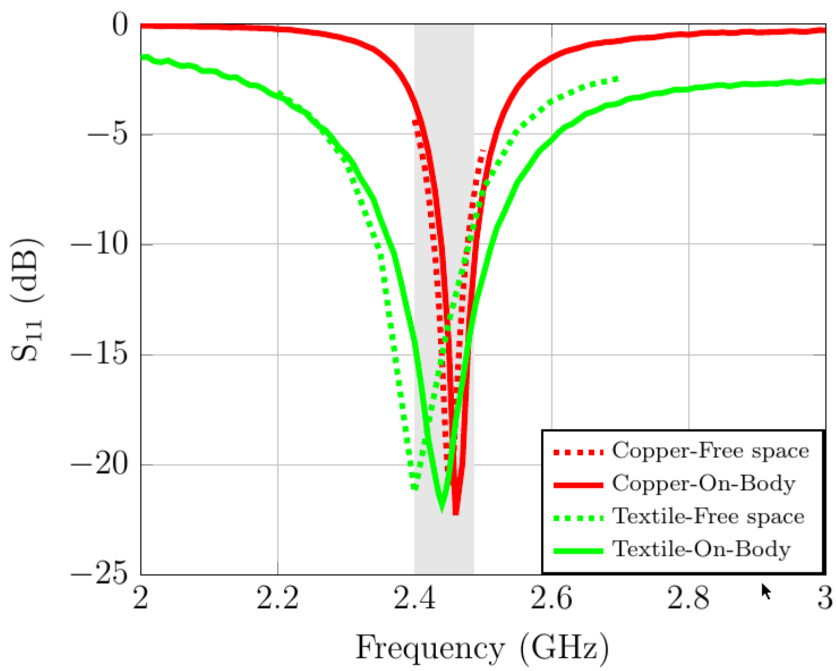


**Figure 5.35** Measured reflection coefficient $S_{11}$ of HMMPA antenna between free space (dotted line) and on-body phantom (solid line)

The HMMPA antenna gain in the direction of maximum radiation ($\theta = 90°$) is given in Fig. 5.36 for the textile and copper patch antennas. The gain performance of the textile patch antenna is found almost 2dB lower than the copper antenna in both free space and on-body cases. This is attributed to the intrinsic ohmic losses of the conductive fabric and conductive thread which form a less efficient radiator. On top of this, the textile ground plane offers less shielding than the copper sheet from the near field interaction with the phantom's body dielectric.

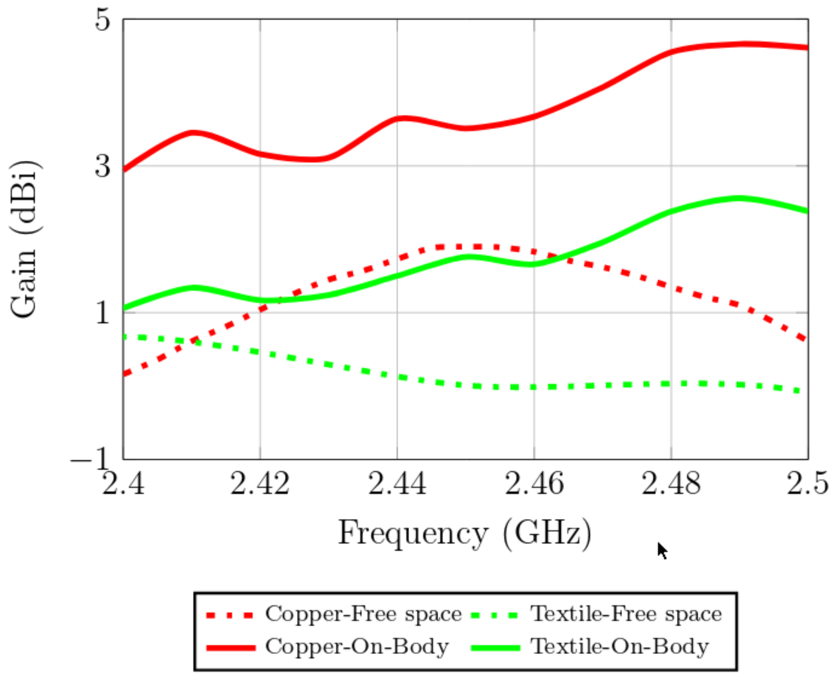


**Figure 5.36** Measured maximum gain of the proposed textile and copper HMMPA antennas

The measured radiation efficiency of the textile antenna in free space was more than 50% Fig. 5.37 while the copper antenna efficiency reached 88% at the resonance frequency. This difference is attributes mainly to the low conductivity of the conductive fabric and thread that were used to fabricate the textile antenna in the embroidery machine.

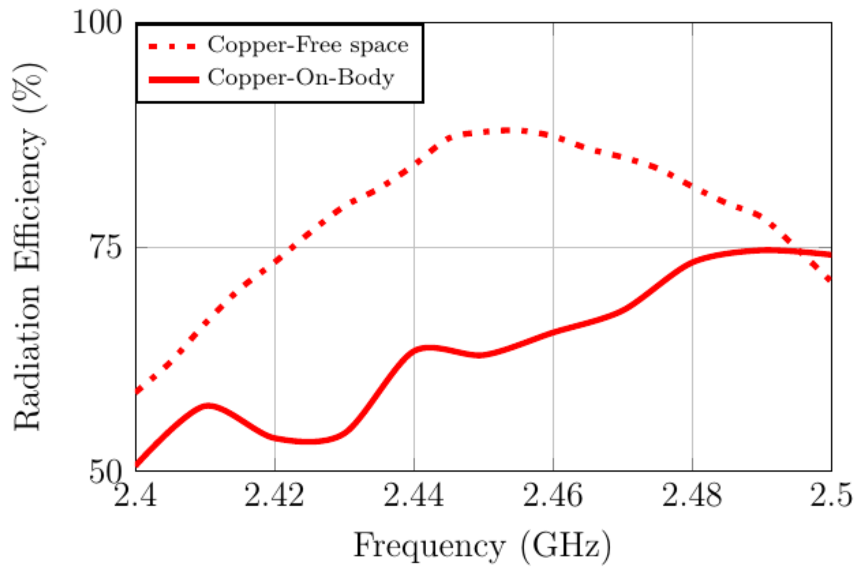


(a)

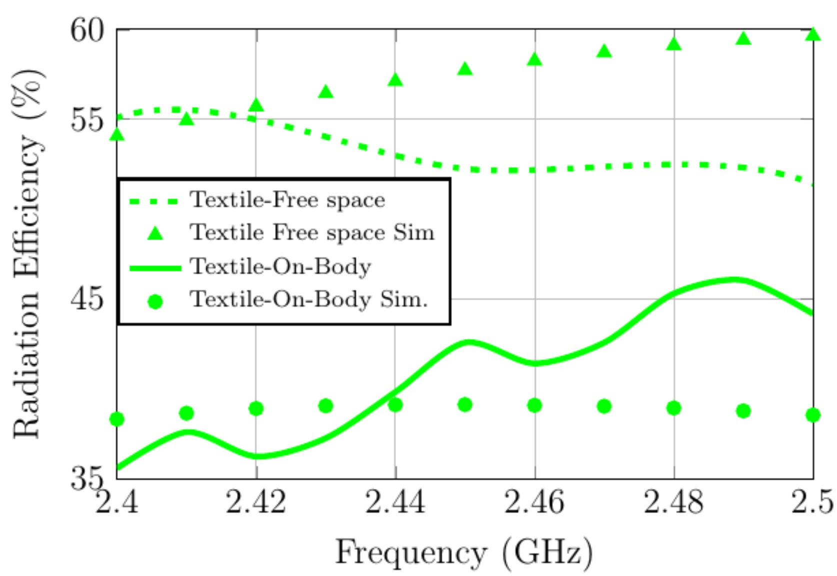


(b)

**Figure 5.37** Measured and simulated radiation efficiency of the (a) copper and (b) textile HMMPA antennas

### 5.4.4 Conclusions on physical properties of full textile model

The focus of this section was the creation and embroidery of the fully textile model, the complete results of the study can be found in [5]. As presented before, the fully textile model was design with a microstrip feed instead of a probe feed. This made a model thinner from 1.4cm in the original copper sheet model to 0.4cm on the full textile model including feeding, as the textile model is side fed. Another advantage is the flexibility of the fully textile model. While with the original one the antenna could not be easily bent due to the copper sheet, with the embroidered model the antenna could be made to conform to the wearers body.

## 5.5 Embroidery techniques and challenges

In this section some embroidery techniques will be discussed. These were developed during the research done during this PhD when trying to embroider more complicated designs. The embroidery machine used is a Entrepreneur Pro PR1000e which was designed for normal embroidery. However, most of the designs presented in the previous chapters have more than one layer of fabric. Depending on the design, embroidering different layers with different patterns presented a challenge when everything had to be aligned.

Another problem when using a normal embroidery machine for these designs, was using the conductive thread Liberator 20. When compared to a normal thread using in embroidery patterns, Liberator 20 has a few different qualities. It is a much harder thread. When the machine does an ending stitch and needs to move the needle for another position, the embroidery process has to be manually paused and the Liberator 20 needs to be cut manually with scissors. The blade that usually cuts the thread is not sharp enough to cut through Liberator. Another problem is that Liberator 20 is prone to unravelling and fraying. This causes different problems in the embroidery machine due to moving parts getting stuck on these frayed strands.

When creating embroidery designs and using Liberator 20, one has to take into account these properties of the thread. In designs where the embroidery machine has to do a lot of start and end stitches, these create a blob of conductive thread on the bottom of the fabric.

One of these problems became apparent when trying to embroider the grounded CPW model. The embroidery process begins by embroidering the central conductor.

After that, it needs to be checked for threads or strands that could get under the side ground planes. In Fig 5.38 it can be seen that there is a piece of thread going out of the central conductor boundary.

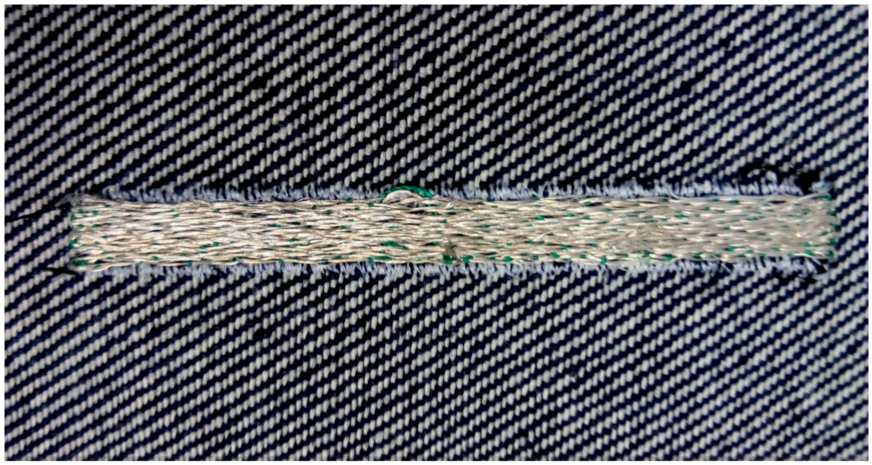

**Figure 5.38** Embroidered central conductor of textile grounded CPW

Something similar can happen after the side planes are embroidered. The model needs to be checked very carefully and overlapping threads have to be removed. After this, a second layer of denim will go under these conductive textile threads. The friction between denim and Liberator 20 can sometimes make the conductive thread fray and create short circuits. To circumvent this, pieces of masking tape were put in the gaps between central conductor and side planes as shown in Fig . This prevents any extra fraying from happening when the extra layer of denim is put in place.

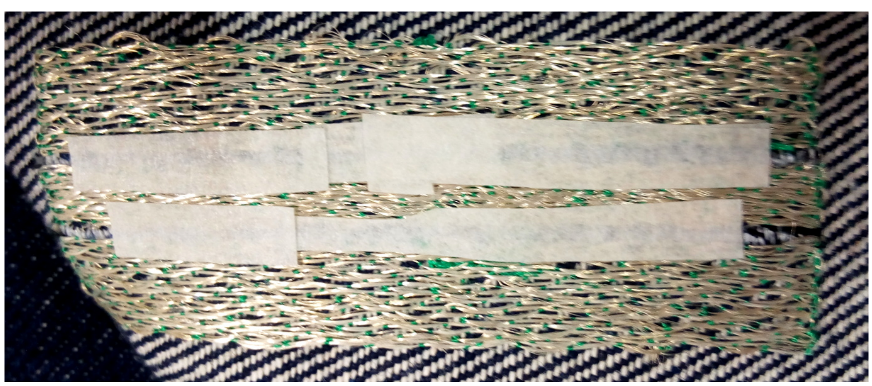

**Figure 5.39** Masking tape used to prevent extra fraying from Liberator 20

The techniques used in this research are presented here so that they can be helpful to others in their research. After all the embroidery machine was not made specifically for multi layered designs or conductive thread.

## References

[1] R. Seager, S. Zhang, A. Chauraya, W. Whittow, Y. Vardaxoglou, T. Acti, and T. Dias, “Effect of the fabrication parameters on the performance of embroidered antennas,” IET Microwaves, Antennas Propagation **7,** 1174–1181 (2013).

[2] M. Kobayashi and K. Takaishi, “Normalized longitudinal current distributions on microstrip lines with finite strip thickness,” IEEE Transactions on Microwave Theory and Techniques **42,** 866–869 (1994).

[3] J. Cserti, G. Széchenyi, and G. Dávid, “Uniform tiling with electrical resistors,” Journal of Physics A: Mathematical and Theoretical **44,** 215201 (2011).

[4] J. G. J. V. M. Pontius, “Embroidermodder,”, 2017.

[5] A. Paraskevopoulos, D. d. S. Fonseca, R. D. Seager, W. G. Whittow, J. C. Vardaxoglou, and A. A. Alexandridis, “Higher-mode textile patch antenna with embroidered vias for on-body communication,” IET Microwaves, Antennas Propagation **10,** 802–807 (2016).

[6] “Nora Dell-CR Conductive Metallized Nylon Fabric,”, http://www.shieldextrading.net/pdfs/NoraDell%20CR.pdf, accessed: 21/11/2014.

[7] “Liberator™ conductive fiber,”, http://www.metalcladfibers.com/liberator-fiber/, accessed: 21/11/2014.

# Chapter 6

# Conclusions and future work

## 6.1 Conclusions

In the area of textile antennas or transmission lines the devices need to be measured and tested to evaluate their properties. This is done by connecting these devices with VNAs or other microwave equipment. Most textile antennas found in the literature are measured by soldering coaxial SMA connectors to the textile or by using conductive epoxy to attach coaxial cables. This has certain disadvantages as these connections cannot be removed easily if the garments need to be washed. The scope of this thesis was to create a textile connection that doesn't have this disadvantage, while maintaining a good connection between textile device and microwave equipment. The requirements were that the connection should not be permanent to be easily removed, and it should also be flexible and conformal to the body.

On Chapter 3 a proof of concept for using magnets to hold the connector in place was presented as well as the microstrip model of the textile connector. The magnets were found to have no negative impact on the results and the connector was successfully characterized and measured with good results up to 2GHz. Afterwards on Chapter 4 a CPW model was made and tested, the same characterization was done. Similarly to the microstrip model, this model has reasonable insertion loss up to 2GHz. This limitation can be due to the denim used being a very lossy dielectric. While this models were created to study the effects of this transition, a usable transition could be made much shorter. This would then reduce the effect of the losses in the denim and improve the results.

A full characterization of the connectors was also done by using de-embedding theory. By extracting the effects of the connection to ABCD parameters, it is possible to predict the effects it will have on the S-parameters of a system where the connection is used.

Work was also done on the effect of using different fillings for the connector. Gradient fillings were used and it was found that when gradients that use less than 53% thread compared to the original model, not much performance is lost. Also on the subject of different filling patterns, a triangular filling was used. It was based on the theory of infinite lattice structures and it was a proof of concept to see how it worked when applied to a textile microstrip line. An open source software was required to directly edit the embroidery files that were created using Matlab code. In the end it did not seem like this type of meshing was ideal for the model created.

Some difficulties regarding the use of conductive textile threads in the embroidery machine were also presented. Due to the characteristics of the thread, Liberator 20 is prone to unravel and that can jam the machine in different moving parts. The way the embroidery machine holds the fabric is also not the easiest if a design has more than one layer. Hopefully as the area develops, more efficient designs for these machines will appear.

A wearable antenna was fully converted to textile materials. Due to the textile materials and being side fed instead of probe fed, the thickness was reduced by 70% from 1.4cm to 0.4cm. Another advantage of the conversion to textile materials is the fact that the antenna can now be bent to conform with the body. Previously the antenna used a rigid copper sheet which was not flexible.

Being one of the first easily removable microwave interconnects, novel work was presented and the work done can influence the research area on how textile antennas are fed. The purpose of this research has been achieved with two different textile connector models created and studied. This tries to bring attention to the lack of removable microwave interconnects in the literature. Some extra work could be done in testing these connectors with different types of textile antennas. This would give extra information on the effects that this connector has with different types of antennas or applications. Another improvement that could be researched would be the way this connector attaches to a textile device. At the moment the connection is on the same plane as the antenna, perhaps a new model could be created that had a vertical connection to said antenna. This way the connector could be attached anywhere and not require a loose piece of the textile feeding system to attach to.

Many textile antennas in the literature are still measured using soldered coaxial cables or metallic connectors, this research could have implications on how new textile antennas are constructed and measured. The connector with better results was the microstrip model, it is not very difficult to create and adapt to textile antennas which are microstrip fed. This could bring full textile antennas already adapted for this type of connection.

In conclusion the following novel work was done within the scope of this thesis:

- A novel method of using magnets in conjunction with the physical type of connection was used. By using magnets for the connection, the act of attaching or removing RF equipment is simple and does not leave permanent metallic parts on the textile system
- The interconnect was fully characterized and the effects of its used extracted
- Multiple measurements using a textile antenna were performed and it was found that the interconnect did not affect the results.

On a closing note continuous research in ways to connect textile antennas to microwave equipment is necessary. If not for a purely academic purpose, for commercial purposes as well. It could make the research in textile antennas and smart clothing more appealing for commercial companies. Presenting textile microwave devices with metallic coaxial SMAs soldered to it is not as appealing as a textile solution with no metallic objects attach to it, while still being able to characterize and study such devices.

## 6.2 Future Work

Future work could be done regarding the triangular filling mesh. With different densities to study the effect this would have on the interconnect. More measurements using different antennas could also be performed. Measurements in an anechoic chamber could also be performed, to check what the effect on the radiation pattern is. Some work could also be done with different threads and if they can be used to improve the designs. Such as a thread with less strands and doesn't fray as much could be used to reduce the gap between the ground plane and central conductor on the CPW design. As for the interconnect itself, future work could be done in making the connection even easier. At the moment this interconnect is attached to the end of fabric. This requires that the feed line of a RF device needs to end at the fabric end. Future work could be done to create an interconnect that attaches vertically to any transmission line. This would give more freedom for the positioning of the textile RF device in test. The coming of 5G with always connected devices can be a good area to apply in the research of wearable electronics. And more good quality interconnects will need to be developed.

# Chapter 7

# Appendices

LIBERATOR®
CONDUCTIVE FIBER

Liberator™fiber, Syscom Advanced Materials' novel conductive metal-clad fiber utilizing Kuraray's Vectran© fiber, gives freedom to design outside the constraints of traditional wires. Liberator™ fiber pairs a light-weight, flexible, and high-strength, Vectran® fiber core with a conductive metal outer layer. The material is designed for use as a shielding braid, bare wire or coated with insulation material.

Properties

- Comparable to 20 bunched ends of 48 AWG wire.
- Seven times greater break strength than 36 AWG (19/48 Type C) copper wire.
- Increased coverage and performance can result in weight savings of over 90%.
- Weighs 56% lighter than copper 36 AWG (19/48 Type C) copper wire.
- Soldered or crimped connections.
- Compatible with braiding equipment used for metal wires.
- Supplied twisted or untwisted on braider bobbins.

**Schematic Liberator™ Fiber-40**

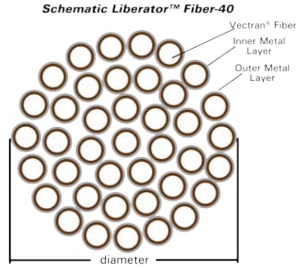


| ***Type: Liberator™ Fiber-20 Ag*** | |
|---|---|
| **Base** | |
| Fiber | Vectran® Fiber |
| Filament Count | 20 |
| Diameter: Filament | 0.00091 in |
| Diameter: Yarn | 0.0062 in |
| **Metalized** | |
| Metalization Layers | Copper/Silver |
| Yarn Diameter | 0.0087 in |
| Flat Width | 0.0252 in |
| % Metal by Weight | 82% |
| Weight | 0.041 LBS/MF |
| DC Resistance | ~2 Ω/ft |
| Break Strength | 5.72 lbs |

The data presented here is provided only as a guide and is based on internal &/or external testing of samples of standard production runs of Liberator™ Fiber. Please contact Syscom Advanced Materials for additional property data or customization options.

syscom
advanced materials

1275 Kinnear Rd. Columbus OH 43212
(614)487.3626
www.metalcladfibers.com

Liberator™ metal clad fiber has excellent thermal stability, strength and cut resistance. Liberator™ fiber utilizes Vectran® fiber and will be available in 20, 40, and 80 filaments with nickel, copper, tin or silver cladding.

www.liberatorfiber.com
info@metalcladfibers.com

**Figure 7.1** Liberator 20 conductive fiber spec sheet visit: www.statex.de — contact: info@statex.de

## Technical Data Sheet

Ag Ni Sn Cu

Shieldex® produced by statex

### Shieldex® Nora Dell

No.: 1401101S80

| | |
|---|---|
| Purpose | Conductive woven fabric for general use (outside skin for EMI/RFI fabric over foam gaskets, shielding material for laminated flat I/O shielding panels, base material for EMI/RFI garments, EMI/RFI cable shielding) |
| Description | Ni/Cu/Ag plated polyamide fabric (RS) |
| Raw material | Parachute silk (polyamide ripstop fabric) |
| Surface resistivity | Average 0.009 Ohms/□ |
| Shielding effectiveness | Average up to 100 db from 30Mhz to 10Ghz |
| Temperature range | -30˚C to 90˚C |
| Total thickness | abt. 0.130mm ± 10% |
| Weight | 95g/m² ± 10% |
| Roll width | 130cm ± 3% |
| Roll length | Average 200m |

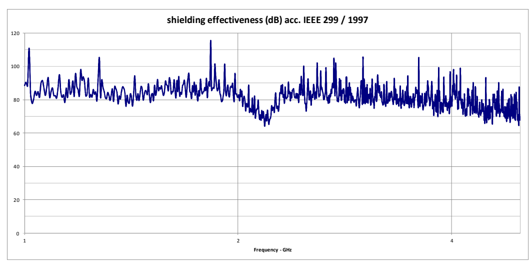


### Compliance and Certification

RoHS
REACH

Alterations Reserved
26.04.13/03

statex

PRODUKTIONS + VERTRIEBS GMBH

Kleiner Ort 11 - 28357 Bremen / Germany
Tel: +49 421 27 50 47 - Fax: +49 421 27 36 43
info@statex.de - www.statex.de

**Figure 7.2** Nora-dell spec sheet